

Fast and Fair Simultaneous Confidence Bands for Functional Parameters

Dominik Liebl*

Matthew Reimherr[†]

Abstract

Quantifying uncertainty using confidence regions is a central goal of statistical inference. Despite this, methodologies for confidence bands in Functional Data Analysis are underdeveloped compared to estimation and hypothesis testing. This work represents a major leap forward in this area by presenting a new methodology for constructing simultaneous confidence bands for functional parameter estimates. These bands possess a number of striking qualities: (1) they have a nearly closed-form expression, (2) they give nearly exact coverage, (3) they have a finite sample correction, (4) they do not require an estimate of the full covariance of the parameter estimate, and (5) they can be constructed adaptively according to a desired criteria. One option for choosing bands we find especially interesting is the concept of *fair bands* which allows us to do fair (or equitable) inference over subintervals and could be especially useful in longitudinal studies over long time scales. Our bands are constructed by integrating and extending tools from Random Field Theory, an area that has yet to overlap with Functional Data Analysis.

Keywords: Functional Data Analysis; Simultaneous Inference; Hypothesis Testing; Kac-Rice Formula

1 Introduction

As part of the big data revolution, statistical tools have made astonishing strides towards handling increasingly complex and structured data. Data gathering technologies have allowed scientists, businesses, and government agencies to collect data on increasingly sophisticated phenomena, including high-dimensional measurements, functions, surfaces, and images. A major tool set that has emerged for handling highly complex and smooth structures is Functional Data Analysis, FDA (Ramsay and Silverman, 2005; Ferraty and Vieu, 2006; Hsing and Eubank, 2015; Kokoszka and Reimherr, 2017). There, one has access to rich, dynamic, and smooth structures, while also having some degree of repetition, allowing researchers to fit complex and flexible nonparametric statistical models.

*Institute of Finance and Statistics, University of Bonn, Adenauerallee 24-42, 53113 Bonn, Germany

[†]Department of Statistics, Penn State University, 411 Thomas Building, University Park, PA 16802

Despite the success and maturity of FDA, some foundational questions remain unanswered or underdeveloped. This work is concerned with a fundamental goal of statistical inference: quantifying estimation uncertainty with simultaneous confidence bands. This problem has received increasing attention in recent years, however, current solutions usually suffer from one of several major drawbacks: (1) they are computationally expensive, (2) they result in bands that are very conservative, or (3) they control only the point-wise type-I error rate.

In this work we present a broad framework based on Random Field Theory (RFT) that provides a seemingly definitive approach that solves the aforementioned issues. Our bands possess a number of desirable qualities, but two are especially striking. First, they can be chosen adaptively to achieve equitable local inference which leads to interpretable bands with locally varying widths. Bands that achieve such a property we call *fair* as they are similar in spirit to recent work on algorithmic fairness (e.g. [Hajian et al., 2016](#); [Friedler et al., 2016](#); [Corbett-Davies et al., 2017](#)). While fair bands seem desirable in general, they could be especially important for applications such as longitudinal pediatric or geriatric studies. In those settings it can be important to treat different ages fairly, in the sense that no age will exert too much control over the shape of the band, especially for studies that contribute to public policy. We are unaware of another FDA or RFT method possessing such a property. Second, which may surprise even some seasoned FDA researchers, is that the bands do not require estimation of the full covariance function of the estimator. Instead, only a narrow band along the diagonal is needed and then only to ascertain the point-wise uncertainty of the estimate and its derivative. No other FDA method in the literature, that we are aware of, for quantifying uncertainty globally possesses such a property. This has broad implications in FDA as many tools are being actively developed for data consisting of fragments, or which are measured longitudinally in a way that makes estimation of the full covariance generally impossible ([Delaigle and Hall, 2016](#); [Descary and Panaretos, 2019](#); [Delaigle et al., 2019](#); [Kneip and Liebl, 2019](#)). Indeed, parametric bootstrap methods, which previously were the only option available for constructing non-conservative bands, still require estimation of the full covariance.

At a broader level this work aims to bridge two branches of statistics, RFT and FDA, which, while seemingly having a great deal in common, have yet to significantly overlap. While Random Field Theory has seen tremendous success in applications related to brain-imaging, subsumed under the term Statistical Parametric Mapping (see, for instance, [Friston et al., 1994, 2007](#)), Functional Data Analysis was originally motivated from curve-like data with applications in health studies, finance, geosciences, etc. ([Ramsay and Silverman, 2005](#)). Though today, FRT and FDA have been successfully applied in many other applications involving both curve and image data. In this work, we demonstrate how methods from RFT can be used in FDA and also provide several new results of interest in RFT. We start by generalizing the so-called Kac-Rice formula ([Kac, 1943](#); [Rice, 1945](#)) to allow for thresholds that vary across the domain. We then develop a very general formula that holds for any elliptical distribution, not just Gaussian processes. Using these tools we provide an entire class of bands that achieve a desired significance level. Lastly, most RFT based methods do not take into account estimation error or that one is working with an estimator that converges in distribution only asymptotically. So we conclude our theoretical work

by showing that the entire class of estimated confidence bands converges asymptotically in Hausdorff distance when the process is asymptotically Gaussian/elliptical.

The central idea behind our methodology is an ingenious connection between the supremum of a stochastic process and the *expected Euler characteristic* of an exceedance set. Consider a real valued random function over a closed interval, $X = \{X(t) : t \in [0, 1]\}$, where restricting the domain to $[0, 1]$ is without loss of generality (for any closed finite interval) and common in FDA to ease notation. Instead of finding the probability that X ever crosses a threshold, $u = \{u(t) : t \in [0, 1]\}$, i.e., $P(\exists t \in [0, 1] : X(t) \geq u(t))$, the expected Euler characteristic inequality suggests to consider the task of counting the events when X crosses u in an upward trajectory. One then uses that the probability of X ever crossing u is less than the expected number of up crossings. While a seemingly small change, the latter ends up being far more tractable. Thus far, the RFT literature has focussed primarily on constant thresholds $u(t) \equiv u \in \mathbb{R}$ for standardized processes (see, for instance, [Adler and Taylor, 2007](#), and [Azaïs and Wschebor, 2009](#)). In this paper, we demonstrate how to handle the more general case of non-constant threshold functions, which, as we will see, opens up the exciting opportunity to produce tight and interpretable bands that adapt to the local dependency structure of the considered process.

The number of up-crossings of X about u on the interval $[0, 1]$ is defined as

$$N_{u,X}([0, 1]) := \#\{0 \leq t \leq 1 : X(t) = u(t), X'(t) > u'(t)\}.$$

If this quantity is zero, then the only way that $X(t)$ could have exceeded $u(t)$ was if X started above of u at $t = 0$, since both functions, X and u , are continuous. This logic leads to the expected Euler characteristic inequality

$$\begin{aligned} P(\exists t \in [0, 1] : X(t) \geq u(t)) &= P(\{X(0) \geq u(0)\} \text{ or } \{N_{u,X}([0, 1]) \geq 1\}) \\ &\leq P(X(0) \geq u(0)) + P(N_{u,X}([0, 1]) \geq 1) \\ &\leq P(X(0) \geq u(0)) + \mathbb{E}[N_{u,X}([0, 1])] = \mathbb{E}[\varphi_u(X)], \end{aligned} \quad (1)$$

where $\varphi_u(X) := \mathbb{1}_{X(0) \geq u(0)} + N_{u,X}([0, 1])$ denotes the Euler (or Euler-Poincaré) characteristic of the excursion set $\{t \in [0, 1] : X(t) \geq u(t)\}$. Intuitively, this quantity counts exceedances by starting at $t = 0$, checking if $X(0) > u(0)$ and then moving through the domain to check for additional up-crossings. For large u , the inequality in (1) gives a very useful and nearly exact approximation. Indeed, for a constant threshold function $u(t) \equiv u$ the results in [Taylor et al. \(2005\)](#) imply that, under some regularity conditions, the approximation error is exponentially smaller than $\mathbb{E}[\varphi_{u,X}(t_0)]$, i.e., $P(\exists t \in [0, 1] : X(t) \geq u) = \mathbb{E}[\varphi_{u,X}(t_0)](1 + o(\exp(-cu^2)))$, for some $c > 0$. As our intended applications are confidence and prediction bands with typically large thresholds u , we will see in our numerical work that the resulting bands are nearly exact.

For variable $u(t)$, it can be useful to start counting at some mid point, $t_0 \in [0, 1]$ and then count crossings moving away from t_0 in both directions. When moving from t_0 down to 0, up-crossings as t decreases are equivalent to down-crossings as t increases (see [Figure 7](#) of the supplementary paper [Liebl and Reimherr \(2019b\)](#)). We therefore work with the

more generalized bound

$$\begin{aligned} P(\exists t \in [0, 1] : X(t) \geq u(t)) &\leq P(X(t_0) \geq u(t_0)) + \mathbb{E}[N_{u,X}^-([0, t_0])] + \mathbb{E}[N_{u,X}([t_0, 1])] \\ &= \mathbb{E}[\varphi_{u,X}(t_0)], \end{aligned} \tag{2}$$

where $N_{u,X}^- := \#\{0 \leq t \leq 1 : X(t) = u(t), X'(t) < u'(t)\}$ denotes the number of down-crossings and t_0 is any fixed value in $[0, 1]$.

The possibility to choose $t_0 \in [0, 1]$ becomes particularly important when using the interpretable fairness property of our bands (see Proposition 2.2) for inference with respect to Regions Of Interest $\text{ROI} = [0, t_0] \subseteq [0, 1]$ or $\text{ROI} = [t_0, 1] \subseteq [0, 1]$. Such ROI analyses are very common, for instance, in the applied neuroimaging and biomechanics literature (Poldrack, 2007; Wager et al., 2008; Pataky et al., 2016; Wen et al., 2018).

Given an expression for $\mathbb{E}[\varphi_{u,X}(t_0)]$ and a significance level, α , solving $\mathbb{E}[\varphi_{u,X}(t_0)] = \alpha/2$ allows one to derive powerful (two-sided) simultaneous confidence bands. For instance, in many applications in FDA, one is interested in estimating a functional parameter, $\theta = \{\theta(t) : t \in [0, 1]\}$, for a particular FDA model. Suppose that $\hat{\theta}(t)$ is an estimator of $\theta(t)$, such that $(\hat{\theta}(t) - \theta(t))$ is a mean zero Gaussian process. Then we can take the standardized Gaussian process $X(t) = (\hat{\theta}(t) - \theta(t)) / (\text{Var}(\hat{\theta}(t)))^{1/2}$, which now has mean zero and unit variance for all $t \in [0, 1]$, and compute the corresponding threshold function $u(t)$ that solves $\mathbb{E}[\varphi_{u,X}(t_0)] = \alpha/2$. Our Theorem 2.1 ensures that

$$[\hat{\theta}_l(t), \hat{\theta}_u(t)] = \hat{\theta}(t) \pm u(t) \sqrt{\text{Var}(\hat{\theta}(t))}, \tag{3}$$

is a valid $(1 - \alpha) \times 100\%$ simultaneous (two-sided) confidence band for the parameter $\theta(t)$. Our Theorem 2.2 ensures that the simultaneous confidence band in (3) holds, at least asymptotically, even when the underlying covariance parameters (and therefore u) are estimated. Moreover, our Corollary 2.3 can be used for finite sample corrections using t -processes to take into account estimation errors in the covariance estimates.

One could also solve $\mathbb{E}[\varphi_{u,X}(t_0)] = \alpha$ to produce one-sided confidence bands, which, while unusual for confidence bands, could prove very useful for forming prediction bands in certain applications. For example, when designing flood barriers to protect against storm surges, one is explicitly interested in an upper bound. In such settings, however, a Gaussian distribution may be too light tailed to accurately model the data directly; therefore, our Theorem 2.1 is stated for general elliptical distributions, which includes the case of heavy tailed processes.

The main hurdle in finding a $u(t)$ that solves $\mathbb{E}[\varphi_{u,X}(t_0)] = \alpha/2$, for some pre-specified α , is to find general expressions for $\mathbb{E}[N_{u,X}^-([0, t_0])]$ and $\mathbb{E}[N_{u,X}([0, t_0])]$, since a formula for the correction term, $P(X(t_0) \geq u(t_0))$, usually follows directly from distributional assumptions on X or from a central limit theorem. As we focus on symmetric distributions, a formula for the up-crossings can be translated into one for the down-crossings since $\mathbb{E}[N_{u,X}^-([0, t])] = \mathbb{E}[N_{-u,X}([0, t])]$. Explicit formulas for $\mathbb{E}[N_{u,X}([0, 1])]$ are grouped together under the famous ‘‘Kac-Rice formulas’’ acknowledging the works of Kac (1943) and Rice (1945). In this paper we generalize the existing Kac-Rice formulas by allowing for adaptive threshold functions $u(t)$. Another apparent challenge is that $\mathbb{E}[\varphi_{u,X}(t_0)] = \alpha/2$ will not,

in general, have a unique solution when we allow for more general $u(t)$, even when t_0 is treated as fixed. However, far from being a liability, we show how this allows one to select bands adaptively according to some desired criteria, such as *fairness*, though other criteria such as minimum squared width are, in principle, possible too.

The recent literature in FDA provides different approaches and methods to simultaneous inference for functional data. Amongst the most successful approaches are the simulation based methods proposed by [Degras \(2011\)](#), [Cao et al. \(2012\)](#) and [Wang et al. \(2019\)](#), which are based on the parametric bootstrap. A further simulation based approach is the interval-wise testing (IWT) procedure proposed by [Pini and Vantini \(2016\)](#) and [Pini and Vantini \(2017b\)](#) which uses permutations. Simulation based approaches, however, are computationally intensive – particularly when used for the practically relevant case of approximating small p-values. Moreover, as shown in our simulation study, the parametric bootstrap based methods tend to over-reject the null hypothesis due to their sensibility against finite sample estimation errors in the covariance. The IWT procedure is able to keep the significance level, but has very low power in detecting local violations of the simultaneous null hypotheses.

Another typical approach is to apply a dimension reduction based on function principal component analysis (FPCA) and to build multivariate confidence ellipses; see, for instance, [Ramsay and Silverman \(2005\)](#), [Yao et al. \(2005\)](#) and [Goldsmith et al. \(2013\)](#). As shown by [Choi and Reimherr \(2018\)](#), however, these procedures lead to ellipses with ‘zero-coverage’. As a solution to this problem, [Choi and Reimherr \(2018\)](#) proposed an approach that allows one to transform confidence hyper-ellipsoids into valid confidence bands. To the best of our knowledge, the \hat{B}_{E_c} band of [Choi and Reimherr \(2018\)](#) is the only band that is able to adapt to the local extent of the multiple testing problem. By minimizing an average squared width criterion, the \hat{B}_{E_c} band becomes narrow in areas with high positive within curve correlations and wider in areas with very weak correlations. However, this band does not fulfill a formal and interpretable fairness property; moreover, the band is quite conservative. Also related are the works of [Ma et al. \(2012\)](#) and [Zheng et al. \(2014\)](#), who focus on the special case of sparsely sampled functional data, which is not the focus of this work. A further recent contribution is the work of [Lundtorp Olsen et al. \(2019\)](#) who adapt the Benjamini-Hochberg procedure to the case of functional data. Inference for partially observed functional data was previously considered by [Kraus \(2019\)](#), who, however, does not consider the case of simultaneous inference.

Early theoretical results on Kac-Rice formulas were developed by [Ito \(1963\)](#), [Cramér and Leadbetter \(1965\)](#), and [Belyaev \(1966\)](#) among others. Fundamental introductions to RFT, including different versions of the Kac-Rice formula, are given in the textbooks of [Adler and Taylor \(2007\)](#), [Azaïs and Wschebor \(2009\)](#), and [Cramér and Leadbetter \(2013\)](#). Results from RFT are also used in other statistical areas; for instance, [Taylor et al. \(2016\)](#) derive a Kac-Rice test-statistic that is useful for lasso-type inferential problems. The RFT based statistical methods have seen a tremendous success in the applied neuroimaging and biomechanics literature (see, for instance, [Friston et al., 2007](#); [Wager et al., 2009](#); [Pataky et al., 2016](#); [Wen et al., 2018](#)), where these methods are subsumed under the term Statistical Parametric Mapping (SPM).

The paper and its contributions are structured as follows. In [Section 2](#) we collect our

methodological and theoretical contributions. Our two main theorems are presented in Section 2.2. Theorem 2.1 contains our generalization of the Kac-Rice formula to variable threshold functions and general elliptical processes and Theorem 2.2 contains our asymptotic results. We introduce a fast algorithm that facilitates selecting interpretable and fair adaptive threshold functions (Section 2.3) and show how these threshold functions lead to interpretable and fair simultaneous confidence bands (Section 2.4). Simulations in Section 3 show the excellent finite-sample behavior of our fair confidence bands for fully observed functions (Section 3.1) and for the challenging case of fragmentary functional data (Section 3.2). Section 4 contains applications to data from sports biomechanics and to fragmentary growth curves. Lastly, Section 5 contains our discussion.

2 Methods and Theory

Our first main result is Theorem 2.1, which establishes the Kac-Rice formula for both variable thresholds, $u = \{u(t) : t \in [0, 1]\}$, and general elliptical processes, $X = \{X(t) : t \in [0, 1]\}$. Interestingly, these results hold even when the process is heavy tailed, making the generality especially useful, for instance, in forecasting and prediction. The results are established under the very mild assumption that the considered process, X , is in $C^1[0, 1]$ and that the threshold function, $u(t)$, is in $C[0, 1]$ and continuously differentiable almost everywhere.

In our second main result, Theorem 2.2, we consider the problem of estimating the confidence/prediction band for a process that is only asymptotically normal/elliptical. A key point is that we only need consistent estimates of the covariance parameters about the diagonal. This interesting property makes our method applicable even for fragmentary functional data where an estimation of the full covariance function is impossible. We discuss how to produce such estimators in Section 2.4. Since we allow for variable threshold functions $u(t)$, the equation $\mathbb{E}[\varphi_{u,X}(t_0)] = \alpha/2$ has, in general, no unique solution, but is solved by a whole class of threshold functions. Therefore, we show that the entire solution class of estimated confidence bands converges in Hausdorff distance as the sample size tends to infinity, $n \rightarrow \infty$. In this way, one can choose some continuous selection criteria (see Section 2.3) to produce adaptive bands that have the correct type-I error rate.

2.1 Elliptical Processes

We consider a centered stochastic process $\{X(t) : t \in \mathcal{T}\}$, where \mathcal{T} is a closed finite interval of \mathbb{R} . For ease of exposition, we rescale the domain so that $\mathcal{T} = [0, 1]$, as is common in FDA. Throughout this paper we will make the following assumption.

Assumption 2.1. *We assume that $X = \{X(t) : 0 \leq t \leq 1\}$ is a centered elliptical process with $X \in C^1[0, 1]$ almost surely.*

The assumption that $X \in C^1[0, 1]$ almost surely means that the realized paths of X will, with probability one, be one time continuously differentiable, which excludes, for instance, Brownian motion. As our methodology is based on counting up-crossings, some

smoothness is required, otherwise the number of up-crossings may be infinite. Of course, not every stochastic process is elliptical, e.g. discrete state Markov chains, but allowing X to be elliptically distributed provides at least two major benefits. First, as we will highlight later on, it allows one to include a finite sample correction into confidence bands by using t -processes, and second it allows for better uncertainty quantification when forecasting heavy tailed processes.

One key aspect of elliptical processes is that they can be expressed as scalar mixtures of Gaussians; see, for instance, [Boente et al. \(2014\)](#) for the case of functional data and [Fang et al. \(2018\)](#) for a general overview in the case of multivariate data.

Lemma 2.1. *If $X = \{X(t) : 0 \leq t \leq 1\}$ is a centered elliptical process, then there exists a strictly positive random variable $V > 0$ and a mean zero Gaussian process, $Z = \{Z(t) : 0 \leq t \leq 1\}$, such that V and Z are independent and satisfy $\{X(t) : 0 \leq t \leq 1\} \stackrel{D}{=} \{VZ(t) : 0 \leq t \leq 1\}$.*

If V is heavy tailed, then $X(t)$ need not even have a finite mean. We will thus refer to the covariance of $Z(t)$, $c(t, s) = \text{Cov}(Z(t), Z(s))$, as the *dispersion function* of $X(t)$. If V has a finite and non-zero variance, then the covariance function of X is given by $\text{Cov}(X(t), X(s)) = \text{Var}(V)c(t, s)$ for all $t, s \in [0, 1]$. In the Gaussian case, where $V \equiv \sigma$, the covariance function of X is given by $\text{Cov}(X(t), X(s)) = \sigma^2 c(t, s)$ for all $t, s \in [0, 1]$.

Since we are working with an arbitrary threshold $u(t)$, we can always assume that it has been scaled by the standard deviation of $Z(t)$, $\sqrt{c(t, t)}$, so that, without loss of generality, we can assume $c(t, t) = 1$ (see Examples 1 and 2).

2.2 Theoretical Results

In this section we present our key theoretical results. We begin with our first theorem, which establishes a generalized Kac-Rice formula for varying thresholds $u(t)$ and elliptical processes $X(t)$. We employ notation such as $\partial_{12}c(t, t)$ to denote partial derivatives of $c(t, s)$ in the first and second coordinates, but then evaluated at $t = s$. Moreover, we write $C_{a.e.}^1[0, 1]$ to denote the space of all continuous functions that are continuously differentiable almost everywhere on $[0, 1]$. Note that $C^1[0, 1] \subset C_{a.e.}^1[0, 1]$, since $C_{a.e.}^1[0, 1]$ also contains, for instance, piece-wise linear functions.

Theorem 2.1. *Let Assumption 2.1 hold and assume that $u \in C_{a.e.}^1[0, 1]$. Let $V > 0$ be the mixing coefficient of X , such that $X(t) \stackrel{D}{=} VZ(t)$, and define $\mathcal{V} = V^{-2}$ along with its moment generating function, $M_{\mathcal{V}}(\cdot)$. Let $\tau(t)^2 = \partial_{12}c(t, t) = \text{Var}(Z'(t))$, where $c(t, s)$ is the dispersion function of $X(t)$, equivalently the covariance function of $Z(t)$. Assume $X(t)$ has a constant pointwise unit dispersion, $c(t, t) = \text{Var}(Z(t)) = 1$, and $\tau(t) > 0$ for all $t \in [0, 1]$.*

Then we have for any fixed $t_0 \in [0, 1]$

$$\begin{aligned} \mathbb{E}[\varphi_{u,X}(t_0)] &= P(X(t_0) \geq u(t_0)) + \int_0^1 \frac{\tau(t)}{2\pi} M_{\mathcal{V}} \left(-\frac{1}{2} \left[u(t)^2 + \frac{u'(t)^2}{\tau(t)^2} \right] \right) dt \\ &\quad + \int_0^{t_0} \int_0^\infty \frac{u'(t)}{2\pi\tau(t)} M'_{\mathcal{V}} \left(-\frac{1}{2} \left[u(t)^2 + \frac{(y - u'(t))^2}{\tau(t)^2} \right] \right) dy dt \\ &\quad - \int_{t_0}^1 \int_0^\infty \frac{u'(t)}{2\pi\tau(t)} M'_{\mathcal{V}} \left(-\frac{1}{2} \left[u(t)^2 + \frac{(y + u'(t))^2}{\tau(t)^2} \right] \right) dy dt. \end{aligned} \tag{4}$$

Note that since \mathcal{V} is strictly positive the above integrals are finite regardless of the mixture distribution, meaning $X(t)$ can be heavy tailed and the expression still holds. Thus $X(t)$ need not even have a finite mean or variance which allows us to model even extreme value processes. The roughness parameter function τ allows to quantify the extent of the local multiple testing problem across the domain $[0, 1]$.

The proof of Theorem 2.1 proceeds in several steps. First, we condition on the mixing parameter $\mathbb{E}[\varphi_{u,X}(t_0)] = \mathbb{E}[\mathbb{E}[\varphi_{u,V,Z}(t_0)|V]] = \mathbb{E}[\mathbb{E}[\varphi_{u/V,Z}(t_0)|V]]$ so that we can exploit the connection to Gaussian processes. Conditioned on V , we build up two key approximations, which are common in RFT, though much more complicated here since u is not restricted to a constant function. One is based on approximating the number of up-crossings by integrating a particular continuous kernel, and the second is based on a linear interpolation along dyadics. Both approximations make the expectation easier to calculate and then we justify taking appropriate limits.

The following three corollaries consider important special cases that simplify the interpretation of our general formula (4) in Theorem 2.1.

Corollary 2.1. (Constant band for elliptical processes) *Let the conditions of Theorem 2.1 hold. If $u(t) \equiv u$ for all $t \in [0, 1]$, then one obtains the elliptical version of the classic Kac-Rice*

$$\mathbb{E}[\varphi_u(X)] = P(X(0) \geq u) + \frac{\|\tau\|_1}{2\pi} M_{\mathcal{V}} \left(-\frac{u^2}{2} \right),$$

where $\varphi_{u,X}(0) = \varphi_u(X)$, and where $\|f\|_1 = \int_0^1 |f(t)| dt$ denotes the L^1 -norm.

Corollary 2.1 directly follows from Theorem 2.1 since $u' \equiv 0$ for constant thresholds, $\tau(t) \geq 0$ for all $t \in [0, 1]$ such that $\int_0^1 \tau(t) dt = \|\tau\|_1$, and $X(t_0) \stackrel{D}{=} X(0)$ for all $t_0 \in [0, 1]$.

Corollary 2.2. (Gaussian processes) *Let the conditions of Theorem 2.1 hold.*

a) *Variable band:* When $X(t)$ is a Gaussian process, we set $V \equiv \sigma$ such that $\text{Var}(X(t)) = \sigma^2 \text{Var}(Z(t)) = \sigma^2$ for all $t \in [0, 1]$. Formula (4) in Theorem 2.1 then leads to

$$\begin{aligned} \mathbb{E}[\varphi_{u,X}(t_0)] &= \Phi \left(\frac{-u(t_0)}{\sigma} \right) + \int_0^1 \frac{\tau(t)}{2\pi} \exp \left\{ -\frac{1}{2\sigma^2} \left[u(t)^2 + \frac{u'(t)^2}{\tau(t)^2} \right] \right\} dt \\ &\quad + \int_0^{t_0} \frac{u'(t)}{\sqrt{2\pi\sigma^2}} \exp \left\{ -\frac{u(t)^2}{2\sigma^2} \right\} \Phi \left(\frac{u'(t)}{\sigma\tau(t)} \right) dt \\ &\quad - \int_{t_0}^1 \frac{u'(t)}{\sqrt{2\pi\sigma^2}} \exp \left\{ -\frac{u(t)^2}{2\sigma^2} \right\} \Phi \left(\frac{-u'(t)}{\sigma\tau(t)} \right) dt. \end{aligned} \tag{5}$$

b) *Constant band:* If additionally $u(t) \equiv u$, one obtains the classic Kac-Rice formula

$$\mathbb{E}[\varphi_u(X)] = \Phi\left(\frac{-u}{\sigma}\right) + \frac{\|\tau\|_1}{2\pi} \exp\left\{-\frac{u^2}{2\sigma^2}\right\}, \quad (6)$$

where $\varphi_{u,X}(0) = \varphi_u(X)$, and where $\|f\|_1 = \int_0^1 |f(t)|dt$ denotes the L^1 -norm.

Corollary 2.3. (t-processes) *Let the conditions of Theorem 2.1 hold.*

a) *Variable band:* When $X(t)$ is a t -process with ν degrees of freedom, meaning $\mathcal{V} \sim \chi_\nu^2/\nu$, formula (4) in Theorem 2.1 leads to

$$\begin{aligned} \mathbb{E}[\varphi_{u,X}(t_0)] &= F_t(-u(t_0); \nu) \\ &+ \int_0^1 \frac{\tau(t)}{2\pi} \left(1 + \frac{u(t)^2}{\nu} + \frac{u'(t)^2}{\nu\tau(t)^2}\right)^{-\nu/2} dt \\ &+ \int_0^{t_0} \frac{u'(t)}{2\pi\tau(t)} \left(1 + \frac{u(t)^2}{\nu}\right)^{-\nu/2-1} \frac{\Gamma((\nu+1)/2)\sqrt{(\nu+1)\pi a(t)}}{\Gamma((\nu+2)/2)} F_t\left(\frac{u'(t)}{a(t)}; \nu+1\right) dt \\ &- \int_{t_0}^1 \frac{u'(t)}{2\pi\tau(t)} \left(1 + \frac{u(t)^2}{\nu}\right)^{-\nu/2-1} \frac{\Gamma((\nu+1)/2)\sqrt{(\nu+1)\pi a(t)}}{\Gamma((\nu+2)/2)} F_t\left(\frac{-u'(t)}{a(t)}; \nu+1\right) dt, \end{aligned} \quad (7)$$

where $a(t)^2 := \nu\tau(t)^2(1 + u(t)^2/\nu)/(\nu+1)$, Γ denotes the gamma function, and $F_t(\cdot; \nu)$ denotes the distribution function of a t -distribution with ν degrees of freedom.

b) *Constant band:* If additionally $u(t) \equiv u$, one obtains the t -version of the classic Kac-Rice formula

$$\mathbb{E}[\varphi_u(X)] = F_t(-u; \nu) + \frac{\|\tau\|_1}{2\pi} \left(1 + \frac{u^2}{\nu}\right)^{-\nu/2}, \quad (8)$$

where $\varphi_{u,X}(0) = \varphi_u(X)$, and where $\|f\|_1 = \int_0^1 |f(t)|dt$ denotes the L^1 -norm.

As commonly with the Gaussian distribution, the t -expression does not have a closed form in general. However, in terms of numerically finding $u(t)$, the above formulations present no complication. Equivalently for more general elliptical distributions, as long as one has a convenient form for M_ν , then the u threshold can be found numerically.

Our second major result concerns statistical estimation of the bands in practice. Here, we assume that $X_n \xrightarrow{D} X$ is only asymptotically Gaussian/elliptical in $C^1[0, 1]$. We also don't assume that we know the dispersion function and thus can't immediately normalize to assume $c(t, t) = 1$. Instead, we assume that we have a sequence of uniformly consistent estimates of the dispersion and partial derivatives.

Assumption 2.2. *Let $c(t, s) = \text{Cov}(Z(t), Z(s))$ be the dispersion function of X and assume the distribution of V is known. Assume that we have a sequence of estimators, $c_n(t, s)$, for $n = 1, 2, \dots$ satisfying,*

$$\begin{aligned} \sup_{0 \leq t \leq 1} |c_n(t, t) - c(t, t)| &= o_P(1) \\ \sup_{0 \leq t \leq 1} |\partial_1 c_n(t, t) - \partial_1 c(t, t)| &= o_P(1) \\ \sup_{0 \leq t \leq 1} |\partial_{12} c_n(t, t) - \partial_{12} c(t, t)| &= o_P(1) \end{aligned}$$

and that $c(t, t) > 0$ for all $0 \leq t \leq 1$.

Since $c(t, s)$ is symmetric, it doesn't matter which coordinate we take the partial derivative in. Practically, this would usually require that c_n converges to c in say C^2 . However, notice that $\partial_1 c(t, t) = \text{Cov}(Z(t), Z'(t))$ and that $\partial_{12} c(t, t) = \text{Var}(Z'(t)) = \tau(t)^2$. Therefore, in some settings, it is possible to estimate these covariance quantities more directly, as for instance in the arguably most relevant case, where $X(t)$ is formed by averaging a random sample of stochastic processes. Equation (19) gives an example of such a more direct estimation of τ which does not require the estimation of derivatives of the covariance function.

Note that we do not require estimation of the full dispersion, $c(t, s)$, only its diagonal and the derivative along the diagonal. By Slutsky's lemma it follows that

$$\tilde{X}_n(t) := c_n^{-1/2}(t, t) X_n(t) \xrightarrow{D} c^{-1/2}(t, t) X(t) = \tilde{X}(t) \quad \text{as } n \rightarrow \infty.$$

The process $\tilde{X}(t)$ has constant variance, so we need only plug in its corresponding $\tilde{\tau}(t)$ into Theorem 2.1 to find corresponding bands. By Assumption 2.2, we can construct a sequence of uniformly consistent estimators $\tilde{\tau}_n(t) \rightarrow \tilde{\tau}(t)$. While this presents a minor notational annoyance, practically, it simply amounts to constructing the band from standardized data or using $c_n(t, s) / \sqrt{c_n(t, t) c_n(s, s)}$ to find $u(t)$.

Our other key assumption is that the space of potential bands, $\mathcal{U} \subseteq C_{a.e.}^1[0, 1]$, is convex, compact, and contains the constant functions (up to an appropriate bound). Compactness is commonly needed in estimation theory to ensure that the estimators are well behaved. The convexity combines with the constant functions to eliminate some pathological limiting problems. In particular, it ensures that if $u \in \mathcal{U}$ isn't on the boundary, then $u(t) + c$ will also be in \mathcal{U} for c small. This helps ensure that no asymptotic band is "isolated", in the sense that one cannot construct a corresponding sequence of estimators for which it is the corresponding limit.

Theorem 2.2. *Let Assumptions 2.1 and 2.2 hold and fix $\alpha \in (0, 1)$ and $t_0 \in [0, 1]$. Define $\tilde{\tau}_n(t) = \partial_{12} \tilde{c}_n(t, s)$ where $\tilde{c}_n(t, s) := c_n(t, s) / \sqrt{c_n(t, t) c_n(s, s)}$ and define $\tilde{\tau}(t)$ analogously. Assume that $\{u \in \mathcal{U}\} \subseteq C_{a.e.}^1[0, 1]$, where \mathcal{U} is convex, compact, and contains the constant functions (up to an appropriate threshold to maintain compactness). For a general $\eta \in C[0, 1]$ with $\eta(t) \geq 0$, define the function*

$$\begin{aligned} f(u, \eta) := & P(X(t_0) \geq u(t_0)) + \int_0^1 \frac{\eta(t)}{2\pi} M_{\mathcal{V}} \left(-\frac{1}{2} \left[u(t)^2 + \frac{u'(t)^2}{\eta(t)^2} \right] \right) dt \\ & + \int_0^{t_0} \int_0^\infty \frac{u'(t)}{2\pi\eta(t)} M'_{\mathcal{V}} \left(-\frac{1}{2} \left[u(t)^2 + \frac{(y - u'(t))^2}{\eta(t)^2} \right] \right) dy dt \\ & - \int_{t_0}^1 \int_0^\infty \frac{u'(t)}{2\pi\eta(t)} M'_{\mathcal{V}} \left(-\frac{1}{2} \left[u(t)^2 + \frac{(y + u'(t))^2}{\eta(t)^2} \right] \right) dy dt, \end{aligned}$$

and the sets

$$S_n := f_{\tilde{\tau}_n}^{-1}(\alpha) = \{u \in \mathcal{U} : f(u, \tilde{\tau}_n) = \alpha\} \quad \text{and} \quad S := f_{\tilde{\tau}}^{-1}(\alpha) = \{u \in \mathcal{U} : f(u, \tilde{\tau}) = \alpha\}.$$

Then we have the following:

1. The sets $\{S_n\}$ and S are nonempty and closed with probability 1.
2. If $\{u_n : n = 1, \dots\}$ is any sequence with $u_n \in S_n$, then $f(u_n, \tilde{\tau}) \xrightarrow{P} \alpha$ as $n \rightarrow \infty$.
3. $S_n \rightarrow S$ in Hausdorff distance¹ with probability one.
4. Let $G : \mathcal{U} \rightarrow [0, \infty)$ be a continuous function used to partially order \mathcal{U} , in the sense that $u_1 \preceq u_2$ if $G(u_1) \leq G(u_2)$. Then $G(S_n) \xrightarrow{P} G(S)$ in Hausdorff distance. Furthermore, if there is a unique $u \in S$ such that $G(u) = \min_{u' \in S} G(u')$, then any sequence u_n that minimizes $G(u')$ for $u' \in S_n$ will converge in probability to u , and such a sequence exists with probability 1.

Theorem 2.2 provides several important asymptotic results that tie consistency of the band to consistency of the functional parameter estimates. The overall message is that if one finds a \hat{u} such that $f(\hat{u}, \tilde{\tau}_n) = \alpha$, then, with probability tending to one, \hat{u} will be close to a u that satisfies $f(u, \tilde{\tau}) = \alpha$, which would be the target, but $\tilde{\tau}$ must be estimated. However, there is a certain awkwardness in stating and establishing these results since α leads to entire set of bands one could use. The first result simply says, with probability one, there exists candidate bands using either the true, $\tilde{\tau}$, or estimate, $\tilde{\tau}_n$. The second result states that any sequence of bands selected using the estimate, $\tilde{\tau}_n$ will asymptotically give the correct coverage. The third result states that, as sets, the collection of bands using the estimate, $\tilde{\tau}_n$, converges to the set one would obtain using the true $\tilde{\tau}$. The fourth and last result states that if one uses some specific criteria to order the bands, then the ‘best’ band using the estimate will converge to the one using the true τ , so long as its unique.

The set \mathcal{U} is used to define the class of bands that one wants to consider. In the case of the classic Kac-Rice formula, one would take \mathcal{U} to be the set of constant functions (up to some bound to ensure compactness). However, our theory allows for more general compact sets. For example, if $\{e_i : i = 1, \dots, m\} \subset C^1[0, 1]$ is a finite collection of linearly independent functions, then we can take $\mathcal{U} = \text{span}\{e_1, \dots, e_m\} \cap B_c(\delta)$, where $B_c(\delta)$ is the closed ball of radius $\delta < \infty$. This gives a convenient form for producing adaptive bands since they will take the form $u(t) = \sum a_i e_i(t)$ and then one need only search over the coefficients. For example, the e_j could be taken to be b-splines or Fourier bases. Note, however, that \mathcal{U} can still be genuinely infinite dimensional, with $m = \infty$, as long as the coefficients are forced to zero in a systematic way, for example, if \mathcal{U} is taken to be an appropriate Sobolev or Reproducing Kernel Hilbert Space (RKHS) ball. In the next section, we present an algorithm for selecting an interpretable threshold function from $\mathcal{U} \subseteq C_{a.e.}^1[0, 1]$.

2.3 Selecting Fair and Interpretable Threshold Functions

As motivated in the introduction, we derive our $(1 - \alpha) \times 100\%$ simultaneous confidence bands by making use of threshold functions $u(t)$ that solve the equation $\mathbb{E}[\varphi_{u,X}(t_0)] = \alpha/2$ for given choices of the significance level $\alpha \in (0, 1)$ and $t_0 \in [0, 1]$. To do so, we use the results of Theorem 2.1 and Corollaries 2.2 and 2.3, which provide explicit expressions for $\mathbb{E}[\varphi_{u,X}(t_0)]$. However, when considering variable threshold functions $u(t)$, $\mathbb{E}[\varphi_{u,X}(t_0)] = \alpha/2$ is solved by an entire family, say \mathcal{U}_α , of possible threshold functions $\mathcal{U}_\alpha = \{u : \mathbb{E}[\varphi_{u,X}(t_0)] = \alpha/2\}$. We use this possibility to select interpretable threshold

¹The Hausdorff distance is given by $d(S_n, S) = \max\{\sup_{u_n \in S_n} \inf_{u \in S} \|u_n - u\|, \sup_{u \in S} \inf_{u_n \in S_n} \|u_n - u\|\}$.

functions that facilitate an equitable fair inference by adapting to the local dependence structure of X . The selection procedure is described in the following algorithm:

Algorithm 1. (Selecting the fair threshold function u_α^*)

0. Preliminaries. Choose any sequence of grid points $0 = a_{-p} < \dots < a_{-1} < a_0 < a_1 < \dots < a_q = 1$, with $p \geq 0$ and $q \geq 1$, that partitions the interval $[0, 1]$ into $p + q$ subintervals such that $t_0 = a_0$. Let $u_{pq}(t)$ denote the following piecewise linear function with $u_{pq}(t) = c_0$ for $t \in [a_0, a_1]$:

$$u_{pq}(t) := c_{-p}(t - a_{-(p-1)})_- + \dots + c_{-1}(t - a_0)_- + c_0 + c_1(t - a_1)_+ + \dots + c_{q-1}(t - a_{q-1})_+,$$

where $(x)_+ = \max\{x, 0\}$ and $(x)_- = \min\{x, 0\}$. In the following, we use $u_{pq}(t)$ and $u'_{pq}(t)$ for modelling $u(t)$ and $u'(t)$ in (4) of Theorem 2.1. By partitioning the integrals in (4) into the intervals $[a_j, a_{j+1}]$, $j = -p, \dots, q-1$, we determine the coefficients c_j , $j = -p, \dots, q-1$, of u_{pq} consecutively.

1. Determine the auxiliary threshold function u_{pqa} . Since $u_{pq}(t) = c_0$ and $u'_{pq}(t) = 0$ for $t \in [a_0, a_1]$, the integrals in (4), restricted to $[a_0, a_1]$, simplify considerably such that the parameter $c_0 = c_{0a}$ can be determined by solving

$$\int_{a_0}^{a_1} \frac{\tau(t)}{2\pi} M_{\mathcal{V}} \left(-\frac{c_{0a}^2}{2} \right) dt = \frac{\mathbf{a}}{2} (a_1 - a_0) \quad (9)$$

for $c_{0a} > 0$ and any given $0 < \mathbf{a} < \alpha$. The variable \mathbf{a} is an auxiliary variable which we use in Step 2 to find the fair threshold function u_α^* .

Given c_{0a} from (9), the parameters $c_j = c_{ja}$, with $j = 1, \dots, q-1$, can be determined by solving

$$\begin{aligned} & \int_{a_j}^{a_{j+1}} \frac{\tau(t)}{2\pi} M_{\mathcal{V}} \left(-\frac{1}{2} \left[u_{pqa}(t)^2 + \frac{u'_{pqa}(t)^2}{\tau(t)^2} \right] \right) dt \\ & - \int_{a_j}^{a_{j+1}} \int_0^\infty \frac{u'_{pqa}(t)}{2\pi\tau(t)} M'_{\mathcal{V}} \left(-\frac{1}{2} \left[u_{pqa}(t)^2 + \frac{(y + u'_{pqa}(t))^2}{\tau(t)^2} \right] \right) dy dt = \frac{\mathbf{a}}{2} (a_{j+1} - a_j) \end{aligned} \quad (10)$$

for $-\infty < c_{ja} < \infty$ in $u_{pqa}(t) = c_{0a} + \sum_{\ell=1}^j c_{j\ell a} (t - a_j)_+$ and in $u'_{pqa}(t) = \sum_{\ell=1}^j c_{j\ell a}$. Equation (10) must be solved *consecutively* for $j = 1, \dots, q-1$, such that each consecutive equation has only one unknown variable, namely, c_{ja} .

Analogously, the parameters $c_j = c_{ja}$, for $j = -1, \dots, -p$, can be determined by solving

$$\begin{aligned} & \int_{a_j}^{a_{j+1}} \frac{\tau(t)}{2\pi} M_{\mathcal{V}} \left(-\frac{1}{2} \left[u_{pqa}(t)^2 + \frac{u'_{pqa}(t)^2}{\tau(t)^2} \right] \right) dt \\ & + \int_{a_j}^{a_{j+1}} \int_0^\infty \frac{u'_{pqa}(t)}{2\pi\tau(t)} M'_{\mathcal{V}} \left(-\frac{1}{2} \left[u_{pqa}(t)^2 + \frac{(y - u'_{pqa}(t))^2}{\tau(t)^2} \right] \right) dy dt = \frac{\mathbf{a}}{2} (a_{j+1} - a_j) \end{aligned} \quad (11)$$

for $-\infty < c_{ja} < \infty$ in $u_{pqa}(t) = c_{0a} + \sum_{\ell=1}^j c_{j\ell a} (t - a_j)_+$ and in $u'_{pqa}(t) = \sum_{\ell=1}^j c_{j\ell a}$. Equation (11) must be solved *consecutively* for $j = -1, \dots, -p$, such that each consecutive equation has only one unknown variable, namely, c_{ja} .

2. Determine the fair threshold function u_α^* . Finally, we can determine the fair threshold function by solving $\mathbb{E}[\varphi_{u_{pq\mathbf{a}^*}, X}(t_0)] = \alpha/2$ for $0 < \mathbf{a}^* < \alpha$, that is, by solving

$$\begin{aligned}
P(X(t_0) \geq u_{pq\mathbf{a}^*}(t_0)) &+ \int_0^1 \frac{\tau(t)}{2\pi} M_{\mathcal{V}} \left(-\frac{1}{2} \left[u_{pq\mathbf{a}^*}(t)^2 + \frac{u'_{pq\mathbf{a}^*}(t)^2}{\tau(t)^2} \right] \right) dt \\
&+ \int_0^{t_0} \int_0^\infty \frac{u'_{pq\mathbf{a}^*}(t)}{2\pi\tau(t)} M'_{\mathcal{V}} \left(-\frac{1}{2} \left[u_{pq\mathbf{a}^*}(t)^2 + \frac{(y - u'_{pq\mathbf{a}^*}(t))^2}{\tau(t)^2} \right] \right) dy dt \\
&- \int_{t_0}^1 \int_0^\infty \frac{u'_{pq\mathbf{a}^*}(t)}{2\pi\tau(t)} M'_{\mathcal{V}} \left(-\frac{1}{2} \left[u_{pq\mathbf{a}^*}(t)^2 + \frac{(y + u'_{pq\mathbf{a}^*}(t))^2}{\tau(t)^2} \right] \right) dy dt = \frac{\alpha}{2}
\end{aligned} \tag{12}$$

for $0 < \mathbf{a}^* < \alpha$.

Results returned by this algorithm:

- (i) the fair threshold function $u_\alpha^* := \{u_{pq\mathbf{a}^*}(t), 0 \leq t \leq 1\}$,
- (ii) the pointwise exceedance probability $P(X(t_0) \geq u_\alpha^*(t_0))$, and
- (iii) the multiple testing component \mathbf{a}^* ,

where $P(X(t_0) \geq u_\alpha^*(t_0)) + \mathbf{a}^*/2 = \alpha/2$.

The shape of the fair threshold function, u_α^* , depends on the given elliptical distribution, through $M_{\mathcal{V}}$, the estimable roughness parameter function, τ , and on the following three parameters that have to be chosen by the user: the significance level α , the value of $t_0 \in [0, 1]$, and the subintervals $[a_j, a_{j+1}]$, $j = -p, \dots, q-1$, for partitioning the domain $[0, 1]$. The choice of the significance level is typically canonical and may be set, for instance, to $\alpha = 0.05$. The choice of t_0 is of minor importance and one may simply set, for instance, $t_0 = 0$ or $t_0 = 1$. However, if the user wants to do fair inference also with respect to a region of interest, $\text{ROI} = [0, t_0]$ or $\text{ROI} = [t_0, 1]$, the value of $t_0 \in [0, 1]$ must be chosen according to the application's region of interest (see Proposition 2.2 and the application in Section 4.1).

The choice and the number of the grid points, $0 = a_{-p} < \dots < a_q = 1$ with $p \geq 0$ and $q \geq 1$, determines how the fair threshold function, u_α^* , adapts to the dependence structure of the process X over the domain $[0, 1]$. For instance, if $p = 0$ and $q = 1$, there is no partitioning of the domain $[0, 1]$ since $[a_0, a_1] = [0, 1]$. In this case, Equations (10) and 11 become redundant and Algorithm (1) leads to a constant threshold function $u_\alpha^*(t) \equiv u_\alpha^*$ that equals the solution of the elliptical version of the Kac-Rice formula in Corollary 2.1. For $p+q > 1$, however, the fair threshold function, u_α^* , becomes adaptive to the dependence structure of X over each of the chosen subintervals $[a_j, a_{j+1}]$, $j = -p, \dots, q-1$. In principle, the users can choose whatever grid points, $0 = a_{-p} < \dots < a_q = 1$, they prefer. In our experience, a good practical choice is to take, for instance, equidistant grid points, $a_{j+1} - a_j = 1/(p+q)$, $j = -p, \dots, q-1$, with three to twelve, i.e. $3 \leq p+q \leq 12$, subintervals in $[0, 1]$.

Besides the fair threshold function, u_α^* , Algorithm 1 returns also the value of $\mathbf{a}^*/2$ which equals, by construction, the mean number of down-crossing events over $[0, t_0]$ plus the mean

number of up-crossing events over $[t_0, 1]$. That is, under the assumptions of Theorem 2.1 we have that

$$\mathbb{E} [N_{u_\alpha^*, X}^-([0, t_0])] + \mathbb{E} [N_{u_\alpha^*, X}([t_0, 1])] = \frac{\mathbf{a}^*}{2}(t_0 - 0) + \frac{\mathbf{a}^*}{2}(1 - t_0) = \frac{\mathbf{a}^*}{2}.$$

From (12) and the generalized expected Euler characteristic inequality (2), we, therefore, have under the conditions of Theorem 2.1 that

$$P(\exists t \in [0, 1] : X(t) \geq u_\alpha^*(t)) \leq P(X(t_0) \geq u_\alpha^*(t_0)) + \frac{\mathbf{a}^*}{2}(t_0 - 0) + \frac{\mathbf{a}^*}{2}(1 - t_0) = \frac{\alpha}{2}. \quad (13)$$

That is, the significance level, $\alpha/2$, is decomposed into the pointwise testing component, $P(X(t_0) \geq u_\alpha^*(t_0))$, and the multiple testing component, $\mathbf{a}^*/2$. These insights, leads to the following proposition.

Proposition 2.1. (Fair and interpretable threshold function u_α^*) *Let the conditions of Theorem 2.1 hold. Then we have for any $t_0 \in [0, 1]$ that*

$$P(\exists t \in [0, t_0] : X(t) \geq u_\alpha^*(t)) \leq P(X(t_0) \geq u_\alpha^*(t_0)) + \frac{\mathbf{a}^*}{2}(t_0 - 0)$$

and $P(\exists t \in [t_0, 1] : X(t) \geq u_\alpha^*(t)) \leq P(X(t_0) \geq u_\alpha^*(t_0)) + \frac{\mathbf{a}^*}{2}(1 - t_0).$

That is, the multiple testing component, $\mathbf{a}^*/2$, is allocated equitably according to the interval lengths, $(t_0 - 0)$ and $(1 - t_0)$, of the two regions of interest $\text{ROI} = [0, t_0]$ and $\text{ROI} = [t_0, 1]$, since Algorithm 1 distributes the multiple testing component, $\mathbf{a}^*/2$, uniform over $[0, 1]$. In the next section, we present Proposition 2.2 which generalizes Proposition 2.1 for the case of simultaneous confidence bands.

2.4 Constructing Fair and Interpretable Confidence Bands

In this section we, first, consider two examples for constructing simultaneous confidence bands using the above described results and methods (Section 2.4.1). Example 1 is a generic example which applies to any asymptotically Gaussian functional parameter estimator $\hat{\theta}$. Example 2 considers the practically relevant special case of t-distributed estimators, $\hat{\theta}$, of the mean function θ . Second, we introduce the interpretable formal fairness property of our simultaneous confidence bands (Section 2.4.2).

2.4.1 Examples

Example 1. (Asymptotically Gaussian estimators) Let $\{\hat{\theta}(t), 0 \leq t \leq 1\}$ be an asymptotically Gaussian (parametric or nonparametric) estimator of a functional parameter $\{\theta(t), 0 \leq t \leq 1\}$ such that

$$\sqrt{r_n} \left(\hat{\theta} - \text{Bias}(\hat{\theta}) - \theta \right) \xrightarrow{D} \mathcal{N}(0, C_\theta) \quad \text{as } n \rightarrow \infty, \quad (14)$$

where r_n denotes the parametric or nonparametric convergence rate of $\hat{\theta}$, $\text{Bias}(\hat{\theta})$ denotes the known (or consistently estimable) possibly non-zero bias operator, and C_θ denotes the known (or consistently estimable) covariance operator. This situation is fairly general and arises, for instance, when estimating the mean or covariance function from sparse or dense functional data (Li and Hsing, 2010; Degras, 2011; Zhang and Wang, 2016), in eigenfunction/value estimation (Kokoszka and Reimherr, 2013; Kraus, 2019), in function-on-scalar regressions (Chen et al., 2016), in concurrent function-on-function regressions (Manrique et al., 2018), etc. Generally, as discussed in Choi and Reimherr (2018), the asymptotic normality in (14) requires *tightness* of the estimate to ensure that the convergence in distribution occurs in the strong topology. Typically, this rules out estimates from ill-posed inverse problems such as, for instance, the classic scalar-on-function regression estimators (cf. Cardot et al., 2007).

From (14) we have that

$$X_n(t) = \frac{\left(\hat{\theta}(t) - \text{Bias}(\hat{\theta}(t)) - \theta(t)\right)}{\sqrt{C_\theta(t, t)/r_n}} \xrightarrow{D} \mathcal{N}(0, 1) \quad \text{for all } t \in [0, 1],$$

such that $X_n \xrightarrow{D} X$, where $X(t) \stackrel{D}{=} VZ(t)$ with $V \equiv \sigma = 1$ for all $t \in [0, 1]$. That is, the covariance function of X equals its dispersion function $\text{Cov}(X(t), X(s)) = c(t, s)$ with $c(t, t) = 1$ for all $t, s \in [0, 1]$ and the only missing parameter required to compute the formula in Corollary 2.2 is the roughness parameter function $\tau(t) = (\partial_{12}c(t, t))^{1/2}$ which quantifies the multiple testing problem locally for each $t \in [0, 1]$. Since $c(t, s) = \text{Cov}(X(t), X(s))$ and $\text{Cov}(X(t), X(s)) = \tilde{C}_\theta(t, s)$ with $\tilde{C}_\theta(t, s) = C_\theta(t, s)/\sqrt{C_\theta(t, t)C_\theta(s, s)}$ it follows that $\tau(t) = (\partial_{12}\tilde{C}_\theta(t, t))^{1/2}$ which is directly computable from the covariance function C_θ .

Plugging in the parameters $\sigma = 1$ and $\tau(t) = (\partial_{12}\tilde{C}_\theta(t, t))^{-1/2}$ into the Gaussian formula of Corollary 2.2 allows us to compute the fair threshold function, u_α^* , as described in Algorithm 1 for given choices of $t_0 \in [0, 1]$, $\alpha \in (0, 1)$, and grid points a_j , $j = -q, \dots, q$. This then leads to the fair simultaneous confidence band

$$\text{FF}_z(t) = [\hat{\theta}_l^*(t), \hat{\theta}_u^*(t)] := \hat{\theta}(t) \pm u_\alpha^*(t)\sqrt{C_\theta(t, t)/r_n} \quad \text{for all } t \in [0, 1], \quad (15)$$

where we denote this simultaneous confidence bands as Fast and Fair (FF) simultaneous confidence bands as it is considerably faster to compute than the alternative simulation based procedures.

Rearranging (13) by using the symmetry of the distribution of X and by applying the generalized expected Euler characteristic inequality (2) yields that, under the conditions of Theorem 2.1,

$$P\left(\exists t \in [0, 1] : \theta(t) \notin [\hat{\theta}_l^*(t), \hat{\theta}_u^*(t)]\right) \leq P\left(\theta(t_0) \notin [\hat{\theta}_l^*(t_0), \hat{\theta}_u^*(t_0)]\right) + \mathbf{a}^* = \alpha \quad (16)$$

or equivalently for the converse probability that

$$P\left(\theta(t) \in [\hat{\theta}_l^*(t), \hat{\theta}_u^*(t)], \forall t \in [0, 1]\right) \geq 1 - P\left(\theta(t_0) \notin [\hat{\theta}_l^*(t_0), \hat{\theta}_u^*(t_0)]\right) - \mathbf{a}^* = 1 - \alpha. \quad (17)$$

That is, under the conditions of Theorem 2.1, the band $[\hat{\theta}_l^*, \hat{\theta}_u^*]$ is a valid $(1 - \alpha) \times 100\%$ simultaneous (two-sided) confidence band with coverage probability of at least $1 - \alpha$. One-sided confidence bands, $[\hat{\theta}_l^*, \infty]$ or $[-\infty, \hat{\theta}_u^*]$, can be constructed from the one-sided version of u_α^* which can be computed using Algorithm 1, but with substituting $\mathbf{a}/2$ and $\alpha/2$ by \mathbf{a} and α .

Usually, we do not know the covariance operator C_θ and have to plug in consistent estimators \hat{C}_θ and $\hat{\tau}$. Then, under the assumptions of Theorem 2.2, the simultaneous confidence band $[\hat{\theta}_l^*, \hat{\theta}_u^*]$ is an asymptotically valid $(1 - \alpha) \times 100\%$ simultaneous confidence band.

The following example demonstrates the practically relevant use of our fair simultaneous confidence band for t-distributed estimators, $\hat{\theta}$, of the mean function θ based on estimated covariances.

Example 2. (t-distributed estimators of the mean function) Let us consider an iid sample $\{S_i\}_{i=1}^n$ from a Gaussian process $\mathcal{N}(\theta, C_\theta)$ with unknown mean function $\theta(t) = \mathbb{E}[S_i(t)]$ and unknown covariance function $C_\theta(t, s) = \text{Cov}(S_i(t), S_i(s))$. We estimate the mean and covariance functions using the standard sample estimators $\hat{\theta}(t) = n^{-1} \sum_{i=1}^n S_i(t)$ and $\hat{C}_\theta(t) = (n - 1)^{-1} \sum_{i=1}^n (S_i(t) - \hat{\theta}(t))(S_i(s) - \hat{\theta}(s))$, for $t, s \in [0, 1]$. This setup yields that

$$X_n(t) = \frac{\hat{\theta}(t) - \theta(t)}{\sqrt{\hat{C}_\theta(t, t)/n}} \sim t_\nu \quad \text{with} \quad \nu = n - 1 \quad \text{for all} \quad t \in [0, 1],$$

such that $X_n(t) \stackrel{D}{=} V_n Z(t)$ with $V_n = \sqrt{\nu/\chi_\nu^2}$ and $Z(t) \sim \mathcal{N}(0, 1)$ for all $t \in [0, 1]$, where $\text{Cov}(X_n(t), X_n(s)) = (\nu/(\nu - 2))c(t, s)$ for all $\nu > 2$ with $c(t, t) = 1$ for all $t, s \in [0, 1]$. Since $\text{Cov}(X_n(t), X_n(s)) = C_\theta(t, s)(C_\theta(t, t)C_\theta(s, s))^{-1/2} \rightarrow c(t, s)$ as $n \rightarrow \infty$ for all $t, s \in [0, 1]$, the roughness parameter function $\tau(t)$ can be estimated consistently by

$$\hat{\tau}_1(t) = (\partial_{12}\hat{c}(t, t))^{1/2} \quad \text{with} \quad \hat{c}(t, s) = \hat{C}_\theta(t, s)(\hat{C}_\theta(t, t)\hat{C}_\theta(s, s))^{-1/2} \quad \text{for} \quad t, s \in [0, 1]. \quad (18)$$

Simple algebraic rearrangements lead to the following equivalent version for $\hat{\tau}_1$:

$$\hat{\tau}_2(t) = \left(\widehat{\text{Var}}(\tilde{S}'_1(t), \dots, \tilde{S}'_n(t)) \right)^{1/2} \quad \text{for} \quad t \in [0, 1], \quad (19)$$

where $\widehat{\text{Var}}(\tilde{S}'_1(t), \dots, \tilde{S}'_n(t)) = (n - 1)^{-1} \sum_{i=1}^n (\tilde{S}'_i(t) - n^{-1} \sum_{i=1}^n \tilde{S}'_i(t))^2$ denotes the empirical variance of the standardized and differentiated sample functions $\tilde{S}_i(t) = (S_i(t) - \hat{\theta}(t))/(\hat{C}_\theta(t, t))^{1/2}$.

Plugging in the degrees of freedom $\nu = n - 1$ and an estimate, $\hat{\tau}_1(t)$ or $\hat{\tau}_2(t)$, of the roughness parameter function $\tau(t)$ into the t-distribution based formula of Corollary 2.3 allows us to compute the fair threshold function, u_α^* , as described in Algorithm 1 for given choices of $t_0 \in [0, 1]$, $\alpha \in (0, 1)$, and grid points a_j , $j = -q, \dots, q$. This then leads to the fair simultaneous confidence band

$$\text{FF}_t(t) = [\hat{\theta}_l^*(t), \hat{\theta}_u^*(t)] := \hat{\theta}(t) \pm \hat{u}_\alpha^*(t) \sqrt{\hat{C}_\theta(t, t)/n}, \quad (20)$$

where the hat in $\hat{u}_\alpha^*(t)$ marks that the threshold function is based on an estimate, $\hat{\tau}_1$ or $\hat{\tau}_2$, of the roughness parameter function τ .

Remark on estimating roughness. *In the case where the random sample functions $\{S_i\}_{i=1}^n$ are fully observed, the estimators $\hat{\tau}_1$ and $\hat{\tau}_2$ in (18) and (19) are equivalent. However, if the sample functions are only sparsely observed, as in Yao et al. (2005), $\hat{\tau}_2$ becomes infeasible since S'_i cannot be computed from sparse functional data. In this case, an estimator similar to $\hat{\tau}_1$ can be used, where the sample estimator \hat{C}_θ has to be substituted by a nonparametric covariance estimator.*

2.4.2 Fair and Interpretable Confidence Bands

The following proposition formally describes the fairness property of our fair simultaneous confidence bands FF_z and FF_t in (15) and (20).

Proposition 2.2. (Fair and interpretable confidence bands) *Let the conditions of Theorem 2.1 hold and let u_α^* be selected by Algorithm 1 with $p + q > 1$. Let $[\hat{\theta}_l^*, \hat{\theta}_u^*]$ denote the simultaneous confidence band FF_z in (15) or FF_t in (20), but with known roughness parameter τ . Then we have for any region of interest $\text{ROI} = [0, t_0]$ or $\text{ROI} = [t_0, 1]$, with $t_0 \in [0, 1]$, that*

$$\begin{aligned} P\left(\exists t \in [0, t_0] : \theta(t) \notin [\hat{\theta}_l^*(t), \hat{\theta}_u^*(t)]\right) &\leq p_{t_0} + \mathbf{a}^*(t_0 - 0) \leq \alpha \\ P\left(\exists t \in [t_0, 1] : \theta(t) \notin [\hat{\theta}_l^*(t), \hat{\theta}_u^*(t)]\right) &\leq p_{t_0} + \mathbf{a}^*(1 - t_0) \leq \alpha \end{aligned} \quad (21)$$

or equivalently for the converse probabilities that

$$\begin{aligned} P\left(\theta(t) \in [\hat{\theta}_l^*(t), \hat{\theta}_u^*(t)], \forall t \in [0, t_0]\right) &\geq 1 - (p_{t_0} + \mathbf{a}^*(t_0 - 0)) \geq 1 - \alpha \\ P\left(\theta(t) \in [\hat{\theta}_l^*(t), \hat{\theta}_u^*(t)], \forall t \in [t_0, 1]\right) &\geq 1 - (p_{t_0} + \mathbf{a}^*(1 - t_0)) \geq 1 - \alpha \end{aligned} \quad (22)$$

with $p_{t_0} := P(\theta(t_0) \notin [\hat{\theta}_l^*(t_0), \hat{\theta}_u^*(t_0)])$, where $p_{t_0} = \alpha - \mathbf{a}^*$.

If the bands are based on consistent estimators \hat{C}_θ and $\hat{\tau}$, Equations (21) and (22) hold asymptotically, for $n \rightarrow \infty$, under the assumptions of Theorem 2.2.

Equation (21) decomposes the overall type-I error budget, α , into the pointwise testing component, p_{t_0} , and the multiple testing component, \mathbf{a}^* , where p_{t_0} and \mathbf{a}^* are both returned by Algorithm 1. Usually, $p_{t_0} \approx 0$ and $\mathbf{a}^* \approx \alpha$ as simultaneous confidence bands are typically wider than ordinary pointwise confidence intervals.

Proposition 2.2 is quite substantial as it makes our fair band, $[\hat{\theta}_l^*, \hat{\theta}_u^*]$, interpretable over any region of interest $\text{ROI} = [0, t_0]$ or $\text{ROI} = [t_0, 1]$ with $t_0 \in [0, 1]$. Indeed, Equation (22) implies that the $(1 - \alpha) \times 100\%$ simultaneous confidence band $[\hat{\theta}_l^*, \hat{\theta}_u^*]$ over $[0, 1]$ is also a valid $(1 - p_{t_0} - \mathbf{a}^*(t_0 - 0)) \times 100\%$ simultaneous confidence band over $[0, t_0]$ and as a valid $(1 - p_{t_0} - \mathbf{a}^*(1 - t_0)) \times 100\%$ simultaneous confidence band over $[t_0, 1]$. Such ROI analyses are very common, for instance, in the applied neuroimaging and biomechanics literature (Poldrack, 2007; Wager et al., 2008; Pataky et al., 2016; Wen et al., 2018), but usually require a complete recomputation of the bands separately for each ROI. By contrast, our band allows for ROI analyses without recomputing separate ROI specific bands. This use of our fair band is also demonstrated in our application in Section 4.1.

Note that this result also holds for non-stationary processes where our fair confidence bands have interpretable adaptive band widths. Consider, for instance, the case of $t_0 = 1/2$ for a non-stationary process with high positive within curve correlations over $[0, 1/2]$, but weak correlations over $[1/2, 1]$. Then our fair band, $[\hat{\theta}_l^*, \hat{\theta}_u^*]$, will be sufficiently narrow over $[0, 1/2]$ and sufficiently wide over $[1/2, 1]$ such that the fair shares, $\alpha^*(1/2) = \alpha^*(1/2)$, of the multiple testing component, α^* , are allocated to each of the two subintervals $[0, 1/2]$ and $[1/2, 1]$. This fair width of our simultaneous confidence band provides a means for sensible visualizations of different local multiple testing problems across the domain $[0, 1]$; see the right column in Figure 1.

None of the existing simultaneous confidence bands has this interpretable fairness feature. In fact, most of the existing simultaneous confidence bands are based on constant threshold functions $u(t) \equiv u$ and, therefore, will be generally ‘too wide’ at areas with high positive within curve correlations and ‘too narrow’ at areas with weak correlations. This can be very problematic in practice where simultaneous confidence bands are often used to detect local differences in functional parameters (Vanrenterghem et al., 2012; Pini et al., 2018).

Computing p-values We can also use our algorithm to generate simultaneous p-value functions for testing the null hypothesis $H_0: \theta = \theta_0$ vs. $H_1: \theta \neq \theta_0$, by finding the smallest α -level such that the confidence band $\{[\hat{\theta}_l^*(t), \hat{\theta}_u^*(t)], 0 \leq t \leq 1\}$ covers the hypothesized parameter θ_0 . That is, to compute a fair simultaneous p-value function we need to select the smallest α -level in Step 2 of Algorithm 1 which calibrates the width of the band $[\hat{\theta}_l^*, \hat{\theta}_u^*]$ pointwise for each $t \in [0, 1]$ such that $\hat{\theta}_l^*(t) = \theta_0(t)$ if $\theta_0(t) \leq \hat{\theta}(t)$ and $\hat{\theta}_u^*(t) = \theta_0(t)$ if $\theta_0(t) > \hat{\theta}(t)$. These pointwise α -levels define then the fair simultaneous p-value function.

3 Simulations

This section contains our simulation study to assess and illustrate the proposed fair simultaneous confidence bands. Section 3.1 considers the case of fully observed random functions and Section 3.2 considers the case of fragmentary functions for which it is impossible to estimate the total covariance operator.

We focus on the practically relevant case of *unknown* covariances, C_θ . All bands are computed based on the standard sample estimators \hat{C}_θ and $\hat{\theta}$ as introduced in Example 2.

3.1 Fully Observed Functions

We generate samples of random functions $\{S_i\}_{i=1}^n \stackrel{\text{iid}}{\sim} \mathcal{N}(\theta, C_\theta)$ with mean function $\theta(t)$, $t \in [0, 1]$, and covariance function $C_\theta(t, s)$, $t, s \in [0, 1]$. The sample functions, S_i , are evaluated at 101 equidistant grid points $t = j/100$, $j = 0, \dots, 100$, to emulate continuous functional data. We consider the following mean function scenarios based on shifting and scaling the polynomial mean function $\theta_0(t) = 10t^3 - 15t^4 + 6t^6$ by some $\Delta \geq 0$:

Mean1 $\theta(t) = \theta_0(t) + \Delta$ (‘shift’)

Mean2 $\theta(t) = \theta_0(t)(1 + \Delta)$ (‘scale’)

Mean3 $\theta(t) = \theta_0(t) + \Delta \mathbb{1}\{(0 \leq t \leq 1/8)\}$ ('local')

The three mean function scenarios, Mean1-3, are shown in the upper row of Figure 2.

For the covariance operator, we take the Matérn covariance $C_\theta(t, s) = 0.25^2(2^{1-\nu}/\Gamma(\nu))(\sqrt{2\nu}|t-s|)^\nu K_\nu(\sqrt{2\nu}|t-s|)$, where Γ is the gamma function, K_ν is the modified Bessel function of the second kind, and where $\nu \geq 0$ controls the roughness of the sample paths $\{S_i(t), 0 \leq t \leq 1\}$. We consider three different covariance scenarios:

Cov1 Stationary Matérn covariance C_θ with $\nu = 3/2$ ('smooth').

Cov2 Stationary Matérn covariance C_θ with $\nu = 1/2$ ('rough').

Cov3 Non-stationary modified Matérn-type covariance $C_\theta(t, s) = 0.25^2(2^{1-\nu_{ts}}/\Gamma(\nu_{ts}))(\sqrt{2\nu_{ts}}|t-s|)^{\nu_{ts}} K_{\nu_{ts}}(\sqrt{2\nu_{ts}}|t-s|)$, where $\nu_{ts} = 2 + \sqrt{\max(t, s)}(1/4 - 2)$ ('smooth to rough').

Cov1 results in smooth continuously differentiable sample functions as typical, for instance, for functional chemometric/spectrometric data (see [Ferraty and Vieu, 2006](#), Ch. 2). Cov2 leads to rough non-differentiable sample functions as considered, for instance, in the literature on functional impact points ([Lindquist and McKeague, 2009](#); [McKeague and Sen, 2010](#); [Kneip et al., 2016](#)) and represents a violation of our smoothness assumption (Assumption 2.1). The non-stationary covariance Cov3 leads to sample functions with inhomogeneous roughness ('smooth to rough'). Exemplary sample paths, S_i , for each of the covariance scenario, Cov1-3, are shown in the upper row of Figure 1. Our simulation setup is similar to that of [Choi and Reimherr \(2018\)](#) except that we consider a more complex and more challenging non-stationary covariance Cov3. The polynomial mean function, θ_0 , was also considered by [Hart and Wehrly \(1986\)](#) and [Degras \(2011\)](#).

Fair Confidence Bands and Benchmarks

The following list describes the specifications of our fair confidence bands and introduces the considered benchmark bands.

FF We denote our simultaneous confidence bands as Fast and Fair (FF) simultaneous confidence bands

$$\text{FF}(t) = [\hat{\theta}_l^*(t), \hat{\theta}_u^*(t)] = \hat{\theta}(t) \pm \hat{u}_\alpha^*(t)(\hat{C}_\theta(t, t)/n)^{1/2}, \quad t \in [0, 1],$$

as they are considerably faster to compute than the alternative simulation based procedures. For estimating the roughness parameter function, τ , we use $\hat{\tau}_2$ in (19). The threshold function, $\hat{u}_\alpha^*(t)$, is computed as described in Algorithm 1. To assess the robustness of Algorithm 1 we consider different values of t_0 and different sets of $p+q$ equidistant grid points $a_j = j/(p+q)$ with $j = 0, 1, \dots, p+q$. When \hat{u}_α^* is based on the Gaussian formula (5) in Corollary 2.2, we write FF_z and when \hat{u}_α^* is based on the t-distribution formula (7) in Corollary 2.3, we write FF_t .

\hat{B}_S The simulation based bootstrap band uses a constant threshold $u_\alpha(t) \equiv u_\alpha$, where u_α is found via the parametric bootstrap based on 10,000 bootstrap replications ([Degras, 2011](#)).

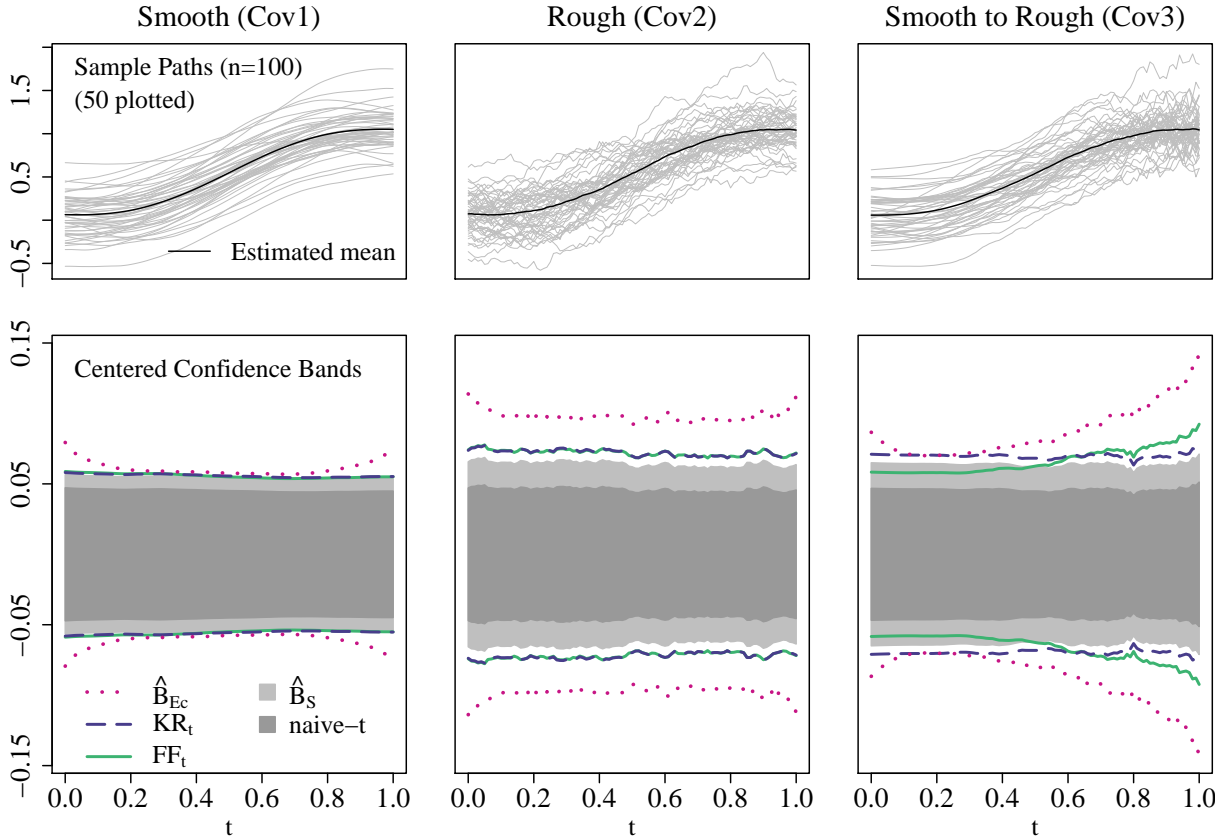


Figure 1: UPPER ROW: Exemplary sample paths and mean estimates, $\hat{\theta}$. LOWER ROW: Exemplary centered 95% confidence bands – centering by $\hat{\theta}$ is applied to optimize the visualization of the bands. The shown FF_t band has parameters $p + q = 9$ and $t_0 = 0$; other parameters lead to similar band shapes.

\hat{B}_{E_c} A modification of Scheffé’s method to transform ellipsoid confidence regions into confidence bands proposed by [Choi and Reimherr \(2018\)](#). The \hat{B}_{E_c} band is chosen adaptively to minimize the average squared width of the band.

KR The Kac-Rice band uses a constant threshold $u_\alpha(t) \equiv u_\alpha$. If u_α is found by solving (6), we write KR_z and if u_α is found by solving (8), we write KR_t .

IWT The Interval-Wise Testing procedure proposed by [Pini and Vantini \(2017b\)](#) and further extended in [Abramowicz et al. \(2018\)](#). This method uses permutation techniques to compute a simultaneous p-value function, $\{p_{IWT}(t), 0 \leq t \leq 1\}$.

naive-t The naive pointwise confidence interval based on the t-distribution without adjusting for multiple testing. Only used as a visual reference.

All methods except the IWT procedure, are implemented in our R-package `ffscb` ([Liebl and Reimherr, 2019a](#)); the IWT procedure is implemented in the R-package `fdatest` ([Pini and Vantini, 2017a](#)).

In the main paper we report the results for the t-distribution based bands FF_t and KR_t which take into account the estimation errors in \hat{C}_θ . The results of the Gaussian versions,

FF_z and KR_z , are summarized in the tables of Appendix B of the supplementary paper [Liebl and Reimherr \(2019b\)](#). In the case of small samples, the Gaussian FF_z and KR_z bands are typically too narrow and have a too low coverages as they ignore the estimation errors in \hat{C}_θ . However, for large samples, the Gaussian FF_z and KR_z bands show a similar and partially even better performances than the t-distribution based bands.

Band shapes The lower row of Figure 1 shows exemplary results of all simultaneous confidence bands for each of the covariance scenarios Cov1-3. In the stationary covariance scenarios, Cov1 and Cov2, the FF_t band and the KR_t band are basically equivalent. The adaptive behavior of the FF_t band can be seen in the non-stationary covariance scenario Cov3, where the FF_t band is narrow over the area with high positive within curve correlations, but wide over the area with low correlations. [Choi and Reimherr \(2018\)](#) report that their band, \hat{B}_{E_c} , works well for smooth processes, but becomes very wide in the case of rough processes – this behavior is well reflected in Figure 1. The bootstrap band, \hat{B}_S , is the tightest simultaneous confidence band; however, as shown below, this band is actually too tight and cannot keep the significance level α .

3.1.1 Hypothesis Testing

To evaluate our fair confidence bands and to compare them with the above introduced alternative approaches, we use the duality of confidence bands with hypothesis tests. We test the hypothesis

$$H_0: \theta(t) = \theta_0(t) \quad \forall t \in [0, 1] \quad \text{vs.} \quad H_1: \exists t \in [0, 1] \text{ s.t. } \theta(t) \neq \theta_0(t)$$

and reject H_0 if θ_0 is not covered by a band for at least one of the evaluation points over the domain $[0, 1]$. Analogously, for the IWT procedure we reject H_0 if $p_{\text{IWT}}(t) < \alpha$ for at least one of the evaluation points $t = j/100$, $j = 0, \dots, 100$. As the significance level we choose $\alpha = 0.05$ which means that we consider 95% simultaneous confidence bands.

Verifying Type-I Error

To verify the type-I error rates, we draw 50,000 Monte Carlo samples $\{\mathcal{S}_i\}_{i=1}^n \stackrel{\text{iid}}{\sim} \mathcal{N}(\theta_0, C_\theta)$ for each covariance function scenario Cov1-3. We examine a quite challenging small sample size of $n = 15$ and a large sample size $n = 100$. Since the IWT procedure is computationally very expensive we had to reduce the number of Monte Carlo replications for this method to 5,000.² Table 1 contains the type-I error rates and we can summarize the results as following:

- (a) The FF_t , KR_t , and \hat{B}_{E_c} bands and the IWT procedure are able to keep nominal α -level in all scenarios and sample sizes.
- (b) The bootstrap band, \hat{B}_S , is too narrow which results in problematic over-rejections of the null hypothesis in all scenarios and sample sizes. The performance is particularly weak for rough processes (Cov2-3) and small samples.

²[Abramowicz et al. \(2018\)](#) use only 1,000 Monte Carlo replications to verify the type-I error rates of their IWT procedure.

Table 1: Type-I error rates.

Band	$n = 15$			$n = 100$		
	Cov1	Cov2	Cov3	Cov1	Cov2	Cov3
$\text{FF}_t (p + q = 3, t_0 = 0)$	0.050	0.037	0.044	0.050	0.030	0.040
$\text{FF}_t (p + q = 3, t_0 = 1)$	0.051	0.037	0.045	0.048	0.031	0.041
$\text{FF}_t (p + q = 9, t_0 = 0)$	0.048	0.037	0.044	0.044	0.031	0.039
$\text{FF}_t (p + q = 9, t_0 = 1)$	0.049	0.034	0.045	0.048	0.031	0.040
KR_t	0.052	0.040	0.045	0.050	0.030	0.039
\hat{B}_{E_c}	0.051	0.037	0.035	0.028	0.001	0.006
IWT	0.036	0.028	0.027	0.036	0.029	0.028
\hat{B}_S	0.090	0.124	0.122	0.057	0.056	0.060

Nominal type-I error rate: $\alpha = 0.05$

(c) Among the methods that are able to keep the α -level, the type-I error rates of the FF_t and KR_t bands are closest to $\alpha = 0.05$. Both methods become moderately conservative for rough processes (Cov2-3).

(d) The IWT procedure and the \hat{B}_{E_c} band are both quite conservative. The \hat{B}_{E_c} band becomes particularly conservative for the rough processes (Cov2-3).

The reason for the weak performance of the bootstrap band, \hat{B}_S , is the sensibility of the parametric bootstrap against the estimation errors in \hat{C}_θ . The bootstrap band performs well under the unrealistic scenario of a known covariance, C_θ (see [Choi and Reimherr, 2018](#)).

Table 2: Average confidence band widths*

Band	$n = 15$			$n = 100$		
	Cov1	Cov2	Cov3	Cov1	Cov2	Cov3
$\text{FF}_t (p + q = 3, t_0 = 0)$	0.335	0.431	0.397	0.120	0.148	0.138
$\text{FF}_t (p + q = 3, t_0 = 1)$	0.336	0.431	0.406	0.120	0.148	0.140
$\text{FF}_t (p + q = 9, t_0 = 0)$	0.335	0.430	0.398	0.120	0.148	0.138
$\text{FF}_t (p + q = 9, t_0 = 1)$	0.335	0.430	0.402	0.120	0.148	0.140
KR_t	0.336	0.432	0.416	0.120	0.148	0.144
\hat{B}_{E_c}	0.324	0.413	0.396	0.131	0.205	0.183
\hat{B}_S	0.297	0.341	0.340	0.117	0.136	0.135

*Cannot be computed for the IWT procedure.

Table 2 summarizes the average widths of the bands where the widths are averaged over the domain $[0, 1]$ and over the Monte Carlo samples. The results confirm the visual impression from Figure 1. The average widths of the FF_t and KR_t bands are slightly (Cov1) and moderately (Cov2-3) larger than the average widths of the too narrow bootstrap band,

\hat{B}_S . The \hat{B}_{Ec} band is comparatively narrow for small samples, but becomes very wide for the rough processes (Cov2-3) and large samples.

Comparing Power

For comparing the power of the hypothesis tests, we generate data using the mean function scenarios Mean1-3 with increasingly large perturbations $\Delta > 0$. The hypothetical mean function, θ_0 , and the different true mean functions, θ , are shown in the upper row of Figure 2. For the small sample scenario, $n = 15$, we consider the perturbations $\Delta \in \{0.05, 0.15, 0.25, 0.35, 0.45\}$ and for the large sample scenario, $n = 100$, we consider the smaller perturbations $\Delta \in \{0.02, 0.04, 0.06, 0.08, 0.1\}$. Each of these mean function perturbations is considered for each of the covariance scenarios Cov1-3. We reduce the number of Monte Carlo repetitions to 10,000, except for the IWT procedure where we keep the 5,000 repetitions.

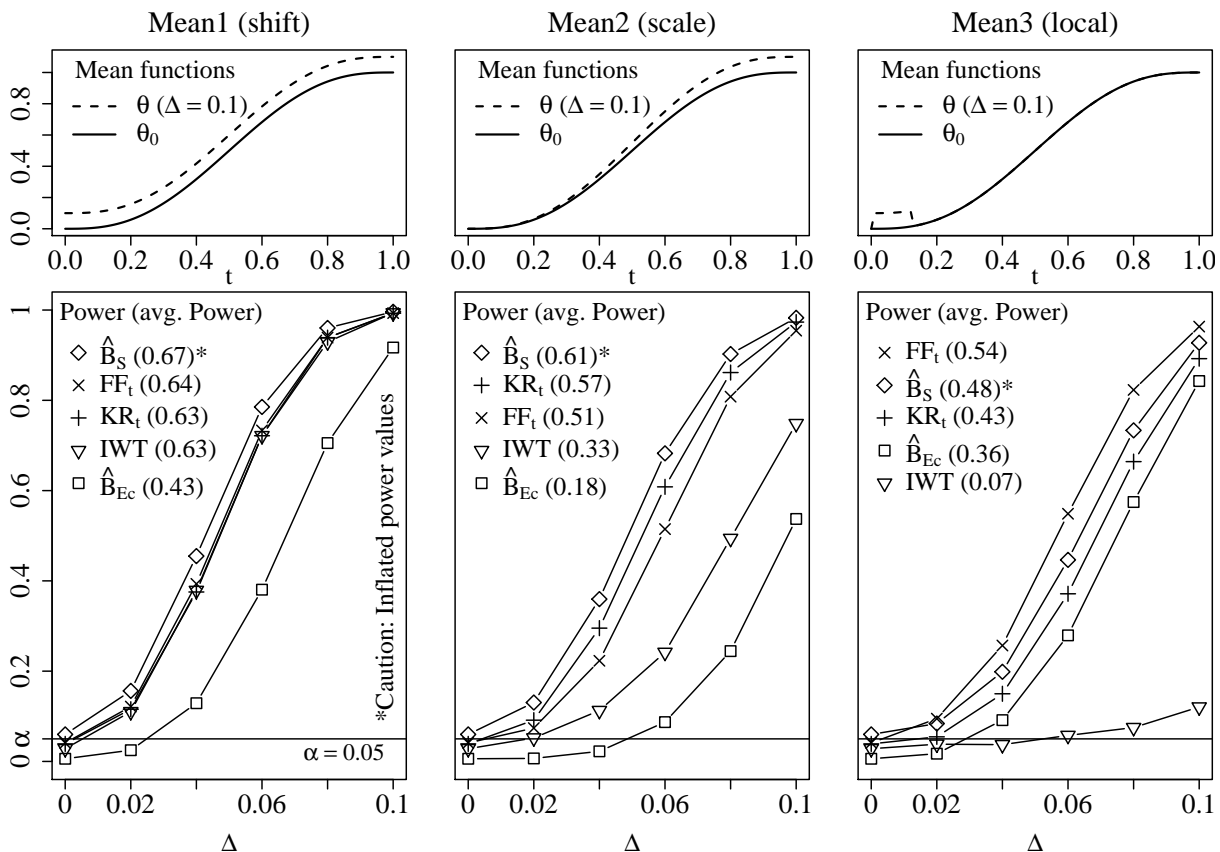


Figure 2: UPPER ROW: Different mean function scenarios Mean 1-3. LOWER ROW: Power comparisons for the ‘smooth to rough’ covariance scenario Cov3 and sample size $n = 100$. The average power values (avg. power) are averages over all mean perturbations $\Delta > 0$. The shown FF_t band has parameters $p + q = 9$ and $t_0 = 0$; other parameters lead to similar results.

The lower row of Figure 2 shows the power plots for the large sample, $n = 100$, and the

challenging non-stationary covariance scenario Cov3. The legends are ranked according to the methods’ average powers over $\Delta > 0$. The results of the FF bands for all parameters $p + q \in \{3, 9\}$ and $t_0 \in \{0, 1\}$ and all scenarios and sample sizes are summarized in the tables of Appendix B of the supplementary paper [Liebl and Reimherr \(2019b\)](#). However, they all lead to the following equivalent conclusions:

- (a) In all scenarios, the power of the bootstrap band, \hat{B}_S , is inflated as this band cannot keep the nominal α -level.
- (b) In scenario Mean1, all procedures that are able to keep the nominal α -level perform essentially equivalent, except for the \hat{B}_{E_c} band which has a relatively low power.
- (c) In scenario Mean2, the KR_t band has the highest power among the methods that are able to keep the nominal α -level. The FF_t band has a slightly lower power than the KR_t since the perturbation of the mean function is largest at the area where the FF_t band is widest (see explanation ‘Fair power of FF band’ below). The IWT procedure and the \hat{B}_{E_c} band have both low powers.
- (d) In scenario Mean3, our FF_t band has the highest power among all methods and performs even better than the size-inflated bootstrap band, \hat{B}_S . The KR_t and the \hat{B}_{E_c} bands have quite a bit lower powers. The IWT method is essentially not able to detect the considered local mean perturbations. The latter is remarkable as the IWT method was originally introduced as a ‘domain-selection’ method ([Pini and Vantini, 2017b](#)).

Fair power of FF band The adaptive fair FF band allocates the multiple testing component, α^* , uniformly over the total domain $[0, 1]$. This causes the FF band to locally adapt its width to the varying within curve correlations of the Cov3 process. An important consequence of this adaptive behavior is an approximately equitable power to detect local deviations from the null hypotheses across the domain $[0, 1]$ – apart from differences in the variances which also affect the power. This explains the result that the local mean differences of the Mean2 and Mean3 scenarios are detected with approximately equal average powers, 0.51 and 0.54, even though the Cov3 process has a non-stationary roughness. In contrast, the non-adaptive KR band has very unbalanced average powers, 0.57 and 0.43, since the KR band is ‘too wide’ in areas with high positive within curve correlations and ‘too narrow’ in areas with weak correlations.

3.1.2 Fair Inference over Regions of Interest

In this section, we assess the interpretable fairness property (Proposition 2.2) of our FF bands which allows us to do fair simultaneous inference over subintervals, or regions of interests, $ROI = [0, t_0]$ and $ROI = [t_0, 1]$. To evaluate this fairness feature, we use again the duality of confidence bands with hypothesis tests. This time, however, we consider the following ROI-specific hypotheses:

$$H_0: \theta(t) = \theta_0(t) \forall t \in ROI \quad \text{vs.} \quad H_1: \exists t \in ROI \text{ s.t. } \theta(t) \neq \theta_0(t),$$

with $ROI = [0, t_0]$ or $ROI = [t_0, 1]$. We reject H_0 if θ_0 is not covered by a band for at least one of the evaluation points over the ROI. In this simulation study we consider three

different t_0 -values, $t_0 \in \{0.25, 0.5, 0.75\}$, which lead to six different ROIs. To check the robustness of our FF_t bands, we consider the two different grid point parameters $p + q = 4$ and $p + q = 8$, where both allow to set $a_0 = t_0$ as needed in Algorithm 1. The simulation study is based again on 50,000 Monte Carlo replications.

Starting points are our FF bands computed as simultaneous 95% confidence bands for the total domain $[0, 1]$. To assess their ROI-specific simultaneous type-I error rates, we compare their empirical ROI-specific type-I error rates with the corresponding nominal ROI-specific significance levels

$$\alpha_{[0,t_0]} = p_{t_0} + \mathbf{a}^*(t_0 - 0) \quad \text{and} \quad \alpha_{[t_0,1]} = p_{t_0} + \mathbf{a}^*(1 - t_0),$$

where the pointwise testing component, p_{t_0} , and the multiple testing component, \mathbf{a}^* , are returned by Algorithm 1 based on the true covariance function. In practice, p_{t_0} and \mathbf{a}^* can be consistently estimated using Algorithm 1 based on the empirical covariance function \hat{C}_θ . As a benchmark we consider the non-adaptive KR_t band.

Table 3: ROI-specific type-I error rates for covariance scenario Cov3.

t_0	Band	ROI = $[0, t_0]$		ROI = $[t_0, 1]$	
		$n = 15$	$n = 100$	$n = 15$	$n = 100$
0.25	$\text{FF}_t (p + q = 4, t_0 = t_0)$	0.021 (0.021)*	0.019 (0.021)	0.036 (0.040)	0.031 (0.040)
	$\text{FF}_t (p + q = 8, t_0 = t_0)$	0.021 (0.021)	0.022 (0.021)	0.033 (0.040)	0.030 (0.040)
	KR_t	0.009 (0.021)	0.007 (0.021)	0.044 (0.040)	0.036 (0.040)
0.50	$\text{FF}_t (p + q = 4, t_0 = t_0)$	0.027 (0.028)	0.027 (0.027)	0.023 (0.028)	0.021 (0.027)
	$\text{FF}_t (p + q = 8, t_0 = t_0)$	0.027 (0.028)	0.026 (0.027)	0.024 (0.028)	0.021 (0.027)
	KR_t	0.014 (0.028)	0.012 (0.027)	0.037 (0.028)	0.033 (0.027)
0.75	$\text{FF}_t (p + q = 4, t_0 = t_0)$	0.035 (0.038)	0.033 (0.038)	0.013 (0.014)	0.011 (0.014)
	$\text{FF}_t (p + q = 8, t_0 = t_0)$	0.034 (0.038)	0.034 (0.038)	0.015 (0.014)	0.012 (0.014)
	KR_t	0.023 (0.038)	0.020 (0.038)	0.030 (0.014)	0.026 (0.014)

*In brackets: nominal ROI-specific type-I error rates $\alpha_{[0,t_0]}$ and $\alpha_{[t_0,1]}$.

Table 3 contains the empirical and the nominal ROI-specific type-I error rates of the adaptive FF_t band and the non-adaptive KR_t band for the case of the challenging non-stationary covariance scenario Cov3. The nominal ROI-specific type-I error rates $\alpha_{[0,t_0]}$ and $\alpha_{[t_0,1]}$ are shown in brackets. The results for the stationary covariance scenarios, Cov1 and Cov2, are reported in the tables of Appendix B of the supplementary paper [Liebl and Reimherr \(2019b\)](#); however, the results for all three covariance scenarios can be summarized as following:

- (a) The FF_t band keeps the nominal ROI-specific type-I error rates for all ROIs, $[0, t_0]$ and $[t_0, 1]$, in all three covariance scenarios Cov1-3 and both sample sizes.
- (b) The FF_t band is slightly conservative if the process is rough, that is, in scenario Cov2 and in the upper parts $[t_0, 1]$ of the non-stationary scenario Cov3.

(c) The non-adaptive KR_t band is able to keep the nominal ROI-specific type-I error rates only in the case of the stationary covariance scenarios Cov1 and Cov2. In case of the non-stationary scenario Cov3, the KR_t band is very conservative over the smooth area $[t_0, 1]$ and over-rejects the null hypothesis over the rough area $[t_0, 1]$.

The results of our FF_t band are remarkable and unique in the literature as none of the existing simultaneous confidence bands allow for ROI-specific inferences for general non-stationary processes.

3.2 Fragmentary Functions

In this section, we consider fragmentized functional data generated from the mean and covariance scenarios, Mean1-3 and Cov1-3. In a first step, we draw random sample functions $\{S_i\}_{i=1}^n \stackrel{\text{iid}}{\sim} \mathcal{N}(\theta, C_\theta)$ and evaluate them at 101 equidistant evaluation points, $t = j/100$ with $j = 0, \dots, 100$, as in Section 3.1. In a second step, we fragmentize the curves by declaring all evaluation points $t \notin [A_i, B_i] \subset [0, 1]$ as missings where $B_i = A_i + 0.4$ and $A_i = \tilde{A}_i/100$ with $\{\tilde{A}_i\}_{i=1}^n \stackrel{\text{iid}}{\sim} \text{BeB}(60, 0.3, 0.3)$ and with $\text{BeB}(N, \alpha, \beta)$ denoting the discrete Beta-Binomial distribution. This leads to a challenging case of fragmentary functions, S_i , since no function covers the total domain $[0, 1]$. Consequently, the covariance, C_θ , can only be estimated over a band along the diagonal, namely, over $\{(t, s) \in [0, 1]^2 : |t - s| \leq 0.4\} \subset [0, 1]^2$. We consider a relatively large sample size of $n = 500$ since fragmentizing the functions reduces the local sample size, $n_t = \sum_{i=1}^n \mathbb{1}\{S_i(t) \text{ is not missing}\} \leq n$, considerably. In our simulation study, the local sample size varied between 44 and 332 across all evaluation points. The upper row in Figure 3 shows exemplary fragmentized sample paths for the mean θ_0 and all covariance scenarios Cov1-3.

For estimating the mean, θ , and covariance, C_θ , we use the following estimators for fragmentary functional data:

$$\hat{\theta}_{\text{frag}}(t) = \frac{I_1(t)}{\sum_{i=1}^n O_i(t)} \sum_{i=1}^n S_i(t) O_i(t),$$

$$\hat{C}_{\text{frag}}(t, s) = \frac{I_2(t, s)}{\sum_{i=1}^n U_i(t, s)} \sum_{i=1}^n U_i(t, s) (S_i(t) - \hat{\theta}_{\text{frag}}(t)) (S_i(s) - \hat{\theta}_{\text{frag}}(s)),$$

where $O_i(t) = \mathbb{1}\{S_i(t) \text{ is not missing}\}$ denotes the missingness process. The operators $I_1(t) = \mathbb{1}\{\sum_{i=1}^n O_i(t) > 0\}$ and $I_2(t, s) = \mathbb{1}\{\sum_{i=1}^n U_i(t, s) > 0\}$, with $U_i(t, s) = O_i(t)O_i(s)$, are necessary to prevent divisions by zero through defining $0/0 := \text{'Missing'}$. Recent works using these estimators are, for instance, [Delaigle and Hall \(2013\)](#), [Kraus \(2015\)](#), and [Liebl and Rameseder \(2019\)](#).

To the best of our knowledge, the KR and our FF bands are the only confidence bands that can be used in the challenging case of fragmentary functional data which prevents estimating the full covariance. The fragment versions, KR_{frag} and FF_{frag} , of the KR and FF bands are defined as following:

$$\text{KR}_{\text{frag}}(t) = [\hat{\theta}_{\text{frag},l}(t), \hat{\theta}_{\text{frag},u}(t)] = \hat{\theta}_{\text{frag}}(t) \pm \hat{u}_{\text{frag},\alpha}(\hat{C}_{\text{frag}}(t, t)/n_t)^{1/2} \quad \text{and}$$

$$\text{FF}_{\text{frag}}(t) = [\hat{\theta}_{\text{frag},l}^*(t), \hat{\theta}_{\text{frag},u}^*(t)] = \hat{\theta}_{\text{frag}}(t) \pm \hat{u}_{\text{frag},\alpha}^*(t)(\hat{C}_{\text{frag}}(t, t)/n_t)^{1/2}, \quad t \in [0, 1],$$

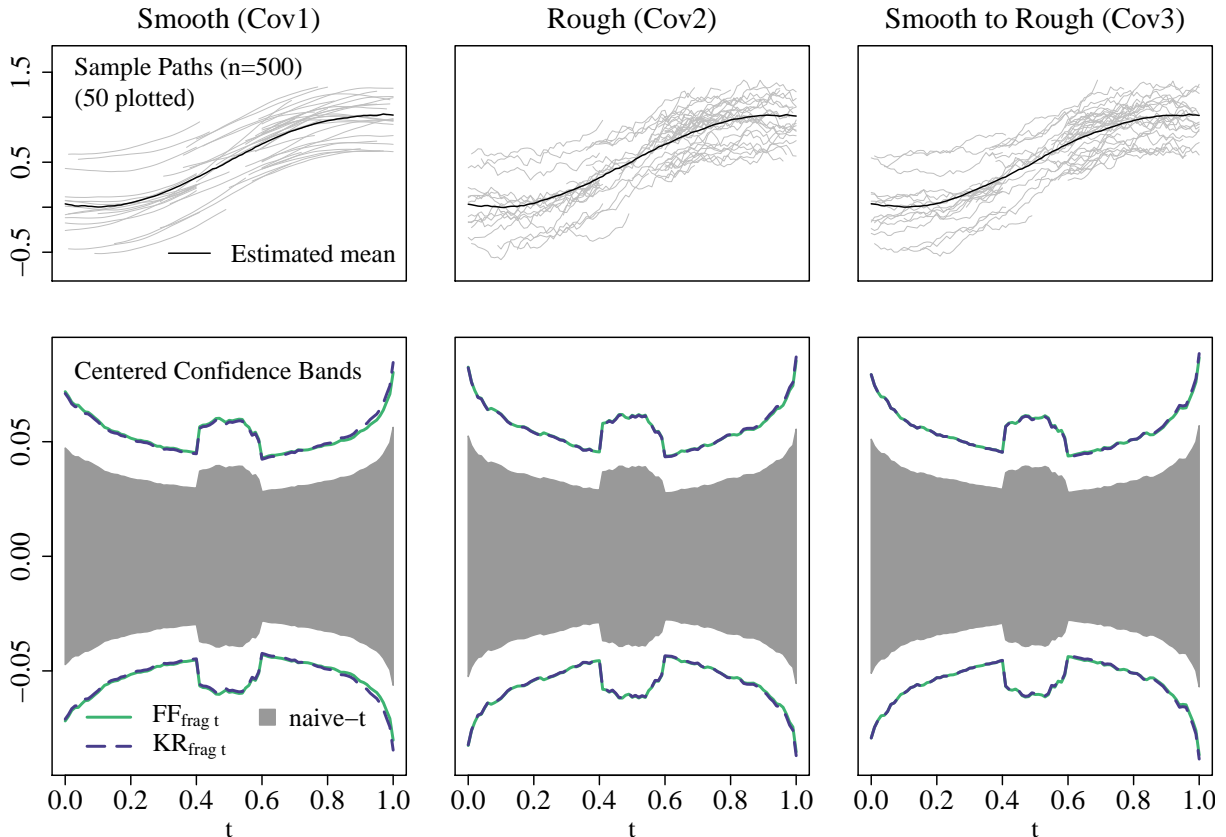


Figure 3: UPPER ROW: Exemplary sample paths and mean estimates, $\hat{\theta}_{\text{frag}}$. LOWER ROW: Exemplary centered 95% confidence bands – centering by $\hat{\theta}_{\text{frag}}$ is applied to optimize the visualization of the bands. The shown $\text{FF}_{\text{frag},t}$ band has parameters $p + q = 9$ and $t_0 = 0$; other parameters lead to similar band shapes.

where the constant threshold, $\hat{u}_{\text{frag},\alpha}$, is computed by solving (6) for $\text{KR}_{\text{frag},t}$ or (8) for $\text{KR}_{\text{frag},z}$, and where the adaptive threshold function, $\hat{u}_{\text{frag},\alpha}^*$, is computed by Algorithm 1 based on (5) for $\text{FF}_{\text{frag},z}$ or (7) for $\text{FF}_{\text{frag},t}$. As the estimator of the roughness parameter function, τ , we use the following fragment version of $\hat{\tau}_1$ in (18):

$$\hat{\tau}_{\text{frag}}(t) = (\partial_{12}\hat{c}_{\text{frag}}(t, t))^{1/2} \quad \text{with} \quad \hat{c}_{\text{frag}}(t, s) = \hat{C}_{\text{frag}}(t, s)(\hat{C}_{\text{frag}}(t, t)\hat{C}_{\text{frag}}(s, s))^{-1/2}$$

for $t, s \in [0, 1]$. This estimator is computable even though the covariance estimate $\hat{C}_{\text{frag}}(t, s)$ may only have non-missing values at a narrow band along the diagonal. We set $\alpha = 0.05$ and $t_0 = 0.5$, use equidistant grid points $a_j = (1/3)j$ with $j = 0, 1, 2, 3$, and test the hypothesis $H_0: \theta(t) = \theta_0(t) \forall t \in [0, 1]$ vs. $H_1: \exists t \in [0, 1]$ s.t. $\theta(t) \neq \theta_0(t)$. For the $\text{KR}_{\text{frag},t}$ band and the $\text{FF}_{\text{frag},t}$ band we use $\nu = \min_t(n_t) - 1$ degrees of freedom.

The lower row of Figure 3 shows examples of the 95% simultaneous confidence bands $\text{KR}_{\text{frag},t}$ and $\text{FF}_{\text{frag},t}$. It is striking that the shapes of the fragment bands are essentially equivalent to each other – even in the case of the non-stationary covariance scenario Cov3. The reason for this is that the missingness process, O_i , introduces an additional source of

roughness into the covariance structure of the estimator $\hat{\theta}_{\text{frag}}$. This additional roughness component becomes here the dominating roughness component leading to equivalent band shapes since we consider the same missingness process for all covariance scenarios Cov1-3. The unusually varying widths of the bands are determined by the varying local sample sizes, n_t , which are driven by the used missingness process. This results in relatively small n_t -values at the boundaries of the domain $[0, 1]$ and over $[0.4, 0.6]$ which makes the bands wide at the boundaries of $[0, 1]$ and causes the characteristic bump over $[0.4, 0.6]$.

Table 4: The type-I error rates and power values of the fragment bands $\text{FF}_{\text{frag},t}$ and $\text{KR}_{\text{frag},t}$ in the non-stationary covariance scenario Cov3.

DGP	Band	H ₀		H ₁				Avg. Power
		$\Delta = 0$	$\Delta = 0.02$	$\Delta = 0.04$	$\Delta = 0.06$	$\Delta = 0.08$	$\Delta = 0.1$	
Mean1	$\text{FF}_{\text{frag},t}$	0.051	0.253	0.806	0.993	1.000	1.000	0.81
Mean1	$\text{KR}_{\text{frag},t}$	0.046	0.248	0.804	0.993	1.000	1.000	0.81
Mean2	$\text{FF}_{\text{frag},t}$	0.051	0.136	0.450	0.830	0.981	0.999	0.68
Mean2	$\text{KR}_{\text{frag},t}$	0.046	0.133	0.449	0.834	0.981	0.999	0.68
Mean3	$\text{FF}_{\text{frag},t}$	0.051	0.095	0.306	0.664	0.925	0.994	0.60
Mean3	$\text{KR}_{\text{frag},t}$	0.046	0.086	0.293	0.654	0.921	0.994	0.59

Table 4 summarizes the type-I error rates and power values of the fragment bands $\text{FF}_{\text{frag},t}$ and $\text{KR}_{\text{frag},t}$ in the challenging non-stationary covariance scenario Cov3. The results for the $\text{FF}_{\text{frag},z}$ and $\text{KR}_{\text{frag},z}$ bands and for the other covariance scenarios (Cov1-2) are summarized in the tables of Appendix B of the supplementary paper [Liebl and Reimherr \(2019b\)](#); however, they all lead to the following conclusions: The $\text{FF}_{\text{frag},t}$ and $\text{KR}_{\text{frag},t}$ bands perform very similar. Both are able to keep the nominal α -level at comparable type-I error rates and both show similar power values.

The possibility to perform simultaneous inference for functional parameters in the case of fragmentary functional data is unique in the literature. This is a strong result for our FF bands and, to the best of our knowledge, was not yet pointed out for the KR bands.

4 Applications

In this section we demonstrate the use of our fair confidence bands in two real data examples. Section 4.1 considers an example from sports biomechanics where scientists often collect and analyze fully observed functional data. Section 4.2 considers the case of fragmentary growth curves where the estimation of the total covariance is impossible.

4.1 Fully Observed Functions

Empirical research in biomechanics uses functional data for describing human (or animal) movements over time ([Vanrenterghem et al., 2012](#); [Hamacher et al., 2016](#); [Warmenhoven et al., 2019](#)). The data shown in Figure 4 comes from a sports biomechanics experiment

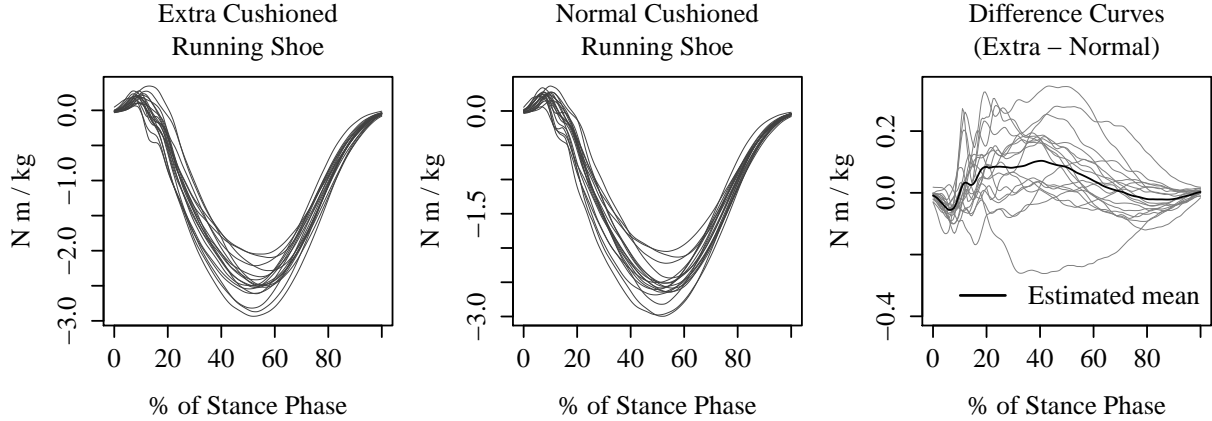


Figure 4: LEFT AND MIDDLE PLOT: Paired sample of $n = 18$ torque curves measured at the ankle joint in sagittal pane. RIGHT PLOT: Sample of $n = 18$ difference-curves computed from the paired sample.

designed to assess the differences between extra cushioned vs. normal cushioned running shoes. The experiment was conducted at the biomechanics lab of the German Sport University, Cologne, Germany. A sample of $n = 18$ recreational runners with a habitual heel strike running pattern were included into the experiment. The outcome of interest are the torque curves describing the temporal torques acting at the right ankle joint in sagittal pane during the ‘stance phase’ of one running stride.³ The torques are measured in Newton metres (N m) standardized by the bodyweights (kg) of the participants. The individual stance phases are standardized to a common unit interval $[0\%, 100\%]$ using simple linear affine time transformations. This simple ‘warping’ method leads to a good alignment of the data and is common in the biomechanics literature. At $t = 0\%$ the heel strikes the ground and at $t = 100\%$ the forefoot leaves the ground. The initially positive curve values represent a net torque in dorsiflexion direction which enables a controlled lowering of the forefoot after the initial heel strike. The subsequent negative curve values represent a net torque in plantarflexion direction which generate the forward movement when running. Further details on the measurement and the computation of the curves can be found in [Liebl et al. \(2014\)](#) who analyze a dataset with essentially equivalent characteristics.

For each participant there are two torque curves – one when running with a certain extra cushioned running shoe and another when running with a certain normal cushioned running shoe (left and middle plots of Figure 4). In order to test for differences in the mean torque curves we consider the pairwise difference-curves (extra minus normal cushioned) shown in the right plot of Figure 4 and test the hypotheses $H_0: \theta(t) = 0 \forall t \in [0\%, 100\%]$ vs. $H_1: \exists t \in [0\%, 100\%]$ s.t. $\theta(t) \neq 0$. To conduct this test, we use our FF_t band with six equidistant grid points $a_j = (20\%)j$, $j = 0, 1, \dots, 5$, and significance level $\alpha = 0.05$. We set $t_0 = 20\%$ since we also want to do inference over the initial ROI = $[0, 20\%]$ which corresponds to the initial heel strike phase where the extra cushioning is supposed to have a particular effect. We compare our adaptive FF_t band with the non-adaptive KR_t band.

³The ‘stance phase’ is the phase of a running stride during which the foot has ground contact.

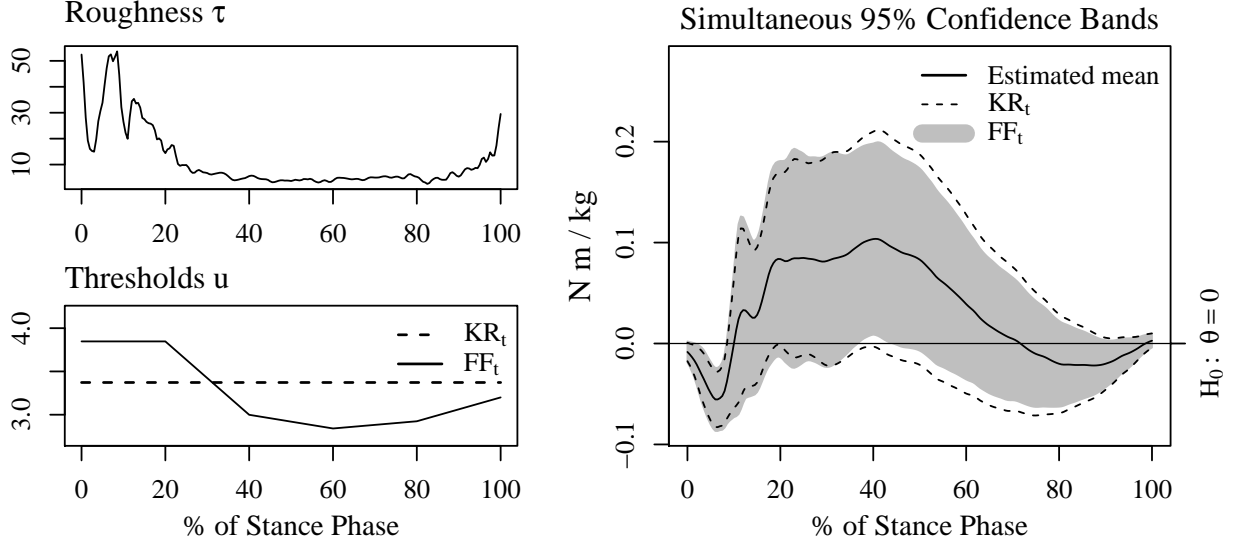


Figure 5: UPPER-LEFT PLOT: Estimated roughness parameter function, $\hat{\tau}$, of the difference-curves. LOWER-LEFT PLOT: Adaptive threshold function \hat{u}_α^* of the FF_t band and constant threshold of the KR_t band. RIGHT PLOT: Simultaneous 95% confidence bands FF_t and KR_t .

The upper-left plot in Figure 5 shows the estimated roughness parameter function, $\hat{\tau}$, for the difference-curves. The roughness is relatively large over the initial interval $[0\%, 20\%]$, relatively low over $[20\%, 90\%]$, and increases again over the final interval $[90\%, 100\%]$. The lower-left plot demonstrates how the adaptive fair threshold function, \hat{u}_α^* , takes into account this roughness pattern. In contrast, the non-adaptive threshold function, \hat{u}_α , of the KR_t band remains constant over the whole domain.

The right plot of Figure 5 shows the simultaneous 95% confidence bands. The FF_t band is wider than the KR_t band over the initially rough first quarter of the domain, $[0\%, 25\%]$, but tighter over the remaining parts. Both bands show significant differences over the initial stance phase from 2% to 8%. Moreover, the FF_t band shows also an additional significant difference over the middle stance phase from 37% to 44% which is not detected by the KR_t band. The two most significant points according to the FF_t band are at $t_1 = 6\%$ and $t_2 = 40\%$ with (simultaneous) p-values $p_{FF_t}(t_1) < 0.001$ and $p_{FF_t}(t_2) = 0.045$.

The specific region of interest in this experiment is the initial ROI = $[0\%, 20\%]$ since this part of the domain corresponds to the initial heel strike phase where the cushioning is supposed to have a particular effect. Over this ROI, the FF_t band corresponds to a $1 - (\hat{p}_{t_0} + \hat{\mathbf{a}}^*(20\% - 0\%)) = 1 - (0.005 + 0.045(20\% - 0\%)) = 98.6\%$ simultaneous confidence band.

4.2 Fragmentary Functional Data

In this section we consider the bone mineral acquisition data described in [Bachrach et al. \(1999\)](#) and further analyzed by [James and Hastie \(2001\)](#), [Delaigle and Hall \(2013\)](#), and [De-](#)

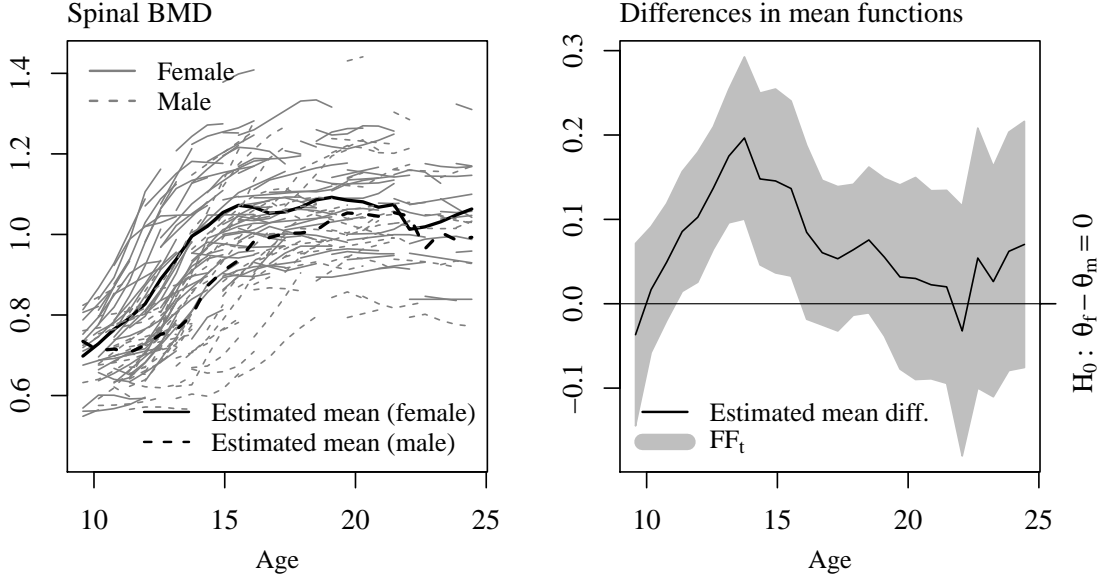


Figure 6: LEFT PLOT: Fragmentary spinal bone mineral density acquisition curves. RIGHT PLOT: Simultaneous 95% confidence bands, FF_t and KR_t , for the difference mean function.

laigle and Hall (2016).⁴ The spinal Bone Mineral Density (BMD) measurements (g/cm^2) were taken for each individual at 2 to 4 time points over short time intervals; therefore, linear interpolations of the measurements give good approximations of the underlying smooth mineral acquisition growth processes. The left plot in Figure 6 shows the fragmentary growth curves of $n_f = 140$ female (f) and $n_m = 113$ male (m) participants after restricting the data to a common domain from 9.6 years to 24.5 years and to at least 2 measurement time points per individual.

In the following we test the hypotheses of equal means $H_0: \theta_f(t) - \theta_m(t) = 0 \forall t \in [9.6 \text{ yr}, 24.5 \text{ yr}]$ vs. $H_1: \exists t \in [9.6 \text{ yr}, 24.5 \text{ yr}]$ s.t. $\theta_f(t) \neq \theta_m(t)$ using the following two-sample (2S) version of our simultaneous confidence band, FF_t ,

$$FF_{\text{frag}}^{2S}(t) = [\hat{\theta}_f^{*2S}(t), \hat{\theta}_m^{*2S}(t)] = (\hat{\theta}_f(t) - \hat{\theta}_m(t)) \pm \hat{u}_{\text{frag}\alpha}^{*2S}(t) (\hat{C}_{\text{frag}}^{2S}(t, t))^{1/2},$$

where the covariance function

$$\hat{C}_{\text{frag}}^{2S}(t, s) = ((n_{ts}^f - 1)\hat{C}_{\text{frag}}^f(t, s) + (n_{ts}^m - 1)\hat{C}_{\text{frag}}^m(t, s)) / (n_{ts}^f + n_{ts}^m - 2)$$

is the usual weighted average of the sample covariances, \hat{C}_{frag}^f and \hat{C}_{frag}^m , with $n_{ts}^m = \sum_{i=1} O_i^m(t)O_i^m(s)$ and $n_{ts}^f = \sum_{i=1} O_i^f(t)O_i^f(s)$ and missingness indicators, $O_i^f(t)$ and $O_i^m(t)$, as defined in Section 3.2. The short fragments of the growth curves allow only an estimation of the covariances, \hat{C}_{frag}^f and \hat{C}_{frag}^m , over narrow bands along the diagonal (see Figure 8 in Appendix B). The threshold function, $\hat{u}_{\text{frag}\alpha}^{*2S}$, is computed using Algorithm 1 with significance level $\alpha = 0.05$, $t_0 = 0$, nine equidistant grid points, and empirical roughness parameter function, $\hat{\tau}^{2S}$, computed from $\hat{C}_{\text{frag}}^{2S}$ using (18) as described in Section 3.2.

⁴The data is freely available at the companion website of the textbook of Friedman et al. (2001).

The right plot in Figure 6 shows a significant difference in the mean growth functions from 11.4 years to 15.5 years. This is the first simultaneous inference result, which confirms the adolescent gender-differences in the bone mineral acquisitions described in [Bachrach et al. \(1999\)](#).

5 Discussion

While this work represents a major methodological leap for confidence bands in FDA, many interesting and important open questions remain unanswered. Concerning confidence regions, it would be useful to extend our work beyond univariate domains. Such extensions exist for the classic Kac-Rice formulas and thus, in principle, should be possible for our bands as well. It would also be useful to explore other criteria for selecting adapting bands beyond fairness. Preliminary simulations have suggested that options such as average width or squared width with splines are possible, but more serious computational efforts are needed since one would need to minimize a non-convex objective function.

Another useful, but highly nontrivial extension would be to further relax the normality or asymptotic normality (or elliptical) assumption. In particular, estimates for models such as scalar-on-function regression do not possess any asymptotic distribution in the strong topology since they are not tight ([Cardot et al., 2007](#)). Instead, such estimates satisfy the CLT only in the weak topology. It is unclear if confidence bands can be constructed for such estimates.

Lastly, our assumptions require the underlying estimate/process to be continuously differentiable. For confidence regions, this is a reasonable assumption, however, for prediction bands it would be useful if this assumption could be relaxed. In particular, for things like daily weather forecasting or tidal levels, it might be useful to only require continuity of the process. However, this would require serious theoretical work as non-differentiable processes can cross a smooth boundary infinitely many times over a compact domain (e.g. Brownian motion).

At a broader level, we also hope this work sparks more interactions between the areas of Random Field Theory and Functional Data Analysis. The two tackle related problems, but using very different techniques and perspectives.

Supplementary materials. The supplementary paper [Liebl and Reimherr \(2019b\)](#) contains the mathematical proofs of our theoretical results, further simulation results, and additional plots. The R-package `ffscb` which implements the introduced methods is available at the first author's GitHub account.

Acknowledgments. We thank the mathematical research institute MATRIX in Creswick, Australia and the Simons Institute for the Theory of Computing at the UC Berkeley where parts of this research was performed. Many thanks go also to Steffen Willwacher (German Sport University Cologne) for providing the data of the biomechanics application in Section 4.1.

References

- Abramowicz, K., C. K. Häger, A. Pini, L. Schelin, S. Sjöstedt de Luna, and S. Vantini (2018). Nonparametric inference for functional-on-scalar linear models applied to knee kinematic hop data after injury of the anterior cruciate ligament. *Scandinavian Journal of Statistics* 45(4), 1036–1061.
- Adler, R. J. and J. E. Taylor (2007). *Random Fields and Geometry*. Springer.
- Azaïs, J.-M. and M. Wschebor (2009). *Level Sets and Extrema of Random Processes and Fields*. John Wiley & Sons.
- Bachrach, L. K., T. Hastie, M.-C. Wang, B. Narasimhan, and R. Marcus (1999). Bone mineral acquisition in healthy asian, hispanic, black, and caucasian youth: A longitudinal study. *The Journal of Clinical Endocrinology & Metabolism* 84(12), 4702–4712.
- Belyaev, Y. K. (1966). On the number of intersections of a level by a gaussian stochastic process. *Theory of Probability & Its Applications* 11(1), 106–113.
- Boente, G., M. S. Barrera, and D. E. Tyler (2014). A characterization of elliptical distributions and some optimality properties of principal components for functional data. *Journal of Multivariate Analysis* 131, 254–264.
- Cao, G., L. Yang, and D. Todem (2012). Simultaneous inference for the mean function based on dense functional data. *Journal of Nonparametric Statistics* 24(2), 359–377.
- Cardot, H., A. Mas, and P. Sarda (2007). Clt in functional linear regression models. *Probability Theory and Related Fields* 138(3-4), 325–361.
- Chen, Y., J. Goldsmith, and R. T. Ogden (2016). Variable selection in function-on-scalar regression. *Stat* 5(1), 88–101.
- Choi, H. and M. Reimherr (2018). A geometric approach to confidence regions and bands for functional parameters. *Journal of the Royal Statistical Society: Series B (Statistical Methodology)* 80(1), 239–260.
- Corbett-Davies, S., E. Pierson, A. Feller, S. Goel, and A. Huq (2017). Algorithmic decision making and the cost of fairness. In *Proceedings of the 23rd ACM SIGKDD International Conference on Knowledge Discovery and Data Mining*, pp. 797–806. ACM.
- Cramér, H. and M. R. Leadbetter (1965). The moments of the number of crossings of a level by a stationary normal process. *The Annals of Mathematical Statistics* 36(6), 1656–1663.
- Cramér, H. and M. R. Leadbetter (2013). *Stationary and related stochastic processes: Sample function properties and their applications*. Courier Corporation.
- Degras, D. A. (2011). Simultaneous confidence bands for nonparametric regression with functional data. *Statistica Sinica* 21(4), 1735–1765.

- Delaigle, A. and P. Hall (2013). Classification using censored functional data. *Journal of the American Statistical Association* 108(504), 1269–1283.
- Delaigle, A. and P. Hall (2016). Approximating fragmented functional data by segments of markov chains. *Biometrika* 103(4), 779–799.
- Delaigle, A., P. Hall, W. Huang, and A. Kneip (2019). Estimating the covariance of fragmented and other incompletely observed functional data. *Working Paper*.
- Descary, M.-H. and V. M. Panaretos (2019). Recovering covariance from functional fragments. *Biometrika* 106(1), 145–160.
- Fang, K.-T., S. Kotz, and K.-W. Ng (2018). *Symmetric Multivariate and Related Distributions* (1. ed.). Chapman and Hall/CRC.
- Ferraty, F. and P. Vieu (2006). *Nonparametric Functional Data Analysis: Theory and Practice*. Springer.
- Friedler, S. A., C. Scheidegger, and S. Venkatasubramanian (2016). On the (im) possibility of fairness. *arXiv preprint arXiv:1609.07236*.
- Friedman, J., T. Hastie, and R. Tibshirani (2001). *The Elements of Statistical Learning*, Volume 1. Springer.
- Friston, K., J. Ashburner, S. Kiebel, T. Nichols, and W. Penny (Eds.) (2007). *Statistical Parametric Mapping: The Analysis of Functional Brain Images*. Academic Press.
- Friston, K. J., A. P. Holmes, K. J. Worsley, J.-P. Poline, C. D. Frith, and R. S. Frackowiak (1994). Statistical parametric maps in functional imaging: A general linear approach. *Human brain mapping* 2(4), 189–210.
- Goldsmith, J., S. Greven, and C. Crainiceanu (2013). Corrected confidence bands for functional data using principal components. *Biometrics* 69(1), 41–51.
- Hajian, S., F. Bonchi, and C. Castillo (2016). Algorithmic bias: From discrimination discovery to fairness-aware data mining. In *Proceedings of the 22nd ACM SIGKDD international conference on knowledge discovery and data mining*, pp. 2125–2126. ACM.
- Hamacher, D., K. Hollander, and A. Zech (2016). Effects of ankle instability on running gait ankle angles and its variability in young adults. *Clinical Biomechanics* 33, 73–78.
- Hart, J. D. and T. E. Wehrly (1986). Kernel regression estimation using repeated measurements data. *Journal of the American Statistical Association* 81(396), 1080–1088.
- Hsing, T. and R. Eubank (2015). *Theoretical Foundations of Functional Data Analysis, with an Introduction to Linear Operators*. John Wiley & Sons.
- Ito, K. (1963). The expected number of zeros of continuous stationary gaussian processes. *Journal of Mathematics of Kyoto University* 3(2), 207–216.

- James, G. M. and T. J. Hastie (2001). Functional linear discriminant analysis for irregularly sampled curves. *Journal of the Royal Statistical Society: Series B (Statistical Methodology)* 63(3), 533–550.
- Kac, M. (1943). On the average number of real roots of a random algebraic equation. *Bulletin of the American Mathematical Society* 49(4), 314–320.
- Kneip, A. and D. Liebl (2019). On the optimal reconstruction of partially observed functional data. *The Annals of Statistics* (forthcoming).
- Kneip, A., D. Poß, and P. Sarda (2016). Functional linear regression with points of impact. *The Annals of Statistics* 44(1), 1–30.
- Kokoszka, P. and M. Reimherr (2013). Asymptotic normality of the principal components of functional time series. *Stochastic Processes and their Applications* 123(5), 1546–1562.
- Kokoszka, P. and M. Reimherr (2017). *Introduction to Functional Data Analysis* (1. ed.). Chapman and Hall/CRC.
- Kraus, D. (2015). Components and completion of partially observed functional data. *Journal of the Royal Statistical Society* 77(4), 777–801.
- Kraus, D. (2019). Inferential procedures for partially observed functional data. *Journal of Multivariate Analysis* 173, 583–603.
- Li, Y. and T. Hsing (2010). Uniform convergence rates for nonparametric regression and principal component analysis in functional/longitudinal data. *The Annals of Statistics* 38(6), 3321–3351.
- Liebl, D. and S. Rameseder (2019). Partially observed functional data: The case of systematically missing parts. *Computational Statistics & Data Analysis* 131, 104 – 115.
- Liebl, D. and M. Reimherr (2019a). *ffscb: Fast and fair simultaneous confidence for functional parameters*. R package version 0.0.9.
- Liebl, D. and M. Reimherr (2019b). Supplement to “fast and fair simultaneous confidence bands for functional parameters”.
- Liebl, D., S. Willwacher, J. Hamill, and G.-P. Brüggemann (2014). Ankle plantarflexion strength in rearfoot and forefoot runners: A novel clusteranalytic approach. *Human Movement Science* 35, 104–120.
- Lindquist, M. A. and I. W. McKeague (2009). Logistic regression with brownian-like predictors. *Journal of the American Statistical Association* 104(488), 1575–1585.
- Lundtorp Olsen, N., A. Pini, and S. Vantini (2019). False discovery rate for functional data. *arXiv preprint arXiv:1908.05272*.

- Ma, S., L. Yang, and R. J. Carroll (2012). A simultaneous confidence band for sparse longitudinal regression. *Statistica Sinica* 22, 95–122.
- Manrique, T., C. Crambes, and N. Hilgert (2018). Ridge regression for the functional concurrent model. *Electronic Journal of Statistics* 12(1), 985–1018.
- McKeague, I. W. and B. Sen (2010). Fractals with point impact in functional linear regression. *The Annals of Statistics* 38(4), 2559–2586.
- Pataky, T. C., M. A. Robinson, and J. Vanrenterghem (2016). Region-of-interest analyses of one-dimensional biomechanical trajectories: Bridging 0d and 1d theory, augmenting statistical power. *PeerJ* 4, e2652.
- Pini, A. and S. Vantini (2016). The interval testing procedure: A general framework for inference in functional data analysis. *Biometrics* 72(3), 835–845.
- Pini, A. and S. Vantini (2017a). *fdatest: Interval wise testing for functional data*. R package version 2.1.0.
- Pini, A. and S. Vantini (2017b). Interval-wise testing for functional data. *Journal of Nonparametric Statistics* 29(2), 407–424.
- Pini, A., S. Vantini, B. M. Colosimo, and M. Grasso (2018). Domain-selective functional analysis of variance for supervised statistical profile monitoring of signal data. *Journal of the Royal Statistical Society: Series C (Applied Statistics)* 67(1), 55–81.
- Poldrack, R. A. (2007). Region of interest analysis for fmri. *Social Cognitive and Affective neuroscience* 2(1), 67–70.
- Ramsay, J. and B. Silverman (2005). *Functional Data Analysis* (2. ed.). Springer.
- Rice, S. O. (1945). Mathematical analysis of random noise. *Bell System Technical Journal* 24, 46–156.
- Taylor, J., A. Takemura, and R. J. Adler (2005). Validity of the expected euler characteristic heuristic. *The Annals of Probability* 33(4), 1362–1396.
- Taylor, J. E., J. R. Loftus, and R. J. Tibshirani (2016). Inference in adaptive regression via the kac-rice formula. *The Annals of Statistics* 44(2), 743–770.
- Vanrenterghem, J., E. Venables, T. Pataky, and M. A. Robinson (2012). The effect of running speed on knee mechanical loading in females during side cutting. *Journal of Biomechanics* 45(14), 2444–2449.
- Wager, T. D., M. L. Davidson, B. L. Hughes, M. A. Lindquist, and K. N. Ochsner (2008). Prefrontal-subcortical pathways mediating successful emotion regulation. *Neuron* 59(6), 1037–1050.

- Wager, T. D., M. A. Lindquist, T. E. Nichols, H. Kober, and J. X. Van Snellenberg (2009). Evaluating the consistency and specificity of neuroimaging data using meta-analysis. *Neuroimage* 45(1), S210–S221.
- Wang, Y., G. Wang, L. Wang, and R. T. Ogden (2019). Simultaneous confidence corridors for mean functions in functional data analysis of imaging data. *Biometrics* (forthcoming).
- Warmenhoven, J., S. Cobley, C. Draper, A. Harrison, N. Bargary, and R. Smith (2019). Considerations for the use of functional principal components analysis in sports biomechanics: examples from on-water rowing. *Sports Biomechanics* 18(3), 317–341.
- Wen, Y., H. Huang, Y. Yu, S. Zhang, J. Yang, Y. Ao, and S. Xia (2018). Effect of tibia marker placement on knee joint kinematic analysis. *Gait & Posture* 60, 99–103.
- Yao, F., H.-G. Müller, and J.-L. Wang (2005). Functional data analysis for sparse longitudinal data. *Journal of the American Statistical Association* 100(470), 577–590.
- Zhang, X. and J.-L. Wang (2016). From sparse to dense functional data and beyond. *The Annals of Statistics* 44(5), 2281–2321.
- Zheng, S., L. Yang, and W. K. Härdle (2014). A smooth simultaneous confidence corridor for the mean of sparse functional data. *Journal of the American Statistical Association* 109(506), 661–673.

Supplement to

Fast and Fair Simultaneous Confidence Bands for Functional Parameters

Dominik Liebl
University of Bonn

Matthew Reimherr
Penn State University

A Proofs

The mathematical arguments are the same for any $t_0 \in [0, 1]$ since the expected number down-crossings about $u(t)$ is equal to the expected number of up-crossings about $-u(t)$. Thus we will fix $t_0 = 0$ in our arguments below. We first establish all of our results conditioned on the mixing coefficient, V , for the elliptical distribution, which can be thought of as computing $\mathbb{E}[\varphi_u(X)|V]$, which is then a Gaussian calculation. After establishing our results for the Gaussian case, we will then reintroduce V and compute the final expectation $\mathbb{E}[\mathbb{E}[\varphi_u(X)|V]]$.

The proof hinges on two approximations that simplify the calculations. The first step is to introduce a smooth approximation of the up-crossing count. This is accomplished using a kernel, $K(x)$. Since the kernel is merely a theoretical device, we will assume it is fairly simple in our lemmas. Intuitively, if $K((u(t) - X(t))/h)$ is large for some small bandwidth, h , then $X(t)$ is very close to crossing $u(t)$. Thus, by integrating this quantity (with appropriate normalizations) we can use it to approximate the up-crossing count.

Our second approximation consists of forming linear interpolations for both $X(t)$ and $u(t)$ on a dyadic grid. In particular, fix an integer k and an index $j = 1, \dots, 2^k$. Then for any $t \in [0, 1]$ such that $j - 1 < t2^k < j$ we form the quantities

$$\begin{aligned}\tilde{X}_k(t) &= X\left(\frac{j-1}{2^k}\right)(j-2^k t) + X\left(\frac{j}{2^k}\right)(2^k t - j + 1), \\ \tilde{u}_k(t) &= u\left(\frac{j-1}{2^k}\right)(j-2^k t) + u\left(\frac{j}{2^k}\right)(2^k t - j + 1), \\ \tilde{X}'_k(t) &= 2^k \left(X\left(\frac{j}{2^k}\right) - X\left(\frac{j-1}{2^k}\right) \right), \\ \tilde{u}'_k(t) &= 2^k \left(u\left(\frac{j}{2^k}\right) - u\left(\frac{j-1}{2^k}\right) \right).\end{aligned}$$

We continuously extend \tilde{X}_k and \tilde{u}_k at the dyadic points, $\tilde{X}_k(j/2^k) = X(j/2^k)$ and $\tilde{u}_k(j/2^k) = u_k(j/2^k)$ for $j = 0, 1, \dots, 2^k$. Since the \tilde{X}'_k and \tilde{u}'_k are step functions, they cannot be continuously extended. For convenience, we take $\tilde{X}'_k(j/2^k) = X'(j/2^k)$ and $\tilde{u}'_k(j/2^k) = u'_k(j/2^k)$, though for the derivatives what happens on a set of measure zero will have no impact on our calculations. This choice also yields the convenient bounds

$$\begin{aligned} \sup_{0 \leq t \leq 1} |\tilde{X}_k(t)| &\leq \sup_{0 \leq t \leq 1} |X(t)| & \sup_{0 \leq t \leq 1} |\tilde{u}_k(t)| &\leq \sup_{0 \leq t \leq 1} |u(t)| \\ \sup_{0 \leq t \leq 1} |\tilde{X}'_k(t)| &\leq \sup_{0 \leq t \leq 1} |X'(t)| & \sup_{0 \leq t \leq 1} |\tilde{u}'_k(t)| &\leq \sup_{0 \leq t \leq 1} |u'(t)|. \end{aligned}$$

A.1 Lemmas

In this section we state our technical lemmas which results in a proof of Corollary 2.2 on the Gaussian case (Lemma A.3).

Lemma A.1. *Let $f \in C[0, 1]$ and suppose there only exists a finite number of zeros $\{t_1, \dots, t_k\}$, that is, $f(t) = 0$ if and only if $t = t_i$ for some $i = 1, \dots, k$. Then for any $\epsilon > 0$ there exists $h > 0$ such that*

$$f^{-1}(-h, h) \subseteq \bigcup_{i=1}^k (t_i - \epsilon, t_i + \epsilon). \quad (23)$$

Proof of Lemma A.1.

Consider a proof by contradiction. Suppose there exists $\epsilon > 0$ such that (23) does not hold for any h . Call the right hand side of (23) B_ϵ . Then consider the sets $A_l = f^{-1}(-2^{-l}, 2^{-l})$ for $l = 1, 2, \dots$. By assumption, $A_l \cap B_\epsilon^c$ is nonempty for any l , so select an infinite sequence $\{x_l\}$ by taking $x_l \in A_l \cap B_\epsilon^c$. By construction, $|f(x_l)| \leq 2^{-l}$, which implies that $f(x_l) \rightarrow 0$ as $l \rightarrow \infty$. However, since $[0, 1]$ is compact, there exists a convergent subsequence $x_{l'}$ such that $x_{l'} \rightarrow x$, which implies $f(x) = 0$. However, $|x - t_i| \geq \epsilon$ for all $i = 1, \dots, k$, which means x cannot be one of the zeros, which is a contradiction. \square

Lemma A.2. Counting Formula.

(a) *Let X be a Gaussian random function with $\text{Var}(X(t)) > 0$ for every $t \in [0, 1]$ and let u be a deterministic function. If $X \in C^1[0, 1]$ almost surely, $u \in C[0, 1]$ and u' is continuous almost everywhere, then the number of up-crossings is*

$$\begin{aligned} N_u(X) &= \#\{t \in [0, 1] : X(t) = u(t), X'(t) - u'(t) > 0\} \\ &= \lim_{h \rightarrow 0} \int_0^1 \frac{1}{h} K\left(\frac{u(t) - X(t)}{h}\right) (X'(t) - u'(t)) \mathbb{1}_{X'(t) - u'(t) > 0} dt < \infty \quad a.s., \end{aligned}$$

where $\mathbb{1}$ denotes the indicator function and K is a symmetric kernel function with compact support, i.e., $K(t) = K(-t) \geq 0$, $K(t) = 0$ if $|t| > 1$, $K(t)$ is continuous on $[-1, 1]$, and $\int K(t) dt = 1$.

(b) Let all requirements in (a) hold, then the dyadic linear interpolations satisfy

$$\begin{aligned}
N_{\tilde{u}_k}(\tilde{X}_k) &= \#\{t \in [0, 1] : \tilde{X}_k(t) = \tilde{u}_k(t), \tilde{X}'_k(t) - \tilde{u}'_k(t) > 0\} \\
&= \lim_{h \rightarrow 0} \int_0^1 \frac{1}{h} K \left(\frac{\tilde{u}_k(t) - \tilde{X}'_k(t)}{h} \right) (\tilde{X}'_k(t) - \tilde{u}'_k(t)) \mathbb{1}_{\tilde{X}'_k(t) - \tilde{u}'_k(t) > 0} dt \\
&\leq \min\{2^k, N_u(X)\},
\end{aligned}$$

almost surely.

Proof of Lemma A.2 Part (a).

First consider the case of no up-crossings, $N_u(X) = 0$, which can happen in only one of two ways. The first possibility is that $X(t) < u(t)$ for all $t \in [0, 1]$ or $X(t) > u(t)$ for all $t \in [0, 1]$. Since $X(t) - u(t)$ is continuous and the domain is compact, there exists an $\epsilon > 0$ such that, $|X(t) - u(t)| \geq \epsilon$ for all $t \in [0, 1]$. This implies that $K((u(t) - X(t))/h) = 0$ for all $t \in [0, 1]$ with $h \leq \epsilon$, thus trivially proving the claim. The second possibility is that we have exactly one down crossing, but no up-crossing. In this case, there is exactly one t_d such that $X(t_d) = u(t_d)$, but $X'(t_d) < u'(t_d)$. Note that t_d is random and equals a discontinuity point of u' with probability zero since u' is continuous almost everywhere. That is, we can take a small enough interval $(t_d - \delta, t_d + \delta)$ such that for all $t \in (t_d - \delta, t_d + \delta)$ we have $\mathbb{1}_{X'(t) > u'(t)} = 0$ with probability one. Then, $|X(t) - u(t)| \geq \epsilon > 0$ for all $t \in [0, t_d - \delta] \cup [t_d + \delta, 1]$ and we can again take h small enough that the integral is exactly zero almost surely.

For the case $N_u(X) = m$ with $m > 0$, define $X_u := X - u$ and let us consider the up-crossings of X_u above 0, which is equivalent to the up-crossings of X above u , that is,

$$\begin{aligned}
N_u(X) &= \#\{t \in [0, 1] : X(t) - u(t) = 0, X'(t) - u'(t) > 0\} \\
&= \#\{t \in [0, 1] : X_u(t) = 0, X'_u(t) > 0\} \\
&= \lim_{h \rightarrow 0} \int_0^1 \frac{1}{h} K \left(\frac{X_u(t) - 0}{h} \right) X'_u(t) \mathbb{1}_{X'_u(t) > 0} dt.
\end{aligned}$$

With probability one, no up-crossing location equals a discontinuity point of u' , thus In addition, with probability one, no up-crossing location equals a discontinuity point of u' , thus the $N_u(X)$ is a well defined quantity. $N_u(X)$ is a well defined quantity. Since $X(0) \neq u(0)$ and $X(1) \neq u(1)$ with probability 1, we can denote the (random) up-crossing locations as $0 < t_1 < \dots < t_m < 1$. By Lemma A.1 for any sufficiently small h , the inverse image of $(-h, h)$ by the function X_u is contained in the union of m pairwise disjoint intervals I_1, \dots, I_m with $t_j \in I_j$, $j = 1, \dots, m$. Observe that $X'_u(t_j) > 0$ for every up-crossing location t_j , $j = 1, \dots, m$, and that X'_u is continuous; therefore, we can take the intervals small enough that the restriction of X_u to I_j is almost surely a diffeomorphism for each $j = 1, \dots, m$.

Since $X'_u(t) = X'(t) + u'(t) > 0$ on I_j almost surely, we can perform a change of variables with $yh = X_u(t)$ and $hdy = X'_u(t)dt$ without changing the orientation of the integral. Since K is compactly supported, we can then take h small enough that

$$\int_{I_j} K \left(\frac{X_u(t)}{h} \right) \frac{X'_u(t)}{h} dt = \int_{-1}^1 K(y) dy = 1, \quad \text{for every } j = 1, \dots, m,$$

which implies that that

$$\begin{aligned} N_u(X) &= \int_0^1 \frac{1}{h} K \left(\frac{u(t) - X(t)}{h} \right) (X'(t) - u'(t)) \mathbb{1}_{X'(t) - u'(t) > 0} dt \\ &= \sum_{j=1}^m \int_{I_j} \frac{1}{h} K \left(\frac{u(t) - X(t)}{h} \right) (X'(t) - u'(t)) \mathbb{1}_{X'(t) > u'(t)} dt = m \end{aligned}$$

for all sufficiently small h .

Finally, the assumption that $X \in C^1([0, 1])$ almost surely implies that the number of up-crossings is finite with probability 1, that is, $N_u(X) = m < \infty$ with probability 1. \square

Proof of Lemma A.2 Part (b).

Since $X(t)$ is a Gaussian process it follows that $\tilde{X}_k(j/2^k) \neq u(j/2^k)$ a.s. for each $j = 0, \dots, 2^k$, meaning an up-crossing occurs only within one of the partitioned intervals $[(j-1)/2^k, j/2^k]$, $j = 1, \dots, 2^k$. Observe that, restricted to an interval $((j-1)/2^k, j/2^k)$, $j = 1, \dots, 2^k$, \tilde{X}_k is just a very simple Gaussian process and \tilde{u}_k is just a linear threshold – both fulfilling the requirements of Lemma A.2 part (a). Thus the result of Lemma A.2 part (a) holds also for each subinterval. So, almost surely, we can count the up-crossings for each partitioned interval and sum up the corresponding integrals

$$N_{\tilde{u}_k}(\tilde{X}_k) = \lim_{h \rightarrow 0} \sum_{j=1}^{2^k} \int_{(j-1)/2^k}^{j/2^k} \frac{1}{h} K \left(\frac{\tilde{u}_k(t) - \tilde{X}_k(t)}{h} \right) (\tilde{X}'_k(t) - \tilde{u}'_k(t)) \mathbb{1}_{\tilde{X}'_k(t) - \tilde{u}'_k(t) > 0} dt,$$

which shows the equality statement.

Since both \tilde{X}_k and \tilde{u}_k are piecewise linear, their difference is also linear. With probability one, this difference is not zero, thus by the fundamental theorem of algebra, there is at most one root/up-crossing. Therefore, the maximum number of up-crossings $N_{\tilde{u}_k}(\tilde{X}_k)$ is bounded by the number of partitioned intervals, 2^k . However, within an interval $[(j-1)/2^k, j/2^k]$, $j = 1, \dots, 2^k$, \tilde{X}_k crossing \tilde{u}_k implies X must cross u by the intermediate value theorem, but the reverse is not true since there can be a subsequent downcrossing. Namely, it is only possible to “miss” up-crossings with the linear interpolation, one cannot add additional crossings, which shows the inequality statement. \square

The result of the following lemma is equivalent to the result in Corollary 2.2 a).

Lemma A.3. Kac-Rice Formula for Non-Constant Thresholds.

Let $\{X(t) : t \in [0, 1]\}$ be a continuously differentiable Gaussian process and $u(t)$ a continuously differentiable function. Let $\tau(t)^2 = \partial_x \partial_y C(x, y)|_{x=y=t}$, where $C(x, y)$ is the covariance function of $X(t)$. Assume $X(t)$ has a constant point-wise unit variance, $\text{Var}(X(t)) = 1$ for all $t \in [0, 1]$. Then the expected value of $\varphi_{u, X}(t_0) = \mathbb{1}_{X(0) \geq u(0)} + N_u(X)$ is

$$\mathbb{E}[\varphi_{u, X}(t_0)] = P(X(0) \geq u(0)) + \int_0^1 \frac{\tau(t)}{2\pi} \exp \left\{ -\frac{1}{2} \left[u(t)^2 + \frac{u'(t)^2}{2\tau(t)^2} \right] \right\} dt - \int_0^1 \frac{u'(t)}{\sqrt{2\pi}} \exp \left\{ -\frac{u(t)^2}{2} \right\} \Phi \left(\frac{-u'(t)}{\tau(t)} \right) dt,$$

where Φ is the standard normal cdf.

Proof of Lemma A.3.

From Lemma A.2 part (b) we have

$$\varphi_{\tilde{u}_k}(\tilde{X}_k) = \mathbb{1}_{X(0) \geq u(0)} + \lim_{h \rightarrow 0} \int_0^1 \frac{1}{h} K \left(\frac{\tilde{u}_k(t) - \tilde{X}_k(t)}{h} \right) (\tilde{X}'_k(t) - \tilde{u}'_k(t)) \mathbb{1}_{\tilde{X}'_k(t) - \tilde{u}'_k(t) > 0} dt \quad a.s.,$$

where we use that $\tilde{X}_k(0) = X(0)$ with probability 1. Let $g_{\tilde{X}_k(t)\tilde{X}'_k(t)}$ denote the joint density of $(\tilde{X}_k(t), \tilde{X}'_k(t))$ and note that by Lemma A.2 part (b) $\int_0^1 (1/h) K((\tilde{u}_k(t) - \tilde{X}_k(t))/h) (\tilde{X}'_k(t) - \tilde{u}'_k(t)) \mathbb{1}_{\tilde{X}'_k(t) - \tilde{u}'_k(t) > 0} dt < 2^k$ (a.s.). Therefore, we can apply the dominated convergence theorem for an arbitrary but fix $k \geq 1$, such that

$$\begin{aligned} \mathbb{E}[\varphi_{\tilde{u}_k}(\tilde{X}_k)] &= P(X(0) \geq u(0)) + \\ &\lim_{h \rightarrow 0} \int_0^1 \frac{1}{h} \int_{-\infty}^{\infty} \int_{\tilde{u}'_k(t)}^{\infty} K \left(\frac{\tilde{u}_k(t) - x}{h} \right) (y - \tilde{u}'_k(t)) g_{\tilde{X}_k(t)\tilde{X}'_k(t)}(x, y) dy dx dt. \end{aligned}$$

Applying a change of variables $x = zh + \tilde{u}_k(t)$, the symmetry and compactness of K yields

$$\begin{aligned} \mathbb{E}[\varphi_u(\tilde{X}_k)] &= P(X(0) \geq u(0)) + \\ &\lim_{h \rightarrow 0} \int_0^1 \int_{-1}^1 \int_{\tilde{u}'_k(t)}^{\infty} K(z) (y - \tilde{u}'_k(t)) g_{\tilde{X}_k(t)\tilde{X}'_k(t)}(zh + \tilde{u}_k(t), y) dy dz dt. \end{aligned}$$

As $g_{\tilde{X}_k(t)\tilde{X}'_k(t)}$ consists of a finite mixture of Gaussian densities for each $t \in [0, 1]$, $g_{\tilde{X}_k(t)\tilde{X}'_k(t)}(x, y)$ it bounded uniformly for all x and y . Therefore, we can bring the limit inside the integral, which yields

$$\mathbb{E}[\varphi_u(\tilde{X}_k)] = P(X(0) \geq u(0)) + \int_0^1 \int_{\tilde{u}'_k(t)}^{\infty} (y - \tilde{u}'_k(t)) g_{\tilde{X}_k(t)\tilde{X}'_k(t)}(\tilde{u}_k(t), y) dy dt. \quad (24)$$

We now finally want to take the limit as $k \rightarrow \infty$. For the left hand side of (24) we immediately have $\mathbb{E}[\varphi_{\tilde{u}_k}(\tilde{X}_k)] \rightarrow \mathbb{E}[\varphi_u(X)]$ as $k \rightarrow \infty$ by the monotone convergence theorem, since $N_u(\tilde{X}_k) \nearrow N_u(X)$ as $k \rightarrow \infty$. For the right hand side of (24), we can rewrite the integral as

$$\int_0^1 \mathbb{E}[(\tilde{X}'_k(t) - \tilde{u}'_k(t)) \mathbb{1}_{\tilde{X}'_k(t) \geq \tilde{u}'_k(t)} | \tilde{X}_k(t) = \tilde{u}_k(t)] g_{\tilde{X}_k(t)}(\tilde{u}_k(t)) dt.$$

To take pass the limit we need to be quite careful with our justification. In particular, we need to pass the limit twice: under the first integral and then under the expectation. We accomplish this in a series of steps.

1. For any $j - 1 \leq t^{2^k} \leq j$ we can write

$$\tilde{X}_k(t) = w_t X((j - 1)/2^k) + (1 - w_t) X(j/2^k),$$

for nonrandom weights $w_t \in [0, 1]$. Since X is continuously differentiable, there exists a k_0 such that for any $k \geq k_0$ we have $\text{Cov}(X((j - 1)/2^k), X(j/2^k)) \geq 0$, which implies that $\text{Var}(\tilde{X}_k(t)) \geq 1$. Thus, for k large, the density $g_{\tilde{X}_k}$ is uniformly bounded by $(2\pi)^{-1/2}$.

2. Next, since $(\tilde{X}_k(t), \tilde{X}'_k(t))$ are jointly mean zero Gaussian random variables (for each t), we have

$$\tilde{X}'_k(t) = b_k(t)\tilde{X}_k(t) + \varepsilon_k(t),$$

where $\varepsilon_k(t)$ and $\tilde{X}_k(t)$ are independent for each t , and b_k are deterministic functions that depend only on the covariance between $\tilde{X}_k(t)$ and $\tilde{X}'_k(t)$. So then we have the bound

$$\begin{aligned} & \mathbb{E}[(\tilde{X}'_k(t) - \tilde{u}'_k(t))1_{\tilde{X}'_k(t) \geq \tilde{u}'_k(t)} | \tilde{X}_k(t) = \tilde{u}_k(t)] \\ & \leq \mathbb{E}[|\tilde{X}'_k(t) - \tilde{u}'_k(t)| | \tilde{X}_k(t) = \tilde{u}_k(t)] \\ & = \mathbb{E}|b_k(t)\tilde{u}_k(t) + \varepsilon_k(t) - \tilde{u}'_k(t)| \leq |b_k(t)\tilde{u}_k(t) - \tilde{u}'_k(t)| + \mathbb{E}|\varepsilon_k(t)|. \end{aligned}$$

Examining the pieces above, a Jensen's inequality implies that

$$\mathbb{E}|\varepsilon_k(t)| \leq \mathbb{E}[X'_k(t)^2]^{1/2} = \tau(t) \leq \sup_{0 \leq t \leq 1} \tau(t).$$

By construction \tilde{u}_k and \tilde{u}'_k are uniformly bounded by sup norms of u and u' respectively. From arguments from step 1, for k large, $\text{Var}(X_k(t)) \geq 1$ and so

$$b_k(t)^2 \leq \mathbb{E}(\tilde{X}'_k(t)^2) \leq \mathbb{E}(\|X'\|_1^2) < \infty.$$

Thus, we have a uniform bound over t for all k large and we can justify passing the limit as $k \rightarrow \infty$ under the integral.

3. Finally, with the limit under the integral we need only that the integrand converges for all or almost all t . Clearly the density term converges

$$g_{\tilde{X}_k(t)}(\tilde{u}_k(t)) \rightarrow \frac{1}{\sqrt{2\pi}} \exp\left\{-\frac{u(t)^2}{2}\right\},$$

since $\text{Var}(X_k(t)) \rightarrow \text{Var}(X(t)) = 1$ and $\tilde{u}_k(t) \rightarrow u(t)$. For the conditional expected value term, using the same arguments as before, we have that

$$\begin{aligned} & \mathbb{E}[(\tilde{X}'_k(t) - \tilde{u}'_k(t))1_{\tilde{X}'_k(t) \geq \tilde{u}'_k(t)} | \tilde{X}_k(t) = \tilde{u}_k(t)] \\ & = \mathbb{E}[(b_k(t)\tilde{u}_k(t) + \varepsilon_k(t) - \tilde{u}'_k(t))1_{b_k(t)\tilde{u}_k(t) + \varepsilon_k(t) \geq \tilde{u}'_k(t)}]. \end{aligned}$$

Clearly we have

$$(b_k(t)\tilde{u}_k(t) + \varepsilon_k(t) - \tilde{u}'_k(t))1_{b_k(t)\tilde{u}_k(t) + \varepsilon_k(t) \geq \tilde{u}'_k(t)} \leq |b_k(t)\tilde{u}_k(t) + \varepsilon_k(t) - \tilde{u}'_k(t)|.$$

As we already showed, $b_k(t)$, $\tilde{u}_k(t)$, and $\tilde{u}'_k(t)$ are uniformly bounded for all k large (and they are deterministic). Turning to $\varepsilon_k(t)$ we have

$$|\varepsilon_k(t)| = |\tilde{X}'_k(t) - b_k(t)\tilde{X}_k(t)| \leq \|X'\|_1 + \|X\|_1(\mathbb{E}\|X'\|_1^2)^{1/2},$$

which has finite expectation. Thus, by the DCT we can pass the limit as $k \rightarrow \infty$ to obtain

$$\begin{aligned} & \mathbb{E}[(b_k(t)\tilde{u}_k(t) + \epsilon_k(t) - \tilde{u}'_k(t))\mathbf{1}_{b_k(t)\tilde{u}_k(t) + \epsilon_k(t) \geq \tilde{u}'_k(t)}] \\ & \rightarrow \mathbb{E}[(b(t)u(t) + \epsilon(t) - u'(t))\mathbf{1}_{b(t)u(t) + \epsilon(t) \geq u'(t)}] \\ & = \mathbb{E}[(X'(t) - u'(t))\mathbf{1}_{X'(t) \geq u'(t)} | X(t) = u(t)], \end{aligned}$$

as desired.

Unraveling the conditional expectation, we have shown that

$$\mathbb{E}[\varphi_u(X)] = P(X(0) \geq u(0)) + \int_0^1 \int_{u'(t)}^\infty (y - u'(t))g_{X(t)X'(t)}(u(t), y) dy dt.$$

Since we assume that $X(t)$ has constant variance, it follows that, for each t , $X(t)$ and $X'(t)$ are uncorrelated and thus independent. So we can express

$$\begin{aligned} \mathbb{E}[\varphi_u(X)] &= P(X(0) \geq u(0)) + \\ & \int_0^1 \left[\frac{1}{\sqrt{2\pi}} \exp\left\{-\frac{u(t)^2}{2}\right\} \int_{u'(t)}^\infty (y - u'(t)) \frac{1}{\sqrt{2\pi\tau(t)^2}} \exp\left\{-\frac{y^2}{2\tau(t)^2}\right\} dy \right] dt. \end{aligned}$$

Turning to the second component, basic calculus implies that

$$\int_{u'(t)}^\infty (y - u'(t)) \frac{1}{\sqrt{2\pi\tau(t)^2}} \exp\left\{-\frac{y^2}{2\tau(t)^2}\right\} dy = \frac{\tau(t)}{\sqrt{2\pi}} \exp\left\{-\frac{u'(t)^2}{2\tau(t)^2}\right\} - u'(t) \Phi\left(\frac{-u'(t)}{\tau(t)}\right),$$

where Φ is the standard normal cdf. This yields the final result

$$\begin{aligned} \mathbb{E}[\varphi_u(X)] &= P(X(0) \geq u(0)) + \\ & \int_0^1 \frac{\tau(t)}{2\pi} \exp\left\{-\frac{u(t)^2}{2} - \frac{u'(t)^2}{2\tau(t)^2}\right\} dt - \int_0^1 \frac{u'(t)}{\sqrt{2\pi}} \exp\left\{-\frac{u(t)^2}{2}\right\} \Phi\left(\frac{-u'(t)}{\tau(t)}\right) dt. \quad \square \end{aligned}$$

This result of Lemma A.3 equals the result in Corollary 2.2 a) for $t_0 = 0$. The general result for any $t_0 \in [0, 1]$ follows now directly from observing that (a), when moving from t_0 down to 0, up-crossings as t decreases are equivalent to down-crossings as t increases, and (b) that the expected number down-crossings about $u(t)$ is equal to the expected number of up-crossings about $-u(t)$. Corollary 2.2 b) follows directly from part a), since $u' \equiv 0$ for constant thresholds $u(t) \equiv u$, $\tau(t) \geq 0$ for all $t \in [0, 1]$ and $X(t_0) \stackrel{D}{=} X(0)$ for all $t_0 \in [0, 1]$

Lemma A.3 allows us now to proof Theorem 2.1.

A.2 Proof of Theorem 2.1

In the following we extend the above result of Lemma A.3 to elliptical distributions. Recall that every elliptical distribution can be expressed as a scalar mixture of a Gaussian and, therefore, our previous calculations were based on conditioning on the scalar mixing coefficient V . Our final expressions simplify if we use the alternative parametrization

$V = \mathcal{V}^{-1/2}$ and work with \mathcal{V} instead. Our previous expectation can then be understood as being conditioned on \mathcal{V} . In particular, if $\dot{u}(t) = \mathcal{V}^{1/2}u(t)$, then by Lemma A.3

$$\begin{aligned} \mathbb{E}[\varphi_u(X)|\mathcal{V}] &= \mathbb{E}[\varphi_{\dot{u}}(X/\mathcal{V}^{1/2})|\mathcal{V}] = P(X(0) \geq u(0)|\mathcal{V}) \\ &+ \int_0^1 \frac{\tau(t)}{2\pi} \exp \left\{ -\mathcal{V} \left[\frac{u(t)^2}{2} + \frac{u'(t)^2}{2\tau(t)^2} \right] \right\} dt \\ &- \int_0^1 \frac{u'(t)\mathcal{V}^{1/2}}{\sqrt{2\pi}} \exp \left\{ -\frac{\mathcal{V}u(t)^2}{2} \right\} \Phi \left(\frac{-u'(t)\mathcal{V}^{1/2}}{\tau(t)} \right) dt. \end{aligned}$$

The expected value of the first component is clearly $P(X(0) \geq u(0))$. For the second component, we can take the expected value and use Fubini's theorem. If $F_{\mathcal{V}}$ is the cdf of \mathcal{V} then this yields

$$\int_0^1 \frac{\tau(t)}{2\pi} \int_0^\infty \exp \left\{ -x \left[\frac{u(t)^2}{2} + \frac{u'(t)^2}{2\tau(t)^2} \right] \right\} dF_{\mathcal{V}}(x) dx dt.$$

Now notice that this is simply a moment generating function (mgf) calculation. Furthermore, it is always finite since \mathcal{V} is strictly positive and the argument is strictly negative. Thus, if $M_{\mathcal{V}}(x)$ is the mgf of \mathcal{V} then we have that the above simplifies to

$$\int_0^1 \frac{\tau(t)}{2\pi} M_{\mathcal{V}} \left(- \left[\frac{u(t)^2}{2} + \frac{u'(t)^2}{2\tau(t)^2} \right] \right) dt.$$

Turning to the third component, we have

$$\begin{aligned} &- \int_0^1 \frac{u'(t)\mathcal{V}^{1/2}}{\sqrt{2\pi}} \exp \left\{ -\frac{\mathcal{V}u(t)^2}{2} \right\} \Phi \left(\frac{-u'(t)\mathcal{V}^{1/2}}{\tau(t)} \right) dt \\ &= - \int_0^1 \frac{u'(t)\mathcal{V}^{1/2}}{\sqrt{2\pi}} \exp \left\{ -\frac{\mathcal{V}u(t)^2}{2} \right\} \int_{\mathcal{V}^{1/2}u'(t)/\tau(t)}^\infty \frac{1}{\sqrt{2\pi}} e^{-x^2/2} dx dt. \end{aligned}$$

Let $y = \tau(t)x/\mathcal{V}^{1/2} - u'(t)$, then the above becomes

$$\begin{aligned} &\int_0^1 \frac{u'(t)\mathcal{V}^{1/2}}{\sqrt{2\pi}} \exp \left\{ -\frac{\mathcal{V}u(t)^2}{2} \right\} \int_0^\infty \frac{\mathcal{V}^{1/2}}{\sqrt{2\pi\tau(t)^2}} e^{-\mathcal{V}(y+u'(t))^2/2\tau(t)^2} dy dt \\ &= \int_0^1 \int_0^\infty \frac{u'(t)\mathcal{V}}{2\pi\tau(t)} \exp \left\{ -\mathcal{V} \left[\frac{u(t)^2}{2} + \frac{(y+u'(t))^2}{2\tau(t)^2} \right] \right\} dy dt. \end{aligned}$$

Now we can take the expected value and use Fubini's theorem to get

$$- \int_0^1 \int_0^\infty \int_0^\infty \frac{u'(t)x}{2\pi\tau(t)} \exp \left\{ -x \left[\frac{u(t)^2}{2} + \frac{(y+u'(t))^2}{2\tau(t)^2} \right] \right\} dF_{\mathcal{V}}(x) dy dt.$$

However as before, the inner integral can be expressed using the mgf of \mathcal{V} , though now with the derivative, resulting in

$$- \int_0^1 \int_0^\infty \frac{u'(t)}{2\pi\tau(t)} M'_{\mathcal{V}} \left(- \left[\frac{u(t)^2}{2} + \frac{(y+u'(t))^2}{2\tau(t)^2} \right] \right) dy dt.$$

So we have the final form for elliptical distributions given as

$$\begin{aligned} \mathbb{E}[\varphi_u(X)] &= P(X(0) \geq u(0)) + \int_0^1 \frac{\tau(t)}{2\pi} M_{\mathcal{V}} \left(- \left[\frac{u(t)^2}{2} + \frac{u'(t)^2}{2\tau(t)^2} \right] \right) dt \\ &\quad - \int_0^1 \int_0^\infty \frac{u'(t)}{2\pi\tau(t)} M'_{\mathcal{V}} \left(- \left[\frac{u(t)^2}{2} + \frac{(y + u'(t))^2}{2\tau(t)^2} \right] \right) dy dt \end{aligned}$$

which equals the result in Theorem 2.1 for $t_0 = 0$. The general result for any $t_0 \in [0, 1]$ follows now directly from observing that (a), when moving from t_0 down to 0, up-crossings as t decreases are equivalent to down-crossings as t increases, and (b) that the expected number down-crossings about $u(t)$ is equal to the expected number of up-crossings about $-u(t)$. \square

A.3 Proof of Corollary 2.3

Maybe the most useful for our purposes is the case where $X(t)$ comes from a t-process. We note that point-wise standardization does not actually produce a t-process, but can still be used to help account for the added uncertainty of estimating the covariance. In this case, the distribution of \mathcal{V} is actually a chi-squared divided by its degrees of freedom. So, if we write $\mathcal{V} = \chi_\nu^2/\nu$, then we have

$$M_{\mathcal{V}}(x) = \left(1 - \frac{2x}{\nu}\right)^{-\nu/2} \quad \text{and} \quad M'_{\mathcal{V}}(x) = \left(1 - \frac{2x}{\nu}\right)^{-\nu/2-1}.$$

Therefore, our expression becomes

$$\begin{aligned} \mathbb{E}[\varphi_u(X)] &= F_t(-u(0); \nu) + \int_0^1 \frac{\tau(t)}{2\pi} \left(1 + \frac{u(t)^2}{\nu} + \frac{u'(t)^2}{\nu\tau(t)^2}\right)^{-\nu/2} dt \\ &\quad - \int_0^1 \int_0^\infty \frac{u'(t)}{2\pi\tau(t)} \left(1 + \frac{u(t)^2}{\nu} + \frac{(y + u'(t))^2}{\nu\tau(t)^2}\right)^{-\nu/2-1} dy dt. \end{aligned}$$

The third term can be further simplified by using the cdf of a t-distribution. In particular, let $\nu' = \nu + 1$ and $a(t)^2 = \nu\tau(t)^2(1 + u(t)^2/\nu)/\nu'$, then we have

$$\begin{aligned} &\int_0^\infty \left(1 + \frac{u(t)^2}{\nu} + \frac{(y + u'(t))^2}{\nu\tau(t)^2}\right)^{-\nu/2-1} dy \\ &= \left(1 + \frac{u(t)^2}{\nu}\right)^{-\nu/2-1} \int_0^\infty \left(1 + \frac{(y + u'(t))^2}{\nu'a(t)^2}\right)^{-\frac{\nu'+1}{2}} dy. \end{aligned}$$

Now use a change of variables $x = y/a(t) + u'(t)/a(t)$ to obtain

$$\begin{aligned}
& \left(1 + \frac{u(t)^2}{\nu}\right)^{-\nu/2-1} a(t) \int_{u'(t)/a(t)}^{\infty} \left(1 + \frac{x^2}{\nu'}\right)^{-\frac{\nu'+1}{2}} dx \\
&= \left(1 + \frac{u(t)^2}{\nu}\right)^{-\nu/2-1} B(1/2, \nu'/2) \sqrt{\nu'} a(t) F_t(-u'(t)/a(t); \nu') \\
&= \left(1 + \frac{u(t)^2}{\nu}\right)^{-\nu/2-1} B(1/2, (\nu+1)/2) \sqrt{\nu+1} a(t) F_t(-u'(t)/a(t); \nu+1) \\
&= \left(1 + \frac{u(t)^2}{\nu}\right)^{-(\nu+1)/2} \frac{\Gamma((\nu+1)/2) \sqrt{(\nu+1)\pi} a(t)}{\Gamma((\nu+2)/2)} F_t(-u'(t)/a(t); \nu').
\end{aligned}$$

where B denotes the beta function, Γ the gamma function, and $F_t(\cdot; \nu')$ denotes the distribution function of a t-distribution with ν' degrees of freedom. This leads to the result in Corollary 2.3 for $t_0 = 0$. The general result for any $t_0 \in [0, 1]$ follows now directly from observing that (a), when moving from t_0 down to 0, up-crossings as t decreases are equivalent to down-crossings as t increases, and (b) that the expected number down-crossings about $u(t)$ is equal to the expected number of up-crossings about $-u(t)$. \square

A.4 Proofs of Propositions 2.1 and 2.2

Proof of Proposition 2.1.

The result of Proposition 2.1 follows directly from the generalized expected Euler characteristic inequality (2) and the construction of u_α^* in Algorithm 1 where the multiple testing component, $\mathbf{a}^*/2$, is uniformly distributed over the domain $[0, 1]$ by allocating the uniform share $(\mathbf{a}^*/2)(a_{j+1} - a_j)$ of the multiple testing component, $\mathbf{a}^*/2$, to each of the $p+q$ intervals $[a_j, a_{j+1}]$, $j = -p, \dots, q-1$. That is, by construction (Algorithm 1) of u_α^* , we have that for any fixed value $t_0 \in [0, 1]$ and significance level $\alpha \in (0, 1)$

$$\begin{aligned}
& P(\exists t \in [0, 1] : X(t) \geq u(t)) \leq \\
& P(X(t_0) \geq u_\alpha^*(t_0)) + \overbrace{\mathbb{E}[N_{u_\alpha^*, X}^-([0, t_0])] + \mathbb{E}[N_{u_\alpha^*, X}([t_0, 1])] }^{=\mathbf{a}^*/2} = \alpha/2, \tag{25} \\
& \qquad \qquad \qquad \underbrace{\hspace{10em}}_{=\mathbf{a}^*(t_0-0)/2} \qquad \qquad \underbrace{\hspace{10em}}_{=\mathbf{a}^*(1-t_0)/2}
\end{aligned}$$

where the value of $\mathbb{E}[N_{u_\alpha^*, X}([t_0, 1])]$ equals the integral in (9) plus the integrals in (10) for $j = 1, \dots, q-1$ with $\mathbf{a} = \mathbf{a}^*$, and where the value of $\mathbb{E}[N_{u_\alpha^*, X}^-([0, t_0])]$ equals the sum of the integrals in (12) for $j = -1, \dots, -p$ with $\mathbf{a} = \mathbf{a}^*$. Partitioning the generalized Euler characteristic inequality (25) into the subintervals $[0, t_0]$ and $[t_0, 1]$ leads to the result of Proposition 2.1. \square

Proof of Propositions 2.2.

Proposition 2.2 is a simple variation of Proposition 2.1 and follows from straight forward calculus exercises equivalent to those leading to (16) and (17). \square

A.5 Proof of Theorem 2.2

The arguments are the same for any elliptical distribution, so we assume that X is a Gaussian process. We recall two classic properties, one from analysis and the other from probability theory. First, if $f(u, \tau)$ is continuous as a mapping from $C^1 \times C \rightarrow \mathbb{R}$, and \mathcal{U} is assumed to be compact, then the collection of functions $\{f_u(\tau) := f(u, \tau) : u \in \mathcal{U}\}$ are equicontinuous. Second, recall that $\tau_n \rightarrow \tau$ in probability if and only if every subsequence $\tau_{n(m)}$ has a further subsequence $\tau_{n(m_l)}$ that converges almost surely.⁵ With a slight abuse of notation we will simply write $n = n(m_l)$. So, we will assume that we are working with such a subsequence $\tau_n \rightarrow \tau$ almost surely. We will then show that this implies that the corresponding properties (1.-4.) of the theorem hold almost surely. By the same logic, this implies that the main claims of the theorem hold in probability, since we will have constructed a subsequence of any subsequence where almost sure convergence holds.

1. The first property follows from the fact that the constant functions are included, and thus a constant band with the desired coverage can always be constructed. That the sets are closed follows from the continuity of $f(u, \tau)$.
2. Since the f_u are equicontinuous, for any $\epsilon > 0$ there exists $\delta > 0$ such that $|f(u, \tau') - f(u, \tau)| \leq \epsilon$ whenever $\|\tau - \tau'\| \leq \delta$ and for all $u \in \mathcal{U}$. Since $\tilde{\tau}_n \rightarrow \tilde{\tau}$ almost surely, we can, with probability 1, find an N large enough such that $n \geq N$ implies $\|\tilde{\tau}_n - \tilde{\tau}\| \leq \delta$. It then follows that if $n \geq N$ then

$$|\alpha - f(u_n, \tilde{\tau})| = |f(u_n, \tilde{\tau}_n) - f(u_n, \tilde{\tau})| \leq \epsilon,$$

which proves the claim.

3. Recall that the Hausdorff distance is given by

$$d(S_n, S) = \max \left\{ \sup_{u_n \in S_n} \inf_{u \in S} \|u_n - u\|, \sup_{u \in S} \inf_{u_n \in S_n} \|u_n - u\| \right\} = \max \{d_{1,n}, d_{2,n}\}.$$

In the following, we examine the terms $d_{1,n}$ and $d_{2,n}$ separately. In the first case, only compactness of \mathcal{U} is needed, while in the second case, both the convexity and the inclusion of the constant functions will be crucial.

- (a) We consider a proof by contradiction, so assume

$$d_{1,n} = \sup_{u_n \in S_n} \inf_{u \in S} \|u_n - u\| \not\rightarrow 0.$$

This implies that, with probability 1, there exists an $\epsilon > 0$ and infinitely many n such that $d_{1,n} \geq \epsilon$. Take a further subsequence such that $d_{1,n} \geq \epsilon$ for all n . Since the sets are compact, this implies that there exists $u_n \in S_n$ such that $\|u_n - u\| \geq \epsilon$, for all n and all $u \in S$. Now take a convergent subsequence of u_n such that $u_n \rightarrow w$. By property 2. we have

$$f(u_n, \tilde{\tau}) \rightarrow \alpha \implies f(w, \tilde{\tau}) = \alpha,$$

which implies that $w \in S$, which is a contradiction since $\|u - w\| \geq \epsilon$ for all $u \in S$. Thus, $d_{1,n} \rightarrow 0$.

⁵See, for instance, Theorem 2.3.2. in: Durrett, R. (2019). *Probability: Theory and Examples*. Cambridge University Press.

(b) We again use a proof by contradiction. Suppose that

$$d_{2,n} = \sup_{u \in S} \inf_{u_n \in S_n} \|u_n - u\| \not\rightarrow 0.$$

As the proof here is more complex, we first provide a high level overview. First, we will show that if $d_{2,n} \not\rightarrow 0$, then we can construct a band, $w \in S$ that is isolated from all but a finite number of the other S_n . We then combine the continuity of f and the convexity of \mathcal{U} to construct a band in S_n with proper coverage, but which must be close to w contradicting this isolation.

Turning to the proof, with probability 1, there exists $\epsilon > 0$ such that $d_{2,n} > 2\epsilon$ for infinitely many n , take an appropriate subsequence such that it holds for all n . Again, since the sets are compact we can find $w_n \in S$, such that $\|w_n - u_n\| > 2\epsilon$ for all $u_n \in S_n$. Now take a further convergent subsequence such that $w_n \rightarrow w$. Then we can find N such that for all $n \geq N$ we have $\|w_n - w\| \leq \epsilon$, which implies that $w \notin S_n$ for $n \geq N$ and even more

$$\|u_n - w\| = \|u_n - w_n + w_n - w\| \geq \|u_n - w_n\| - \|w_n - w\| \geq \epsilon$$

for all $u_n \in S_n$. This implies that w is isolated from the S_n , that is, there is a ball of radius ϵ about w that does not intersect with any S_n .

We now have to utilize the form for f more than previously. In particular, since the constant functions are in \mathcal{U} and \mathcal{U} is convex, this means that $w + 1c \in \mathcal{U}$ (1 is the constant function) if $c \in \mathbb{R}$ is small (if w is on the boundary then enlarge \mathcal{U} slightly) and so for any $\tilde{\tau}$, $f(w + 1c, \tilde{\tau})$ is monotonically decreasing with c (since the band raises uniformly). If ϕ is the density of $X(0)$ then

$$|c|\phi(w(0) + |c|) \leq |P(X(0) \geq w(0) + c) - P(X(0) \geq w(0))| \leq |c|\phi(w(0) - |c|),$$

which means that we can raise/lower the band by c and produce a change in α at least as large in magnitude as the corresponding quantity above (note the integrals in $f(w, \tilde{\tau})$ will increase/decrease in the same direction).

Coming back to the problem at hand, we have that $f(w, \tilde{\tau}) = \alpha$, which implies that $f(w, \tilde{\tau}_n) \rightarrow \alpha$. So take N such that for all $n \geq N$ we have

$$|f(w, \tilde{\tau}_n) - \alpha| < \delta := (\epsilon/2)\phi(u(0) + \epsilon/2).$$

However, now by construction we have that there exists $u_1, u_2 \in \mathcal{U}$ with $|u_i - w| \leq \epsilon$ such that

$$f(u_1, \tau_n) < \alpha \quad \text{and} \quad f(u_2, \tau_n) > \alpha,$$

where $u_i = w + c_i 1$, for some $|c_i| \leq \epsilon/2$. However, $B_c(u', \epsilon) \cap \mathcal{U}$ is convex and $f(u_1 t + (1-t)u_2, \tau_n)$ is continuous in $t \in [0, 1]$ thus there must exist a $u \in B_c(w, \epsilon) \cap \mathcal{U}$ such that $f(u, \tau_n) = \alpha$ implying $u \in S_n$, which is a contradiction since no element of S_n is within ϵ of w . Thus $d_{2,n} \rightarrow 0$.

4. Both properties follow immediately from the continuity of Γ and property 3.

B Additional Simulation Results and Figures

Table 5: Size and Power for Cov1 and $n = 15$. (Section 3.1.1 in the main paper.)

Scenario	n	Band	Mean perturbation Δ						Avg. Power
			0	0.05	0.15	0.25	0.35	0.45	
Mean1 Cov1	15	$FF_t (t_0 = 0, p + q = 3)$	0.050	0.121	0.632	0.972	1.000	1.000	0.745
Mean1 Cov1	15	$FF_t (t_0 = 1, p + q = 3)$	0.051	0.117	0.625	0.970	1.000	1.000	0.742
Mean1 Cov1	15	$FF_t (t_0 = 0, p + q = 9)$	0.048	0.113	0.628	0.971	1.000	1.000	0.742
Mean1 Cov1	15	$FF_t (t_0 = 1, p + q = 9)$	0.049	0.112	0.625	0.967	1.000	1.000	0.741
Mean1 Cov1	15	KR-t	0.052	0.123	0.637	0.971	1.000	1.000	0.746
Mean1 Cov1	15	$FF_z (t_0 = 0, p + q = 3)$	0.085	0.176	0.730	0.986	1.000	1.000	0.778
Mean1 Cov1	15	$FF_z (t_0 = 1, p + q = 3)$	0.086	0.173	0.722	0.986	1.000	1.000	0.776
Mean1 Cov1	15	$FF_z (t_0 = 0, p + q = 9)$	0.082	0.168	0.719	0.985	1.000	1.000	0.774
Mean1 Cov1	15	$FF_z (t_0 = 1, p + q = 9)$	0.082	0.170	0.722	0.984	1.000	1.000	0.775
Mean1 Cov1	15	KR_z	0.086	0.178	0.733	0.986	1.000	1.000	0.779
Mean1 Cov1	15	\hat{B}_{E_c}	0.051	0.119	0.628	0.968	1.000	1.000	0.743
Mean1 Cov1	15	\hat{B}_S	0.090	0.186	0.742	0.987	1.000	1.000	0.783
Mean1 Cov1	15	IWT	0.036	0.097	0.585	0.953	0.999	1.000	0.727
Mean2 Cov1	15	$FF_t (t_0 = 0, p + q = 3)$	0.050	0.085	0.445	0.897	0.996	1.000	0.685
Mean2 Cov1	15	$FF_t (t_0 = 1, p + q = 3)$	0.051	0.083	0.445	0.899	0.996	1.000	0.685
Mean2 Cov1	15	$FF_t (t_0 = 0, p + q = 9)$	0.048	0.092	0.455	0.900	0.995	1.000	0.688
Mean2 Cov1	15	$FF_t (t_0 = 1, p + q = 9)$	0.049	0.085	0.455	0.899	0.995	1.000	0.687
Mean2 Cov1	15	KR-t	0.052	0.089	0.448	0.895	0.996	1.000	0.685
Mean2 Cov1	15	$FF_z (t_0 = 0, p + q = 3)$	0.085	0.134	0.552	0.943	0.999	1.000	0.726
Mean2 Cov1	15	$FF_z (t_0 = 1, p + q = 3)$	0.086	0.130	0.554	0.940	0.999	1.000	0.724
Mean2 Cov1	15	$FF_z (t_0 = 0, p + q = 9)$	0.082	0.140	0.555	0.943	0.998	1.000	0.727
Mean2 Cov1	15	$FF_z (t_0 = 1, p + q = 9)$	0.082	0.130	0.562	0.943	0.998	1.000	0.727
Mean2 Cov1	15	KR_z	0.086	0.136	0.553	0.942	0.998	1.000	0.726
Mean2 Cov1	15	\hat{B}_{E_c}	0.051	0.083	0.434	0.891	0.996	1.000	0.681
Mean2 Cov1	15	\hat{B}_S	0.090	0.142	0.564	0.946	0.998	1.000	0.730
Mean2 Cov1	15	IWT	0.036	0.049	0.218	0.605	0.923	0.997	0.558
Mean3 Cov1	15	$FF_t (t_0 = 0, p + q = 3)$	0.050	0.087	0.460	0.905	0.998	1.000	0.690
Mean3 Cov1	15	$FF_t (t_0 = 1, p + q = 3)$	0.051	0.085	0.456	0.912	0.998	1.000	0.690
Mean3 Cov1	15	$FF_t (t_0 = 0, p + q = 9)$	0.048	0.084	0.459	0.909	0.997	1.000	0.690
Mean3 Cov1	15	$FF_t (t_0 = 1, p + q = 9)$	0.049	0.090	0.461	0.908	0.999	1.000	0.692
Mean3 Cov1	15	KR-t	0.052	0.090	0.460	0.904	0.998	1.000	0.690
Mean3 Cov1	15	$FF_z (t_0 = 0, p + q = 3)$	0.085	0.140	0.576	0.952	0.999	1.000	0.734
Mean3 Cov1	15	$FF_z (t_0 = 1, p + q = 3)$	0.086	0.138	0.573	0.955	1.000	1.000	0.733
Mean3 Cov1	15	$FF_z (t_0 = 0, p + q = 9)$	0.082	0.136	0.571	0.952	0.999	1.000	0.732
Mean3 Cov1	15	$FF_z (t_0 = 1, p + q = 9)$	0.082	0.145	0.580	0.954	1.000	1.000	0.736
Mean3 Cov1	15	KR_z	0.086	0.142	0.577	0.951	0.999	1.000	0.734
Mean3 Cov1	15	\hat{B}_{E_c}	0.051	0.078	0.434	0.901	0.998	1.000	0.682
Mean3 Cov1	15	\hat{B}_S	0.090	0.146	0.588	0.954	0.999	1.000	0.737
Mean3 Cov1	15	IWT	0.036	0.038	0.057	0.120	0.282	0.615	0.222

Table 6: Size and Power for Cov1 and $n = 100$. (Section 3.1.1 in the main paper.)

Scenario	n	Band	Mean perturbation Δ						Avg. Power
			0	0.05	0.15	0.25	0.35	0.45	
Mean1 Cov1	100	$FF_t (t_0 = 0, p + q = 3)$	0.050	0.128	0.378	0.703	0.921	0.988	0.624
Mean1 Cov1	100	$FF_t (t_0 = 1, p + q = 3)$	0.048	0.118	0.383	0.711	0.920	0.989	0.624
Mean1 Cov1	100	$FF_t (t_0 = 0, p + q = 9)$	0.044	0.132	0.376	0.705	0.921	0.987	0.624
Mean1 Cov1	100	$FF_t (t_0 = 1, p + q = 9)$	0.048	0.135	0.385	0.717	0.921	0.989	0.629
Mean1 Cov1	100	KR-t	0.050	0.128	0.379	0.704	0.921	0.988	0.624
Mean1 Cov1	100	$FF_z (t_0 = 0, p + q = 3)$	0.055	0.136	0.394	0.717	0.927	0.989	0.632
Mean1 Cov1	100	$FF_z (t_0 = 1, p + q = 3)$	0.052	0.127	0.398	0.724	0.925	0.990	0.633
Mean1 Cov1	100	$FF_z (t_0 = 0, p + q = 9)$	0.049	0.139	0.390	0.717	0.926	0.989	0.632
Mean1 Cov1	100	$FF_z (t_0 = 1, p + q = 9)$	0.052	0.141	0.401	0.730	0.927	0.990	0.638
Mean1 Cov1	100	KR _z	0.055	0.136	0.394	0.718	0.927	0.989	0.633
Mean1 Cov1	100	\hat{B}_{E_c}	0.028	0.081	0.283	0.590	0.861	0.968	0.556
Mean1 Cov1	100	\hat{B}_S	0.057	0.141	0.404	0.726	0.930	0.990	0.638
Mean1 Cov1	100	IWT	0.036	0.113	0.350	0.680	0.900	0.983	0.605
Mean2 Cov1	100	$FF_t (t_0 = 0, p + q = 3)$	0.050	0.088	0.261	0.542	0.812	0.954	0.531
Mean2 Cov1	100	$FF_t (t_0 = 1, p + q = 3)$	0.048	0.092	0.252	0.545	0.816	0.957	0.532
Mean2 Cov1	100	$FF_t (t_0 = 0, p + q = 9)$	0.044	0.095	0.266	0.554	0.815	0.958	0.537
Mean2 Cov1	100	$FF_t (t_0 = 1, p + q = 9)$	0.048	0.088	0.249	0.535	0.813	0.951	0.527
Mean2 Cov1	100	KR-t	0.050	0.089	0.262	0.540	0.812	0.954	0.531
Mean2 Cov1	100	$FF_z (t_0 = 0, p + q = 3)$	0.055	0.096	0.274	0.558	0.825	0.957	0.542
Mean2 Cov1	100	$FF_z (t_0 = 1, p + q = 3)$	0.052	0.098	0.266	0.559	0.826	0.960	0.542
Mean2 Cov1	100	$FF_z (t_0 = 0, p + q = 9)$	0.049	0.101	0.279	0.569	0.824	0.961	0.547
Mean2 Cov1	100	$FF_z (t_0 = 1, p + q = 9)$	0.052	0.096	0.263	0.550	0.825	0.955	0.538
Mean2 Cov1	100	KR _z	0.055	0.095	0.274	0.557	0.824	0.957	0.541
Mean2 Cov1	100	\hat{B}_{E_c}	0.028	0.053	0.169	0.405	0.701	0.905	0.447
Mean2 Cov1	100	\hat{B}_S	0.057	0.100	0.281	0.565	0.830	0.959	0.547
Mean2 Cov1	100	IWT	0.036	0.053	0.112	0.224	0.429	0.672	0.298
Mean3 Cov1	100	$FF_t (t_0 = 0, p + q = 3)$	0.050	0.091	0.254	0.556	0.826	0.967	0.539
Mean3 Cov1	100	$FF_t (t_0 = 1, p + q = 3)$	0.048	0.093	0.256	0.549	0.821	0.967	0.537
Mean3 Cov1	100	$FF_t (t_0 = 0, p + q = 9)$	0.044	0.092	0.247	0.537	0.820	0.960	0.531
Mean3 Cov1	100	$FF_t (t_0 = 1, p + q = 9)$	0.048	0.098	0.263	0.556	0.835	0.970	0.544
Mean3 Cov1	100	KR-t	0.050	0.092	0.255	0.556	0.826	0.967	0.539
Mean3 Cov1	100	$FF_z (t_0 = 0, p + q = 3)$	0.055	0.098	0.270	0.572	0.836	0.971	0.549
Mean3 Cov1	100	$FF_z (t_0 = 1, p + q = 3)$	0.052	0.100	0.266	0.566	0.833	0.972	0.547
Mean3 Cov1	100	$FF_z (t_0 = 0, p + q = 9)$	0.049	0.098	0.260	0.552	0.832	0.966	0.542
Mean3 Cov1	100	$FF_z (t_0 = 1, p + q = 9)$	0.052	0.105	0.276	0.574	0.844	0.973	0.554
Mean3 Cov1	100	KR _z	0.055	0.098	0.270	0.572	0.837	0.971	0.550
Mean3 Cov1	100	\hat{B}_{E_c}	0.028	0.048	0.155	0.407	0.704	0.920	0.447
Mean3 Cov1	100	\hat{B}_S	0.057	0.103	0.279	0.582	0.843	0.975	0.556
Mean3 Cov1	100	IWT	0.036	0.038	0.043	0.051	0.074	0.100	0.061

Table 7: Size and Power for Cov2 and $n = 15$. (Section 3.1.1 in the main paper.)

Scenario	n	Band	Mean perturbation Δ						Avg. Power
			0	0.05	0.15	0.25	0.35	0.45	
Mean1 Cov2	15	$FF_t (t_0 = 0, p + q = 3)$	0.037	0.093	0.590	0.963	1.000	1.000	0.729
Mean1 Cov2	15	$FF_t (t_0 = 1, p + q = 3)$	0.037	0.094	0.581	0.964	1.000	1.000	0.728
Mean1 Cov2	15	$FF_t (t_0 = 0, p + q = 9)$	0.037	0.092	0.582	0.962	1.000	1.000	0.727
Mean1 Cov2	15	$FF_t (t_0 = 1, p + q = 9)$	0.034	0.096	0.578	0.964	0.999	1.000	0.727
Mean1 Cov2	15	KR-t	0.040	0.097	0.598	0.964	1.000	1.000	0.732
Mean1 Cov2	15	$FF_z (t_0 = 0, p + q = 3)$	0.088	0.189	0.747	0.988	1.000	1.000	0.785
Mean1 Cov2	15	$FF_z (t_0 = 1, p + q = 3)$	0.087	0.186	0.741	0.990	1.000	1.000	0.783
Mean1 Cov2	15	$FF_z (t_0 = 0, p + q = 9)$	0.089	0.180	0.744	0.988	1.000	1.000	0.782
Mean1 Cov2	15	$FF_z (t_0 = 1, p + q = 9)$	0.084	0.188	0.744	0.990	1.000	1.000	0.784
Mean1 Cov2	15	KR_z	0.091	0.192	0.749	0.989	1.000	1.000	0.786
Mean1 Cov2	15	\hat{B}_{E_c}	0.037	0.101	0.623	0.973	1.000	1.000	0.739
Mean1 Cov2	15	\hat{B}_S	0.124	0.238	0.809	0.995	1.000	1.000	0.808
Mean1 Cov2	15	IWT	0.028	0.100	0.632	0.980	1.000	1.000	0.742
Mean2 Cov2	15	$FF_t (t_0 = 0, p + q = 3)$	0.037	0.061	0.376	0.841	0.989	1.000	0.653
Mean2 Cov2	15	$FF_t (t_0 = 1, p + q = 3)$	0.037	0.063	0.369	0.843	0.990	1.000	0.653
Mean2 Cov2	15	$FF_t (t_0 = 0, p + q = 9)$	0.037	0.063	0.370	0.838	0.992	1.000	0.653
Mean2 Cov2	15	$FF_t (t_0 = 1, p + q = 9)$	0.034	0.063	0.360	0.832	0.988	1.000	0.649
Mean2 Cov2	15	KR-t	0.040	0.064	0.379	0.840	0.988	1.000	0.654
Mean2 Cov2	15	$FF_z (t_0 = 0, p + q = 3)$	0.088	0.135	0.549	0.929	0.998	1.000	0.722
Mean2 Cov2	15	$FF_z (t_0 = 1, p + q = 3)$	0.087	0.136	0.543	0.930	0.997	1.000	0.721
Mean2 Cov2	15	$FF_z (t_0 = 0, p + q = 9)$	0.089	0.140	0.541	0.929	0.998	1.000	0.722
Mean2 Cov2	15	$FF_z (t_0 = 1, p + q = 9)$	0.084	0.138	0.531	0.926	0.997	1.000	0.719
Mean2 Cov2	15	KR_z	0.091	0.138	0.550	0.928	0.998	1.000	0.723
Mean2 Cov2	15	\hat{B}_{E_c}	0.037	0.062	0.404	0.866	0.994	1.000	0.665
Mean2 Cov2	15	\hat{B}_S	0.124	0.184	0.625	0.951	0.999	1.000	0.752
Mean2 Cov2	15	IWT	0.028	0.045	0.225	0.695	0.961	0.998	0.585
Mean3 Cov2	15	$FF_t (t_0 = 0, p + q = 3)$	0.037	0.053	0.314	0.802	0.987	1.000	0.631
Mean3 Cov2	15	$FF_t (t_0 = 1, p + q = 3)$	0.037	0.054	0.319	0.812	0.989	1.000	0.635
Mean3 Cov2	15	$FF_t (t_0 = 0, p + q = 9)$	0.037	0.051	0.295	0.801	0.987	1.000	0.627
Mean3 Cov2	15	$FF_t (t_0 = 1, p + q = 9)$	0.034	0.059	0.312	0.807	0.989	1.000	0.633
Mean3 Cov2	15	KR-t	0.040	0.056	0.317	0.801	0.986	1.000	0.632
Mean3 Cov2	15	$FF_z (t_0 = 0, p + q = 3)$	0.088	0.117	0.488	0.918	0.997	1.000	0.704
Mean3 Cov2	15	$FF_z (t_0 = 1, p + q = 3)$	0.087	0.127	0.494	0.921	0.998	1.000	0.708
Mean3 Cov2	15	$FF_z (t_0 = 0, p + q = 9)$	0.089	0.114	0.479	0.912	0.997	1.000	0.701
Mean3 Cov2	15	$FF_z (t_0 = 1, p + q = 9)$	0.084	0.127	0.493	0.915	0.998	1.000	0.707
Mean3 Cov2	15	KR_z	0.091	0.121	0.490	0.916	0.997	1.000	0.705
Mean3 Cov2	15	\hat{B}_{E_c}	0.037	0.048	0.317	0.830	0.993	1.000	0.637
Mean3 Cov2	15	\hat{B}_S	0.124	0.163	0.572	0.949	0.999	1.000	0.737
Mean3 Cov2	15	IWT	0.028	0.030	0.056	0.136	0.376	0.722	0.264

Table 8: Size and Power for Cov2 and $n = 100$. (Section 3.1.1 in the main paper.)

Scenario	n	Band	Mean perturbation Δ						Avg. Power
			0	0.05	0.15	0.25	0.35	0.45	
Mean1 Cov2	100	$\text{FF}_t (t_0 = 0, p + q = 3)$	0.030	0.102	0.335	0.686	0.915	0.989	0.605
Mean1 Cov2	100	$\text{FF}_t (t_0 = 1, p + q = 3)$	0.031	0.101	0.343	0.686	0.918	0.988	0.607
Mean1 Cov2	100	$\text{FF}_t (t_0 = 0, p + q = 9)$	0.031	0.096	0.338	0.675	0.912	0.987	0.602
Mean1 Cov2	100	$\text{FF}_t (t_0 = 1, p + q = 9)$	0.031	0.102	0.344	0.671	0.914	0.990	0.605
Mean1 Cov2	100	KR-t	0.030	0.102	0.336	0.688	0.915	0.989	0.606
Mean1 Cov2	100	$\text{FF}_z (t_0 = 0, p + q = 3)$	0.035	0.115	0.360	0.711	0.925	0.990	0.620
Mean1 Cov2	100	$\text{FF}_z (t_0 = 1, p + q = 3)$	0.037	0.113	0.369	0.711	0.927	0.989	0.622
Mean1 Cov2	100	$\text{FF}_z (t_0 = 0, p + q = 9)$	0.036	0.108	0.361	0.701	0.923	0.989	0.617
Mean1 Cov2	100	$\text{FF}_z (t_0 = 1, p + q = 9)$	0.036	0.113	0.371	0.696	0.924	0.993	0.619
Mean1 Cov2	100	KR _z	0.035	0.115	0.362	0.713	0.925	0.990	0.621
Mean1 Cov2	100	\hat{B}_{E_c}	0.001	0.007	0.049	0.216	0.542	0.837	0.330
Mean1 Cov2	100	\hat{B}_S	0.056	0.161	0.443	0.778	0.949	0.995	0.665
Mean1 Cov2	100	IWT	0.029	0.111	0.376	0.717	0.932	0.993	0.626
Mean2 Cov2	100	$\text{FF}_t (t_0 = 0, p + q = 3)$	0.030	0.064	0.198	0.459	0.753	0.919	0.478
Mean2 Cov2	100	$\text{FF}_t (t_0 = 1, p + q = 3)$	0.031	0.064	0.191	0.463	0.756	0.927	0.480
Mean2 Cov2	100	$\text{FF}_t (t_0 = 0, p + q = 9)$	0.031	0.065	0.194	0.465	0.750	0.930	0.481
Mean2 Cov2	100	$\text{FF}_t (t_0 = 1, p + q = 9)$	0.031	0.066	0.189	0.455	0.747	0.921	0.476
Mean2 Cov2	100	KR-t	0.030	0.063	0.200	0.461	0.754	0.919	0.479
Mean2 Cov2	100	$\text{FF}_z (t_0 = 0, p + q = 3)$	0.035	0.073	0.216	0.484	0.773	0.929	0.495
Mean2 Cov2	100	$\text{FF}_z (t_0 = 1, p + q = 3)$	0.037	0.073	0.208	0.487	0.777	0.937	0.497
Mean2 Cov2	100	$\text{FF}_z (t_0 = 0, p + q = 9)$	0.036	0.075	0.213	0.492	0.773	0.938	0.498
Mean2 Cov2	100	$\text{FF}_z (t_0 = 1, p + q = 9)$	0.036	0.075	0.206	0.480	0.769	0.931	0.492
Mean2 Cov2	100	KR _z	0.035	0.073	0.217	0.487	0.774	0.930	0.496
Mean2 Cov2	100	\hat{B}_{E_c}	0.001	0.003	0.020	0.091	0.289	0.589	0.198
Mean2 Cov2	100	\hat{B}_S	0.056	0.110	0.287	0.567	0.829	0.953	0.549
Mean2 Cov2	100	IWT	0.029	0.052	0.122	0.268	0.493	0.762	0.339
Mean3 Cov2	100	$\text{FF}_t (t_0 = 0, p + q = 3)$	0.030	0.053	0.161	0.414	0.718	0.921	0.453
Mean3 Cov2	100	$\text{FF}_t (t_0 = 1, p + q = 3)$	0.031	0.056	0.165	0.412	0.722	0.927	0.456
Mean3 Cov2	100	$\text{FF}_t (t_0 = 0, p + q = 9)$	0.031	0.048	0.153	0.403	0.708	0.917	0.446
Mean3 Cov2	100	$\text{FF}_t (t_0 = 1, p + q = 9)$	0.031	0.053	0.166	0.413	0.719	0.919	0.454
Mean3 Cov2	100	KR-t	0.030	0.053	0.162	0.416	0.719	0.922	0.454
Mean3 Cov2	100	$\text{FF}_z (t_0 = 0, p + q = 3)$	0.035	0.062	0.178	0.444	0.742	0.932	0.472
Mean3 Cov2	100	$\text{FF}_z (t_0 = 1, p + q = 3)$	0.037	0.067	0.183	0.438	0.745	0.937	0.474
Mean3 Cov2	100	$\text{FF}_z (t_0 = 0, p + q = 9)$	0.036	0.056	0.172	0.431	0.733	0.929	0.464
Mean3 Cov2	100	$\text{FF}_z (t_0 = 1, p + q = 9)$	0.036	0.061	0.185	0.439	0.743	0.930	0.472
Mean3 Cov2	100	KR _z	0.035	0.062	0.180	0.445	0.744	0.932	0.473
Mean3 Cov2	100	\hat{B}_{E_c}	0.001	0.001	0.013	0.071	0.242	0.542	0.174
Mean3 Cov2	100	\hat{B}_S	0.056	0.093	0.239	0.531	0.810	0.960	0.527
Mean3 Cov2	100	IWT	0.029	0.030	0.042	0.059	0.080	0.116	0.065

Table 9: Size and Power for Cov3 and $n = 15$. (Section 3.1.1 in the main paper.)

Scenario	n	Band	Mean perturbation Δ						Avg. Power
			0	0.05	0.15	0.25	0.35	0.45	
Mean1 Cov3	15	$FF_t (t_0 = 0, p + q = 3)$	0.044	0.109	0.631	0.975	1.000	1.000	0.743
Mean1 Cov3	15	$FF_t (t_0 = 1, p + q = 3)$	0.047	0.116	0.647	0.979	1.000	1.000	0.748
Mean1 Cov3	15	$FF_t (t_0 = 0, p + q = 9)$	0.044	0.106	0.632	0.973	1.000	1.000	0.742
Mean1 Cov3	15	$FF_t (t_0 = 1, p + q = 9)$	0.045	0.112	0.628	0.974	1.000	1.000	0.743
Mean1 Cov3	15	KR-t	0.045	0.112	0.642	0.975	1.000	1.000	0.746
Mean1 Cov3	15	$FF_z (t_0 = 0, p + q = 3)$	0.092	0.195	0.776	0.992	1.000	1.000	0.793
Mean1 Cov3	15	$FF_z (t_0 = 1, p + q = 3)$	0.098	0.205	0.779	0.994	1.000	1.000	0.796
Mean1 Cov3	15	$FF_z (t_0 = 0, p + q = 9)$	0.093	0.191	0.768	0.993	1.000	1.000	0.790
Mean1 Cov3	15	$FF_z (t_0 = 1, p + q = 9)$	0.096	0.200	0.767	0.990	1.000	1.000	0.791
Mean1 Cov3	15	KR_z	0.099	0.203	0.783	0.992	1.000	1.000	0.796
Mean1 Cov3	15	\hat{B}_{E_c}	0.035	0.095	0.605	0.968	1.000	1.000	0.734
Mean1 Cov3	15	\hat{B}_S	0.122	0.237	0.818	0.995	1.000	1.000	0.810
Mean1 Cov3	15	IWT	0.027	0.094	0.625	0.976	1.000	1.000	0.739
Mean2 Cov3	15	$FF_t (t_0 = 0, p + q = 3)$	0.044	0.073	0.375	0.843	0.992	1.000	0.657
Mean2 Cov3	15	$FF_t (t_0 = 1, p + q = 3)$	0.045	0.077	0.422	0.881	0.995	1.000	0.675
Mean2 Cov3	15	$FF_t (t_0 = 0, p + q = 9)$	0.044	0.066	0.363	0.840	0.991	1.000	0.652
Mean2 Cov3	15	$FF_t (t_0 = 1, p + q = 9)$	0.045	0.075	0.393	0.858	0.995	1.000	0.664
Mean2 Cov3	15	KR-t	0.045	0.095	0.513	0.929	0.998	1.000	0.707
Mean2 Cov3	15	$FF_z (t_0 = 0, p + q = 3)$	0.092	0.151	0.572	0.945	0.998	1.000	0.733
Mean2 Cov3	15	$FF_z (t_0 = 1, p + q = 3)$	0.095	0.157	0.614	0.955	0.999	1.000	0.745
Mean2 Cov3	15	$FF_z (t_0 = 0, p + q = 9)$	0.093	0.139	0.574	0.946	0.998	1.000	0.732
Mean2 Cov3	15	$FF_z (t_0 = 1, p + q = 9)$	0.096	0.157	0.597	0.949	0.999	1.000	0.740
Mean2 Cov3	15	KR_z	0.099	0.180	0.670	0.974	0.999	1.000	0.765
Mean2 Cov3	15	\hat{B}_{E_c}	0.035	0.063	0.358	0.850	0.992	1.000	0.652
Mean2 Cov3	15	\hat{B}_S	0.122	0.212	0.717	0.982	1.000	1.000	0.782
Mean2 Cov3	15	IWT	0.027	0.048	0.231	0.681	0.958	0.997	0.583
Mean3 Cov3	15	$FF_t (t_0 = 0, p + q = 3)$	0.044	0.078	0.428	0.894	0.996	1.000	0.679
Mean3 Cov3	15	$FF_t (t_0 = 1, p + q = 3)$	0.045	0.090	0.457	0.901	0.998	1.000	0.689
Mean3 Cov3	15	$FF_t (t_0 = 0, p + q = 9)$	0.044	0.082	0.452	0.904	0.998	1.000	0.687
Mean3 Cov3	15	$FF_t (t_0 = 1, p + q = 9)$	0.045	0.084	0.452	0.912	0.998	1.000	0.689
Mean3 Cov3	15	KR-t	0.045	0.058	0.273	0.756	0.978	1.000	0.613
Mean3 Cov3	15	$FF_z (t_0 = 0, p + q = 3)$	0.092	0.145	0.552	0.947	0.999	1.000	0.729
Mean3 Cov3	15	$FF_z (t_0 = 1, p + q = 3)$	0.095	0.158	0.579	0.953	0.999	1.000	0.738
Mean3 Cov3	15	$FF_z (t_0 = 0, p + q = 9)$	0.093	0.150	0.567	0.950	1.000	1.000	0.733
Mean3 Cov3	15	$FF_z (t_0 = 1, p + q = 9)$	0.096	0.154	0.577	0.955	1.000	1.000	0.737
Mean3 Cov3	15	KR_z	0.099	0.129	0.432	0.880	0.994	1.000	0.687
Mean3 Cov3	15	\hat{B}_{E_c}	0.035	0.058	0.366	0.869	0.995	1.000	0.658
Mean3 Cov3	15	\hat{B}_S	0.122	0.155	0.486	0.909	0.997	1.000	0.709
Mean3 Cov3	15	IWT	0.027	0.033	0.053	0.137	0.363	0.714	0.260

Table 10: Size and Power for Cov3 and $n = 100$. (Section 3.1.1 in the main paper.)

Scenario	n	Band	Mean perturbation Δ						Avg. Power
			0	0.05	0.15	0.25	0.35	0.45	
Mean1 Cov3	100	$FF_t (t_0 = 0, p + q = 3)$	0.040	0.119	0.374	0.718	0.933	0.992	0.627
Mean1 Cov3	100	$FF_t (t_0 = 1, p + q = 3)$	0.041	0.122	0.393	0.733	0.939	0.993	0.636
Mean1 Cov3	100	$FF_t (t_0 = 0, p + q = 9)$	0.039	0.120	0.384	0.720	0.934	0.992	0.630
Mean1 Cov3	100	$FF_t (t_0 = 1, p + q = 9)$	0.040	0.121	0.381	0.719	0.936	0.994	0.630
Mean1 Cov3	100	KR-t	0.039	0.116	0.375	0.722	0.939	0.993	0.629
Mean1 Cov3	100	$FF_z (t_0 = 0, p + q = 3)$	0.046	0.129	0.396	0.738	0.943	0.993	0.640
Mean1 Cov3	100	$FF_z (t_0 = 1, p + q = 3)$	0.046	0.133	0.416	0.754	0.946	0.994	0.649
Mean1 Cov3	100	$FF_z (t_0 = 0, p + q = 9)$	0.045	0.131	0.409	0.742	0.940	0.993	0.643
Mean1 Cov3	100	$FF_z (t_0 = 1, p + q = 9)$	0.046	0.135	0.405	0.739	0.944	0.994	0.644
Mean1 Cov3	100	KR _z	0.045	0.126	0.400	0.744	0.946	0.994	0.642
Mean1 Cov3	100	\hat{B}_{E_c}	0.006	0.025	0.129	0.381	0.705	0.917	0.431
Mean1 Cov3	100	\hat{B}_S	0.060	0.156	0.455	0.785	0.960	0.996	0.671
Mean1 Cov3	100	IWT	0.028	0.110	0.379	0.722	0.929	0.994	0.627
Mean2 Cov3	100	$FF_t (t_0 = 0, p + q = 3)$	0.040	0.072	0.209	0.479	0.759	0.934	0.490
Mean2 Cov3	100	$FF_t (t_0 = 1, p + q = 3)$	0.041	0.074	0.223	0.515	0.808	0.954	0.515
Mean2 Cov3	100	$FF_t (t_0 = 0, p + q = 9)$	0.039	0.069	0.199	0.460	0.754	0.935	0.484
Mean2 Cov3	100	$FF_t (t_0 = 1, p + q = 9)$	0.040	0.073	0.210	0.496	0.783	0.947	0.502
Mean2 Cov3	100	KR-t	0.039	0.091	0.295	0.608	0.862	0.973	0.566
Mean2 Cov3	100	$FF_z (t_0 = 0, p + q = 3)$	0.046	0.080	0.232	0.511	0.786	0.945	0.511
Mean2 Cov3	100	$FF_z (t_0 = 1, p + q = 3)$	0.046	0.085	0.247	0.545	0.827	0.961	0.533
Mean2 Cov3	100	$FF_z (t_0 = 0, p + q = 9)$	0.045	0.080	0.222	0.495	0.783	0.947	0.505
Mean2 Cov3	100	$FF_z (t_0 = 1, p + q = 9)$	0.046	0.083	0.233	0.531	0.806	0.955	0.522
Mean2 Cov3	100	KR _z	0.045	0.104	0.315	0.633	0.875	0.977	0.581
Mean2 Cov3	100	\hat{B}_{E_c}	0.006	0.007	0.022	0.087	0.244	0.537	0.180
Mean2 Cov3	100	\hat{B}_S	0.060	0.131	0.360	0.682	0.902	0.983	0.612
Mean2 Cov3	100	IWT	0.028	0.052	0.113	0.242	0.494	0.748	0.330
Mean3 Cov3	100	$FF_t (t_0 = 0, p + q = 3)$	0.040	0.086	0.239	0.525	0.801	0.959	0.522
Mean3 Cov3	100	$FF_t (t_0 = 1, p + q = 3)$	0.041	0.095	0.257	0.549	0.823	0.963	0.537
Mean3 Cov3	100	$FF_t (t_0 = 0, p + q = 9)$	0.039	0.087	0.251	0.540	0.818	0.967	0.532
Mean3 Cov3	100	$FF_t (t_0 = 1, p + q = 9)$	0.040	0.095	0.261	0.543	0.822	0.965	0.537
Mean3 Cov3	100	KR-t	0.039	0.054	0.150	0.371	0.664	0.892	0.426
Mean3 Cov3	100	$FF_z (t_0 = 0, p + q = 3)$	0.046	0.093	0.253	0.543	0.815	0.964	0.534
Mean3 Cov3	100	$FF_z (t_0 = 1, p + q = 3)$	0.046	0.105	0.271	0.564	0.834	0.969	0.548
Mean3 Cov3	100	$FF_z (t_0 = 0, p + q = 9)$	0.045	0.096	0.265	0.556	0.830	0.971	0.543
Mean3 Cov3	100	$FF_z (t_0 = 1, p + q = 9)$	0.046	0.103	0.274	0.559	0.834	0.969	0.548
Mean3 Cov3	100	KR _z	0.045	0.064	0.163	0.396	0.689	0.905	0.443
Mean3 Cov3	100	\hat{B}_{E_c}	0.006	0.017	0.091	0.279	0.575	0.843	0.361
Mean3 Cov3	100	\hat{B}_S	0.060	0.084	0.199	0.447	0.733	0.927	0.478
Mean3 Cov3	100	IWT	0.028	0.038	0.037	0.058	0.075	0.121	0.066

Table 11: ROI-specific type-I error rates for Cov1. (Section 3.1.2 in the main paper.)

t_0	Band	ROI = $[0, t_0]$		ROI = $[t_0, 1]$	
		$n = 15$	$n = 100$	$n = 15$	$n = 100$
0.25	FF.t ($p + q = 4, t_0 = t_0$)	0.025 (0.026)*	0.026 (0.025)	0.040 (0.042)	0.041 (0.042)
	FF.t ($p + q = 8, t_0 = t_0$)	0.025 (0.026)	0.025 (0.025)	0.042 (0.042)	0.040 (0.042)
	KR.t	0.026 (0.026)	0.026 (0.025)	0.042 (0.042)	0.041 (0.042)
0.50	FF.t ($p + q = 4, t_0 = t_0$)	0.034 (0.034)	0.032 (0.034)	0.034 (0.034)	0.032 (0.034)
	FF.t ($p + q = 8, t_0 = t_0$)	0.033 (0.034)	0.033 (0.034)	0.034 (0.034)	0.033 (0.034)
	KR.t	0.035 (0.034)	0.032 (0.034)	0.036 (0.034)	0.033 (0.034)
0.75	FF.t ($p + q = 4, t_0 = t_0$)	0.042 (0.042)	0.041 (0.042)	0.024 (0.026)	0.026 (0.025)
	FF.t ($p + q = 8, t_0 = t_0$)	0.043 (0.042)	0.041 (0.042)	0.026 (0.026)	0.025 (0.025)
	KR.t	0.043 (0.042)	0.041 (0.042)	0.025 (0.026)	0.026 (0.025)

*In brackets: nominal ROI-specific type-I error rates $\alpha_{[0, t_0]}$ and $\alpha_{[t_0, 1]}$.

Table 12: ROI-specific type-I error rates for Cov2. (Section 3.1.2 in the main paper.)

t_0	Band	ROI = $[0, t_0]$		ROI = $[t_0, 1]$	
		$n = 15$	$n = 100$	$n = 15$	$n = 100$
0.25	FF.t ($p + q = 4, t_0 = t_0$)	0.013 (0.015)*	0.012 (0.014)	0.028 (0.038)	0.024 (0.038)
	FF.t ($p + q = 8, t_0 = t_0$)	0.013 (0.015)	0.012 (0.014)	0.028 (0.038)	0.026 (0.038)
	KR.t	0.014 (0.015)	0.012 (0.014)	0.030 (0.038)	0.024 (0.038)
0.50	FF.t ($p + q = 4, t_0 = t_0$)	0.021 (0.026)	0.018 (0.026)	0.020 (0.026)	0.018 (0.026)
	FF.t ($p + q = 8, t_0 = t_0$)	0.021 (0.026)	0.019 (0.026)	0.021 (0.026)	0.018 (0.026)
	KR.t	0.022 (0.026)	0.018 (0.026)	0.022 (0.026)	0.018 (0.026)
0.75	FF.t ($p + q = 4, t_0 = t_0$)	0.028 (0.038)	0.026 (0.038)	0.014 (0.015)	0.012 (0.014)
	FF.t ($p + q = 8, t_0 = t_0$)	0.029 (0.038)	0.024 (0.038)	0.013 (0.015)	0.012 (0.014)
	KR.t	0.030 (0.038)	0.026 (0.038)	0.015 (0.015)	0.012 (0.014)

*In brackets: nominal ROI-specific type-I error rates $\alpha_{[0, t_0]}$ and $\alpha_{[t_0, 1]}$.

Table 13: ROI-specific type-I error rates for Cov3. (Section 3.1.2 in the main paper.)

t_0	Band	ROI = $[0, t_0]$		ROI = $[t_0, 1]$	
		$n = 15$	$n = 100$	$n = 15$	$n = 100$
0.25	FF.t ($p + q = 4, t_0 = t_0$)	0.021 (0.021)*	0.019 (0.021)	0.036 (0.040)	0.031 (0.040)
	FF.t ($p + q = 8, t_0 = t_0$)	0.021 (0.021)	0.022 (0.021)	0.033 (0.040)	0.030 (0.040)
	KR.t	0.009 (0.021)	0.007 (0.021)	0.044 (0.040)	0.036 (0.040)
0.50	FF.t ($p + q = 4, t_0 = t_0$)	0.027 (0.028)	0.027 (0.027)	0.023 (0.028)	0.021 (0.027)
	FF.t ($p + q = 8$)	0.027 (0.028)	0.026 (0.027)	0.024 (0.028)	0.021 (0.027)
	KR.t	0.014 (0.028)	0.012 (0.027)	0.037 (0.028)	0.033 (0.027)
0.75	FF.t ($p + q = 4, t_0 = t_0$)	0.035 (0.038)	0.033 (0.038)	0.013 (0.014)	0.011 (0.014)
	FF.t ($p + q = 8, t_0 = t_0$)	0.034 (0.038)	0.034 (0.038)	0.015 (0.014)	0.012 (0.014)
	KR.t	0.023 (0.038)	0.020 (0.038)	0.030 (0.014)	0.026 (0.014)

*In brackets: nominal ROI-specific type-I error rates $\alpha_{[0, t_0]}$ and $\alpha_{[t_0, 1]}$.

Table 14: The type-I error rates and power values of the fragment bands $\text{FF}_{\text{frag-t}}$ and $\text{KR}_{\text{frag-t}}$ in the non-stationary covariance scenario Cov1. (Section 3.2 in the main paper.)

DGP	Band	H ₀		H ₁				Avg.
		$\Delta = 0$	$\Delta = 0.02$	$\Delta = 0.04$	$\Delta = 0.06$	$\Delta = 0.08$	$\Delta = 0.1$	Power
Mean1 Cov1	FF-t	0.053	0.266	0.779	0.990	1.000	1.000	0.81
Mean1 Cov1	FF-z	0.061	0.298	0.814	0.993	1.000	1.000	0.82
Mean1 Cov1	KR-t	0.044	0.248	0.771	0.989	1.000	1.000	0.80
Mean1 Cov1	KR-z	0.057	0.288	0.814	0.993	1.000	1.000	0.82
Mean2 Cov1	FF-t	0.053	0.136	0.430	0.798	0.970	0.998	0.67
Mean2 Cov1	FF-z	0.061	0.154	0.468	0.830	0.978	0.999	0.69
Mean2 Cov1	KR-t	0.044	0.121	0.420	0.798	0.969	0.998	0.66
Mean2 Cov1	KR-z	0.057	0.147	0.467	0.827	0.976	0.999	0.68
Mean3 Cov1	FF-t	0.053	0.104	0.309	0.670	0.928	0.995	0.60
Mean3 Cov1	FF-z	0.061	0.118	0.340	0.704	0.943	0.996	0.62
Mean3 Cov1	KR-t	0.044	0.088	0.290	0.660	0.926	0.994	0.59
Mean3 Cov1	KR-z	0.057	0.108	0.330	0.698	0.941	0.996	0.61

Table 15: The type-I error rates and power values of the fragment bands $\text{FF}_{\text{frag-t}}$ and $\text{KR}_{\text{frag-t}}$ in the non-stationary covariance scenario Cov2. (Section 3.2 in the main paper.)

DGP	Band	H ₀		H ₁				Avg.
		$\Delta = 0$	$\Delta = 0.02$	$\Delta = 0.04$	$\Delta = 0.06$	$\Delta = 0.08$	$\Delta = 0.1$	Power
Mean1 Cov2	FF-t	0.047	0.264	0.805	0.994	1.000	1.000	0.81
Mean1 Cov2	FF-z	0.060	0.305	0.845	0.995	1.000	1.000	0.83
Mean1 Cov2	KR-t	0.044	0.262	0.805	0.994	1.000	1.000	0.81
Mean1 Cov2	KR-z	0.058	0.302	0.843	0.995	1.000	1.000	0.83
Mean2 Cov2	FF-t	0.047	0.134	0.449	0.829	0.982	1.000	0.68
Mean2 Cov2	FF-z	0.060	0.165	0.502	0.861	0.988	1.000	0.70
Mean2 Cov2	KR-t	0.044	0.133	0.445	0.829	0.982	0.999	0.68
Mean2 Cov2	KR-z	0.058	0.164	0.501	0.860	0.988	1.000	0.70
Mean3 Cov2	FF-t	0.047	0.081	0.282	0.656	0.925	0.993	0.59
Mean3 Cov2	FF-z	0.060	0.104	0.322	0.705	0.941	0.996	0.61
Mean3 Cov2	KR-t	0.044	0.077	0.279	0.651	0.923	0.993	0.58
Mean3 Cov2	KR-z	0.058	0.102	0.320	0.702	0.940	0.996	0.61

Table 16: The type-I error rates and power values of the fragment bands $\text{FF}_{\text{frag-t}}$ and $\text{KR}_{\text{frag-t}}$ in the non-stationary covariance scenario Cov3. (Section 3.2 in the main paper.)

DGP	Band	H ₀		H ₁				Avg.
		$\Delta = 0$	$\Delta = 0.02$	$\Delta = 0.04$	$\Delta = 0.06$	$\Delta = 0.08$	$\Delta = 0.1$	Power
Mean1 Cov3	FF-t	0.051	0.253	0.806	0.993	1.000	1.000	0.81
Mean1 Cov3	FF-z	0.063	0.296	0.845	0.995	1.000	1.000	0.83
Mean1 Cov3	KR-t	0.046	0.248	0.804	0.993	1.000	1.000	0.81
Mean1 Cov3	KR-z	0.060	0.292	0.842	0.996	1.000	1.000	0.83
Mean2 Cov3	FF-t	0.051	0.136	0.450	0.830	0.981	0.999	0.68
Mean2 Cov3	FF-z	0.063	0.163	0.493	0.858	0.986	1.000	0.70
Mean2 Cov3	KR-t	0.046	0.133	0.449	0.834	0.981	0.999	0.68
Mean2 Cov3	KR-z	0.060	0.161	0.499	0.860	0.987	1.000	0.70
Mean3 Cov3	FF-t	0.051	0.095	0.306	0.664	0.925	0.994	0.60
Mean3 Cov3	FF-z	0.063	0.115	0.342	0.704	0.942	0.996	0.62
Mean3 Cov3	KR-t	0.046	0.086	0.293	0.654	0.921	0.994	0.59
Mean3 Cov3	KR-z	0.060	0.109	0.334	0.697	0.937	0.996	0.61

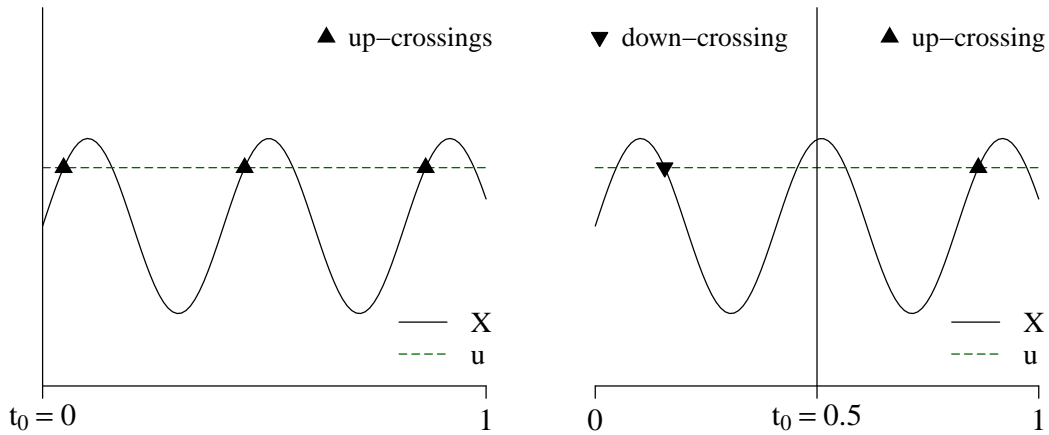


Figure 7: LEFT PLOT: Three exceedance events counted as three up-crossing events to the right of $t_0 = 0$. RIGHT PLOT: The same three exceedance events, but counted as one down-crossing event to the left of $t_0 = 0.5$, one exceedance event at $t_0 = 0.5$, and one up-crossing event to the right of $t_0 = 0.5$.

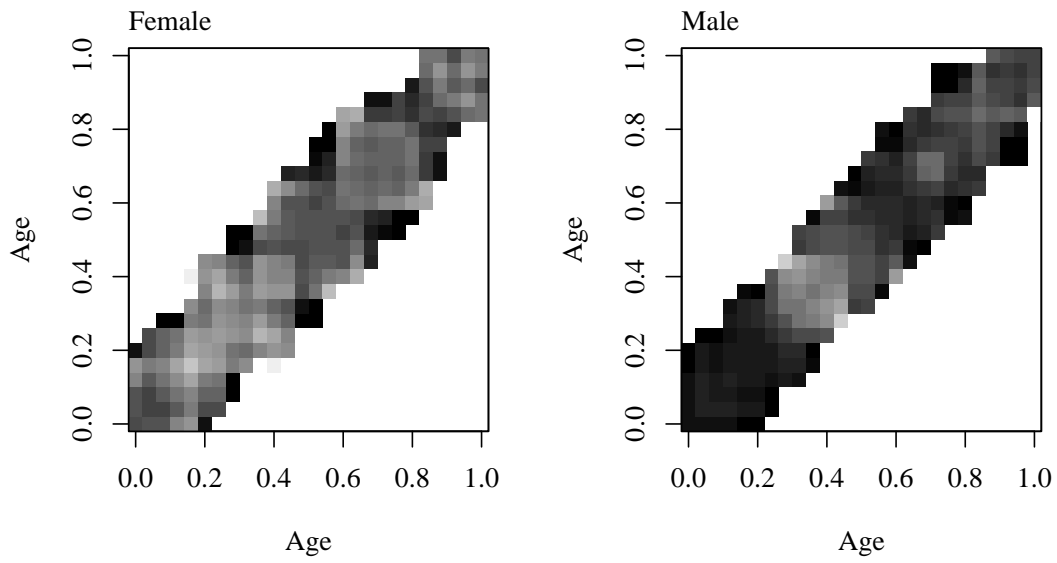


Figure 8: The estimable parts of the sample covariances, \hat{C}_{frag}^f and \hat{C}_{frag}^m , of the bone mineral acquisition data application in Section 4.2.